

**VALIDATION OF RADARSAT-2 SURFACE SOIL MOISTURE
MEASUREMENTS**

DIANA CAROLINA ROMERO-SUAREZ

**Submitted in Partial Fulfillment
of the Requirements for the
Masters in Science in Hydrology**

**NEW MEXICO INSTITUTE OF MINING AND TECHNOLOGY
SOCORRO, NEW MEXICO
June 2010**

ABSTRACT

Soil moisture is an important hydrological parameter in energy, water and ecological processes and models. It has been proposed that the RADARSAT-2 sensor can provide effective and accurate acquisition of soil moisture, under all atmospheric and surface conditions. The focus of this study was to validate the RADARSAT-2 maps by comparing the estimated soil moisture with field measurements. Five sites (Alpha, Beta, Creosote, Nichole, Tripp) with different surface and moisture conditions were chosen in the Rio Grande valley, close to Socorro, NM, USA. Results showed that the application of RADARSAT-2 for water content estimation has specific limitations, related to the features of the terrain (surface roughness, vegetation coverage) and antecedent soil moisture conditions (previous rainfall events).

The highest correlation between RADARSAT-2 soil moisture maps and field measurements are found in the Alpha and Tripp sites, which exhibit: ideal surface conditions (bare and flat/ with homogeneous vegetation) and moderate moisture conditions (Volumetric Water Content (VWC) between 4 and 28%). These characteristics satisfy the requirements of the Oh model (2004), which is used for generating the RADARSAT-2 soil moisture maps. The Beta, Creosote and Nichole sites have non-ideal surface conditions (e.g. rough and/or vegetated) and their moisture values are out of the range required by the model ($4\% < \text{VWC} < 28\%$). Furthermore, data suggest that the correlation between the measurements and the accuracy of the RADARSAT-2 maps decrease as the scale of study decreases from site ($100 \times 100 \text{ m}^2$) to point scale ($10 \times 10 \text{ m}^2$).

RADARSAT-2 maps with asymmetric volumetric correction were also evaluated during this study. The comparison with field water content measurements indicated that there is no significant change in the accuracy and the correlation with the RADARSAT-2 maps, in the site with ideal conditions (Alpha). However, the correlations and accuracy on the other sites, which are covered by vegetation, were reduced significantly.

Finally, comparison with field measurements show that RADARSAT-2 measures soil moisture between 0 to 3 cm depth, which confirm the theoretical estimates of the penetration depth of the radar signal in soils.

ACKNOWLEDGMENTS

First, thanks to the Department of Defense for their financial support of this project. I also want to thank the MDA Company for access to the RADARSAT-2 maps, and special thanks to Bernhard Rasbus for technical support throughout this research.

I want to express my gratitude to my advisor Dr. Jan Hendrickx for his unconditional support, his patience and his advice during this educational process. Also, thanks to my committee members, Dr. Bruce Harrison and Dr. Brian Borchers for all their help during the research process and for encouraging me to keep my spirits high.

I owe special gratitude to all the people who helped me in technical procedures: the sampling process (20 graduate and undergraduate NMT students) lab procedures (Karen Karen, Jeremy Billiot, Alex Rinehart) and review of the body of my thesis (Penny Bencomo and Julianne Newmark).

Finally, but no less important, thanks to all my family and friends who supported me during this process and encourage me every day to do my best for reaching this goal. All my gratitude to my parents, Manuel and MariaO for understanding me and respecting my decisions through all my life - I know it has not been easy to deal with my style of life and I do appreciate all your support and love. Also, thanks to Camilo Casadiego, who encouraged me to keep walking, despite the challenge that it was representing to me. I want to thank Omar Marcillo for his unconditional support for the last 2 years. Thanks to all my good friends in Colombia (Odette, Giovanna, Manuel, Jaime, Pocho, Giovanni A, Andres A, Alberto F, Maye, Natalia, Vlado...) and my friends in Socorro (Vyoma, Marty, Cath, Luis, Maya, Carlos...), who always gave me their good energy and wishes.

Table of Contents

1	INTRODUCTION	1
2	STUDY AREA	5
2.1	Study site.....	5
2.1.1	Geology.....	11
2.1.2	Soils.....	13
3	METHODS AND MATERIALS.....	16
3.1	Estimation of soil moisture data from RADARSAT-2 signal acquisition.....	16
3.2	Field sampling.....	20
3.2.1	Gravimetric Water Content (GWC).....	20
3.2.2	Soil profiles.....	23
3.2.3	Soil bulk density	23
3.3	Lab procedures and calculations.....	24
3.3.1	Gravimetric water content.....	24
3.3.2	Soil bulk density calculation.....	24
3.3.3	Volumetric Water Content.....	25
3.3.4	Soil particle size.....	26
3.3.5	Carbonate content calculation.....	26
3.4	Post-processing RADARSAT-2 soil moisture maps	27
3.5	Comparison of field measurements and RADARSAT-2.....	31
4	RESULTS AND DISCUSSIONS.....	36
4.1	Field observations	36
4.1.1	General characteristics of soils	36
4.1.2	Soil moisture	42
4.2	RADARSAT-2 soil moisture maps	62
4.2.1	Coverage of RADARSAT-2 soil moisture maps obtained with Oh model. .	62
4.2.2	Coverage of RADARSAT-2 soil moisture maps with asymmetric volumetric correction	68
4.2.3	Soil moisture values obtained through RADARSAT-2.....	73
4.3	Comparison and analysis of soil moisture field measurements and RADARSAT-2 soil moisture maps	78
4.3.1	Correlation between soil moisture values from field and RADARSAT- 2 soil moisture maps.	79
4.3.2	Correlation between soil moisture values from field and RADARSAT- 2 maps with asymmetric volumetric correction.....	90
5	CONCLUSIONS.....	100
6	REFERENCES	104

List of Tables

Table 1: Surface characteristics of sampling sites	8
Table 2: Characteristics of RADARSAT-2 images during the study time. This is part of the routine left and right looking capability (Morena et al, 2004). During the ascending orbit, made during afternoon hours in the study area, the image was taken using right looking orientation; whereas during the descending orbit in the morning it was used the left looking orientation. The fact that the satellite overpasses the study area under ascending and descending orbits, allows a more frequent monitoring and measurement of the soil moisture.....	18
Table 3: Collection dates in coincidence with RADARSAT-2 in five study sites	21
Table 4: Soil horizons characteristics in Alpha, Beta, Creosote, Nichole and Tripp sites. A: Mineral horizon formed at surface, has high pedogenesis; B: Subsurface mineral horizon, accumulation of clays, iron minerals, etc; C: Mineral horizon with little pedogenesis; v: vesicular; k: carbonate accumulation; w: weak accumulation of materials; h: humus/organic matter accumulation; g: strong gleyed.	39
Table 5: Bulk densities in study area. First and second columns show the mean of the bulk density values (ρ_b) for the 8 points sampled at each site, at depths 0-5 and 5-10 cm, respectively. The third column shows the mean of the bulk density values (ρ_b) of the soil horizons identified at each soil pit in each site.....	40
Table 6: Percentage of coverage of each site per day in RADARSAT-2 maps	65
Table 7. Percentage of coverage of each site per day in RADARSAT-2 maps with asymmetric volumetric correction.	72
Table 8. Comparison of the percent coverage between the first version of the soil moisture maps (1) and the RADARSAT-2 maps with asymmetric correction (2)...	77
Table 9. Statistical parameters calculated between mean VWC % from RADARSAT-2 maps and mean VWC % of 5 sites.....	84
Table 10: Statistical parameters calculated between mean VWC % from corrected RADARSAT-2 maps and mean field VWC % of 5 sites	94

List of Figures

Figure 1. Location of five sampling sites in study area.	7
Figure 2. Precipitation during study period 2008	9
Figure 3. Temperature during study period 2008	10
Figure 4. Geologic Map of study area. The study area is covered by young Cenozoic geologic units. Qsg: sand and gravel (Holocene); Qal: alluvium (Holocene); Qf: Mud and sand (Holocene); Qae: Eolian deposits; Qpy: younger piedmont alluvium (upper Pleistocene); Qpo: older piedmont alluvium (middle to lower Pleistocene); Qtsa: axial-river facies (Sierra Ladrones formation, SantaFe group); Qtst: transitional axial-piedmont facies (Sierra Ladrones formation, SantaFe group). Source: Cather and Colpitts, 2005.	12
Figure 5. Soils map of study area. 621: Arizo-Riverwash complex; 635: Wink- Pajarito Complex; 60: Typic Ustifluent; 26: Popotosa clay loam. Other references can be obtained at USDA, 1988.	15
Figure 6. Diagram of collection points into a study site.	22
Figure 7. : Extraction of pixels covering each collection site. Pixels vary from red (dry conditions 4% VWC) to blue (wet conditions 28% VWC).	28
Figure 8. Dimensions of each area extracted from RADARSAT-2 soil moisture maps. Pixels vary from red (dry conditions 4% VWC) to blue (wet conditions 28% VWC).	29
Figure 9. Extraction of pixels covering an area of 10x10 m around each point. Pixels vary from red (dry conditions 4% VWC) to blue (wet conditions 28% VWC). The area around the sampling point may be covered by 4 or 6 pixels.	30
Figure 10. Comparison between mean VWC % from RADARSAT-2 maps and mean VWC % of the entire site at each site	33
Figure 11. Comparison between VWC % from RADARSAT-2 maps and VWC % of each sampling point at each site.....	34
Figure 12. Comparison between mean VWC % from RADARSAT-2 maps and mean VWC % of the five sampling sites at each day.....	35
Figure 13. Soil particle size classification for the five sampling sites.....	41
Figure 14. Distribution of GWC in the 5 sites at: a) June 12; b) June 14. For June 14 there was sampling just Creosote site.	45
Figure 15. Distribution of GWC in the 5 sites at: a) July 08; b) August 01	46
Figure 16. Distribution of GWC in the 5 sites at: a) August 23; b) August 25	47
Figure 17 Distribution of GWC in the 5 sites at: a) September 16; b) September 18	48
Figure 18. Distribution of GWC in the 5 sites at a) October 10; b) October 10.....	49
Figure 19. Distribution of VWC in the 5 sites at: a) June 12; b) June 14.....	50
Figure 20. Distribution of VWC in the 5 sites at: a) July 08; b) August 01	51
Figure 21. Distribution of VWC in the 5 sites at: a) August 23; b) August 25	52
Figure 22 Distribution of VWC in the 5 sites at: a) September 16; b) September 18	53
Figure 23. Distribution of VWC in the 5 sites at a) October 10; b) October 12.....	54

Figure 24. Precipitation events and VWC % field measurements for Alpha site.....	55
Figure 25. Precipitation events and VWC % field measurements for Beta site	56
Figure 26. Precipitation events and VWC % field measurements for Creosote site	57
Figure 27. Precipitation events and VWC % field measurements for Nichole site.....	58
Figure 28. Precipitation events and VWC % field measurements for Tripp site.....	59
Figure 29. Comparison of VWC (%) between moist and dry conditions...continue.	60
Figure 30. Comparison dates with different moisture conditions. Soil moisture VWC ranges from 4% (red) to 28% (blue). During extremely wet (July 08) or extremely dry (September 18) conditions, the percent coverage is less than during days with moderate moisture conditions (October 10 or August 01).....	64
Figure 31. Comparison dates with different moisture conditions in RADARSAT-2 soil moisture maps with asymmetric volumetric correction. Soil moisture VWC ranges from 4% (red) to 28% (blue).....	71
Figure 32. Mean of VWC % from RADARSAT-2 maps, in the 5 sites at the 10 study dates. Days: 1:June 12; 2: June 14; 3: July 08; 4: August 01; 5: August 23; 6: August 25; 7: September 16; 8: September 18; 9: October 10; 10: October 12.	75
Figure 33. Mean of VWC % from RADARSAT-2 maps with asymmetric volumetric correction, in the 5 sites at the 10 study dates. Days: 1:June 12; 2: June 14; 3: July 08; 4: August 01; 5: August 23; 6: August 25; 7: September 16; 8: September 18; 9: October 10; 10: October 12.....	76
Figure 34. VWC % RADARSAT-2 maps vs. VWC% field values Alpha site	85
Figure 35. VWC % RADARSAT-2 maps vs. VWC% field values Beta site	86
Figure 36. VWC % RADARSAT-2 maps vs. VWC% field values Creosote site.....	87
Figure 37. VWC % RADARSAT-2 maps vs. VWC% field values Nichole site	88
Figure 38. VWC % RADARSAT-2 maps vs. VWC% field values Tripp site.....	89
Figure 39. VWC % corrected RADARSAT-2 maps vs. VWC% field values Alpha site	95
Figure 40. VWC % corrected RADARSAT-2 maps vs. VWC% field values Beta site..	96
Figure 41. VWC % corrected RADARSAT-2 maps vs. VWC% field values Creosote site	97
Figure 42. VWC % corrected RADARSAT-2 maps vs. VWC% field values Nichole site	98
Figure 43. VWC % corrected RADARSAT-2 maps vs. VWC% field values Tripp site	99

LIST OF ACRONYMS

- M_v**: Volumetric water content ($\text{cm}^3 / \text{cm}^3$)
- ρ_b** : Soil bulk density (gr / cm^3)
- VWC**: Volumetric Water Content (%)
- GWC**: Gravimetric Water Content (%)
- σ_{hh}** : Backscatter coefficient horizontal-horizontal
- σ_{vv}** : Backscatter coefficient vertical-vertical
- σ_{hv}** : Backscatter coefficient horizontal-vertical
- σ_{vh}** : Backscatter coefficient vertical-horizontal
- p**: Co-polarized ratio ($\sigma_{hh} / \sigma_{vv}$)
- q**: Cross- polarized ratio ($\sigma_{vh} / \sigma_{vv}$)
- θ** : Incident angle of radar signal
- κ** : Wavelength
- s**: Root mean square (RMS) height.

This thesis is accepted on behalf of the Faculty of the Institute by the following committee:

Dr. Jan Hendrickx

Dr. Bruce Harrison

Dr. Brian Borchers

Date

I release this document to the New Mexico Institute of Mining and Technology.

Student's signature

Date

1 INTRODUCTION

Soil moisture is an important parameter in energy, hydrology and ecological processes. In energy processes, soil water content determines the partitioning of net radiation into soil, sensible and latent heat fluxes. In hydrology, soil moisture controls the infiltration rate of precipitation into the soil, and the subsequent generation of runoff (Findell and Eltahir, 1997; Grayson et al., 1997); rainfall intensity and soil characteristics also play an important role in these processes. Finally, water content governs the atmosphere-water-vegetation interaction in ecological processes (Ma et al., 2004). Given its large influence on ecosystem processes, estimation of soil moisture has become a priority in many areas of land use including agriculture, cartography, disaster management, and hydrology.

There are several techniques for measuring soil water content in-situ (Jury and Horton, 2004). The most common manual technique is the gravimetric method, in which the soil sample is oven dried until it reaches a constant weight. Then, the water content related to the weigh loss of the sample is calculated. However, this technique requires much time, personnel and money; furthermore, it disturbs the soil. There are automated methods that can measure soil moisture efficiently, such as tensiometry, electromagnetism, soil dielectric constant, and nuclear techniques. (Walker et al., 2004; Schmutge et al., 1980). These techniques collect the information efficiently, requiring less man power and time than the gravimetric method. However, some of these methods are more expensive, require calibration for each type of soil, and/ or are highly sensitive

to non-ideal conditions of the sampling area (i.e. climate, light movements of the sensor). Furthermore, the field measurements are not always representative of the actual amount of water in the soil, because this varies spatially and temporally at watershed (>10 ha), field (1-10 ha) and site (<1 ha) scales (Thoma et al., 2008). Consequently, this generates an up-scaling problem, because the value estimated at a point will not always represent the soil moisture of the area around that spot. The variability results mainly from factors such as changes in vegetation coverage, micro-topography, and soil texture (Cantón et al., 2004; English et al., 2005; Zhu and Shao, 2008).

Remote sensing has the potential to estimate surface soil moisture at different scales and with high temporal and spatial accuracy (Hall et al., 1995; Schneider et al., 2008). Optical remote sensors, like Landsat and SPOT, detect the electromagnetic radiation that comes from the sun and is reflected from the Earth's surface (Campbell, 2007). However, optical remote sensors cannot operate under all atmospheric conditions and sometimes the temporal resolution is not as high as with radar sensors (Heilman et al., 1977; Li et al., 2008).

In contrast to optical sensors, radar sensors can operate under all atmospheric conditions, improving the potential for surface soil moisture estimation (Engman and Chauhan, 1995; Lakhankar et al., 2009; D'Urso and Minacapilli, 2006). Several studies have shown the potential for estimating surface soil moisture by using different radar sensors, like GPR systems (Huisman et al., 2001; Lun et al., 2005), passive microwave (Mohanty and Skaggs, 2001; Schmugge, 1998), ENVISAR (Baup et al., 2007), ERS 1 and 2 (Blumberg and Freilikher, 2001; Quesney et al., 2000), RADARSAT-1 (Baghdadi

et al., 2007; Sahebi et al., 2003; Jackson, and Wood, 2001). However, several studies (e.g. Alvarez-Mozos et al., 2009; Baghdadi et al., 2007; Loew, 2008; Moran et al., 2000) have shown that the radar signal is highly influenced by surface roughness, vegetation type and heterogeneity, and soil texture. Consequently, surface soil moisture estimation is not straightforward, either at watershed or field scale (Thoma et al., 2008).

In order to obtain accurate soil moisture values from radar images, several theoretical, empirical and semi-empirical models have been developed. The most common methods are the Integral Equation Model (IEM) (Fung et al., 1992), the Oh Model (OM) (Oh et al., 2002; Oh, 2004), and the Dubuois Model (DM) (Dubois et al., 1995). These and other models have been improved (e.g. Wang et al., 2004; Zhang et al., 2009), by taking into account parameters that were not initially considered, such as vegetation and surface roughness. In addition, some models have been improved and developed specifically for each radar sensor, such as ENVISAT/ASAR (M. Zribi et al., 2005), ERS 1 and 2 (Blumberg and Freilikher, 2001), and RADARSAT-1 (Baghdadi and Zribi, 2006; Sahebi and Angles, 2009). Furthermore, a combination of passive and active sensors have been used (e.g. Moran et al, 1997; Pierdicca et al., 2010; Sanli et al., 2007), to obtain more accurate soil moisture maps, using the best features of each type of sensor.

Despite significant research, many factors still influence the accurate estimation of soil moisture. RADARSAT-2, a new Synthetic Aperture Radar (SAR) sensor, has been developed with several technological improvements, such as quad-polarization and multiple angular approaches. A description of this satellite is summarized in section 2 of this thesis and is explained in detailed by Ali et al., (2004); Fox et al., (2004); Morena et

al., (2004). The enhanced features of RADARSAT-2 have been described as the necessary tools for estimating soil water content without the influence of surface factors (i.e. Sahebi and Angles, 2009; Ulaby et al., 1996; Van der Sanden, 2004; Verhoest et al., 2008). RADARSAT-2 derived soil moisture maps have not yet been validated.

The main objective of this research is to validate the RADARSAT-2 soil moisture maps, by correlation with field Gravimetric Water Content (GWC) and Volumetric Water Content (VWC) measurements. In general, previous validation studies of active sensors for estimating soil moisture have been carried out in areas with ideal conditions (bare, flat surfaces) for the backscatter of the radar signal (i.e. Leconte and Brissette, 2004; Wickel and Jackson, 1999). The present study has been performed in areas with both ideal and non-ideal (rough, vegetated) surface conditions in Socorro, New Mexico (USA). The distribution of soil moisture in semiarid environments such as New Mexico is mainly governed by topographic features, soil texture, vegetation density, and the distribution of rainfall (Kears, 1998; NMBMMR 1981). This study will evaluate the factors which influence the backscatter of the radar signal, and consequently the estimation of surface soil moisture.

The radar signal is thought to penetrate less than 10 cm into the soil profile (Schmugge, 1998; Lakhankar et al., 2009). However by comparing field water content values at one cm increments for the top 10 cm of the soil, the effective depth of penetration of the radar signal could be determined. By understanding the behaviour of soil moisture under ideal and non ideal surface conditions and its response to the radar signal, the acquisition and processing of the soil moisture maps can be improved.

2 STUDY AREA

2.1 Study site

The research was performed in the Rio Grande Valley on the Hilton Ranch, located in Socorro County, New Mexico, USA (Figure 1). This region is characterized by a heterogeneous distribution of landforms; common landforms include alluvial fans, terraces, and flood plains. Vegetation consists of species of semiarid communities including, creosote, mesquite, grasses and juniper, as well as species of riparian areas, such as salt cedar and cottonwood (close to the Rio Grande) (e.g. Alkov, 2008; Engle, 2009.)

Five sites with different surface characteristics were chosen for the validation of RADARSAT-2 derived soil moisture maps. These sites are named Alpha, Beta, Creosote, Nichole, and Tripp. Figure 1 shows the location and Table 1 lists the characteristics of each site. By choosing these sites, the validation can be performed in areas with ideal (bare, flat) and non- ideal (heterogeneous vegetation, rough surface) conditions for radar signal acquisition.

According to historic records from 1914 through 2005 from the Western Regional Climate Center (WRCC <http://www.wrcc.dri.edu>), the average monthly maximum temperature is 34 °C in July, whereas the average minimum monthly average is -5 °C in January. Annual average precipitation is 240 mm, which occurs mainly in July and August. March and April are the driest months of the year. For 2008, when the present study was performed, the conditions of precipitation and temperature follow the historic

trend described above (<http://www.wrcc.dri.edu>). The highest daily precipitation occurred during the summer months, between May and August, with a maximum of 25 mm/day, on August 16 (Figure 2). August had the highest monthly precipitation (63 mm/month) and the larger number of rain days (13 days) (Figure 2), as observed in Figure 2. March and April had no precipitation during the entire time of this study (2008). Temperatures were also the highest during summer months (Figure 3), with an average daily maximum of 31 C, and a maximum monthly average temperature 26.3 C during June, when no precipitation was reported in the study area. The coldest months were December and January.

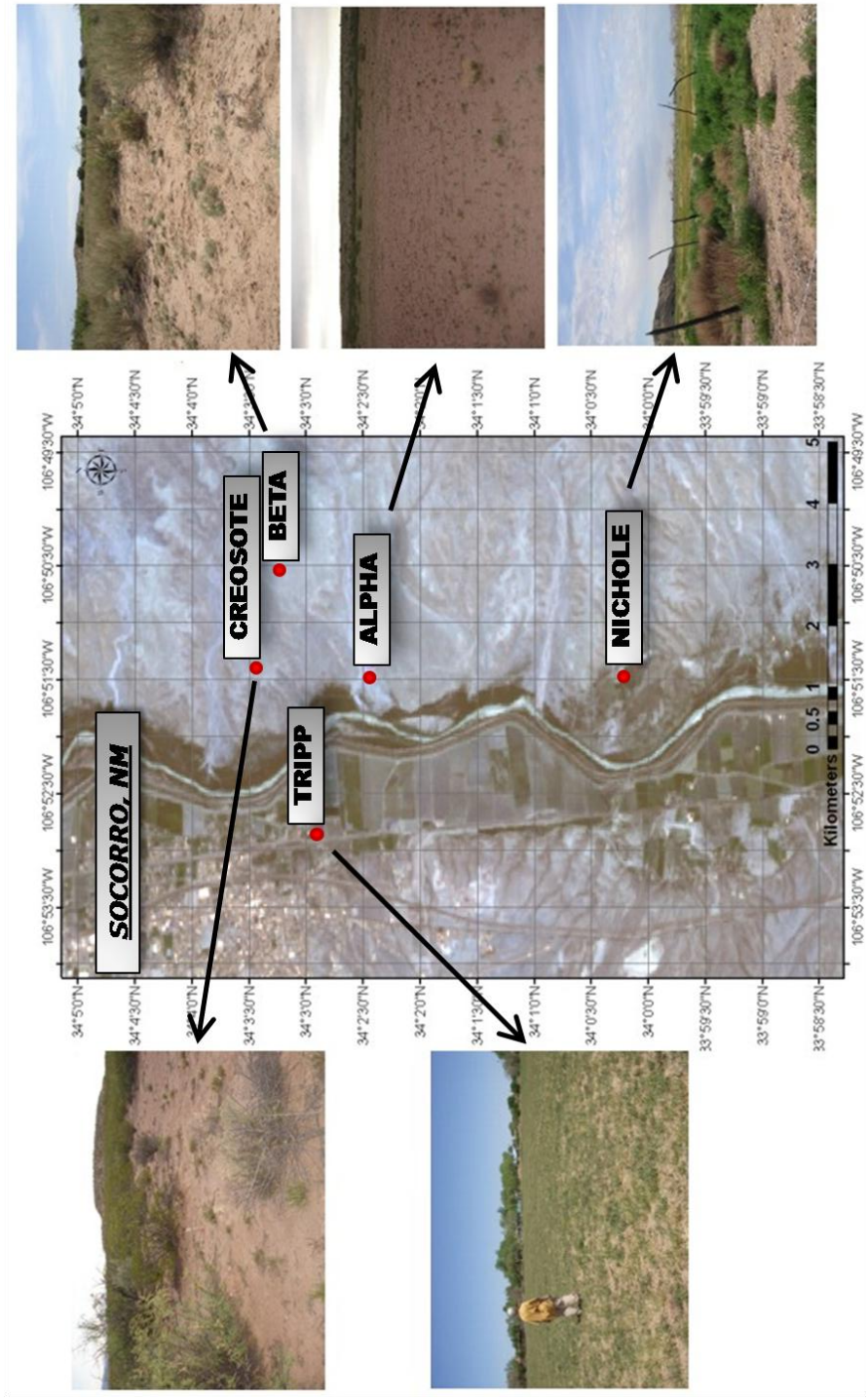


Figure 1. Location of five sampling sites in study area.

Site	Surface roughness	Vegetation cover
Alpha	Flat	Bare
Beta	Undulated	Heterogeneous vegetation with salt bushes, mesquite, Juniper.
Creosote	Undulated	Creosote bushes and mesquite
Nichole	Flat	Heterogeneous vegetation with tamarisk, cottonwood, willows, mesquite, grasses.
Tripp	Flat	Irrigated pasture

Table 1: Surface characteristics of sampling sites

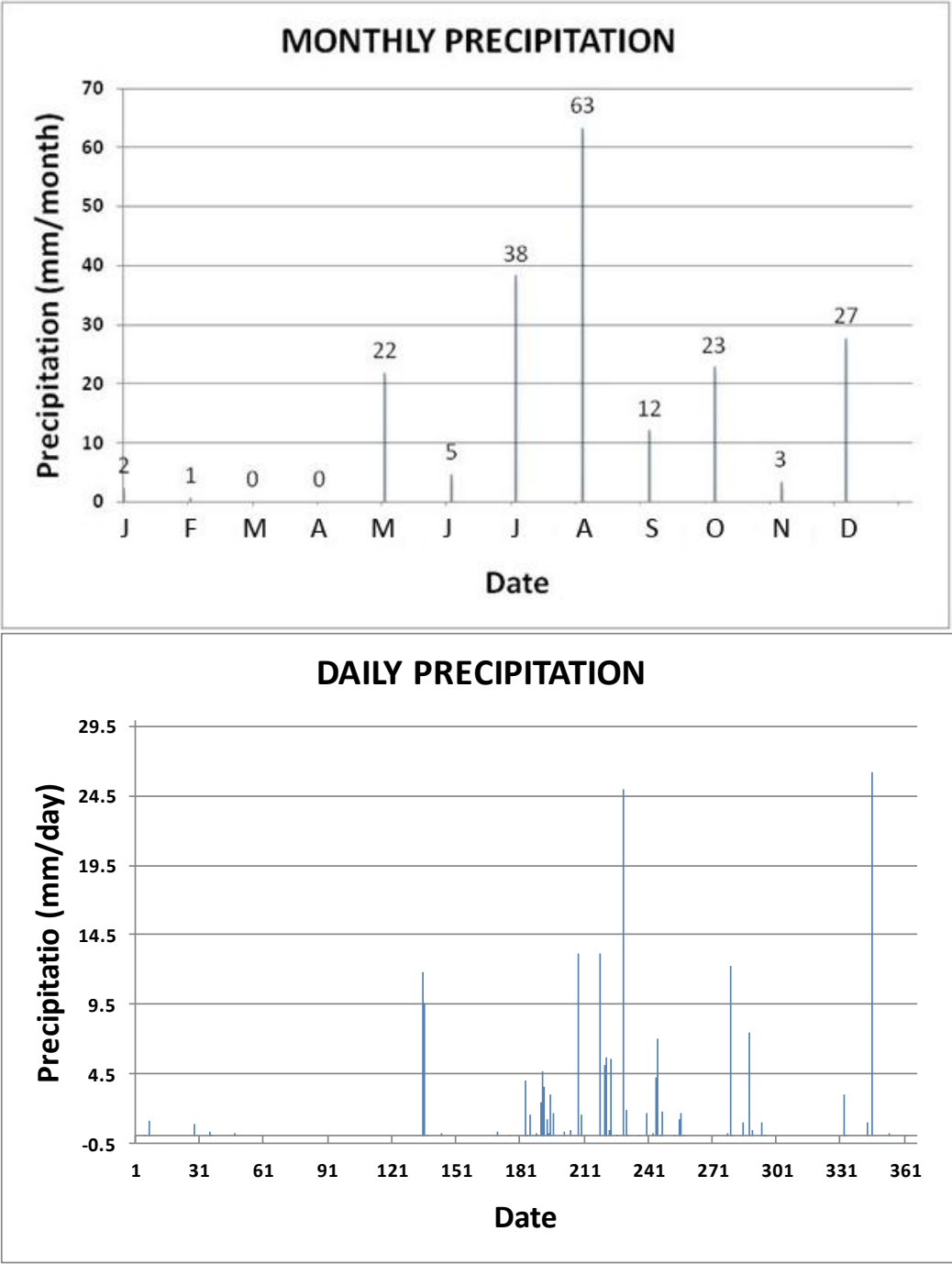


Figure 2. Precipitation during study period 2008

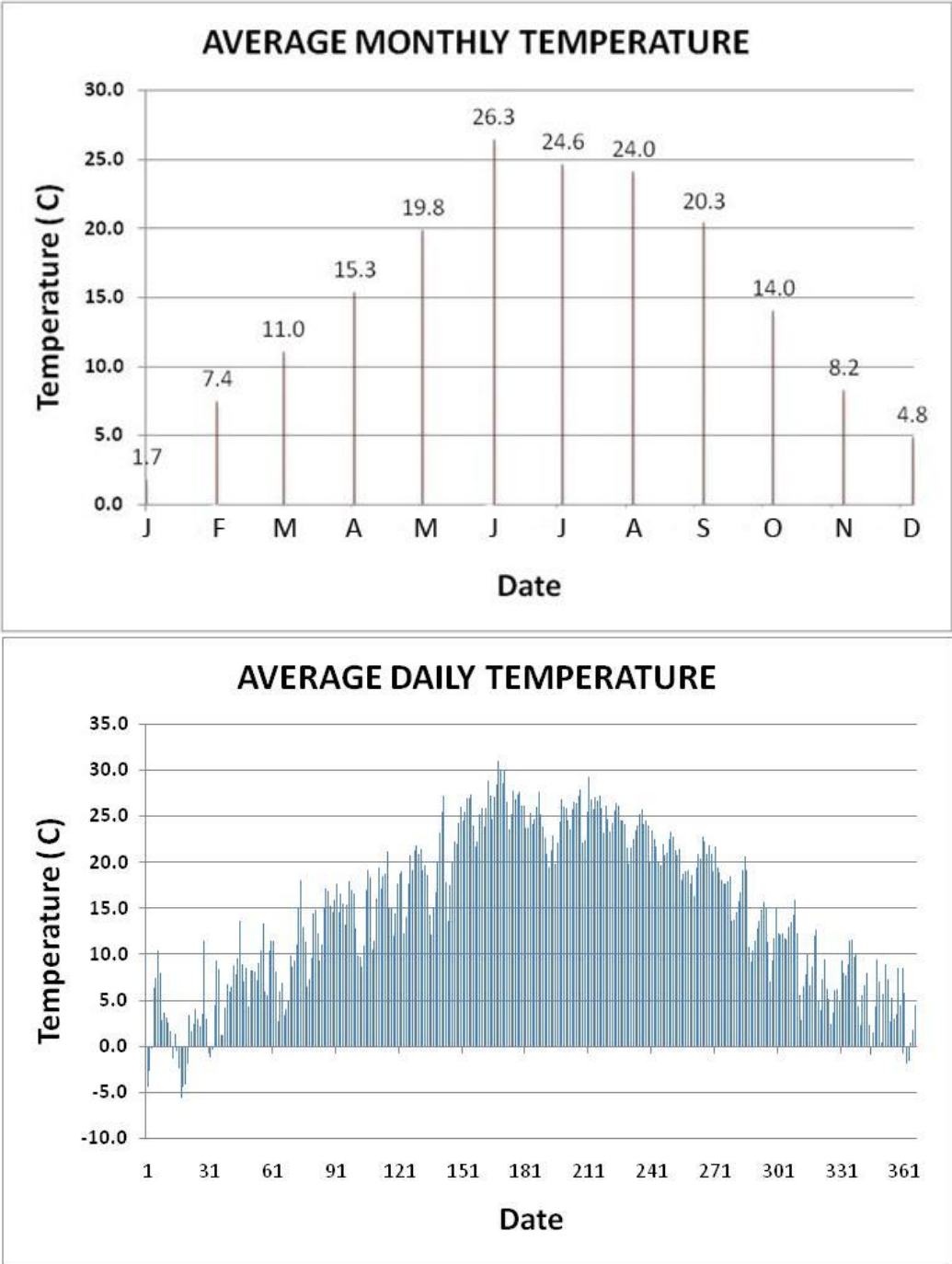


Figure 3. Temperature during study period 2008

2.1.1 Geology

The five sampling sites are located on a combination of Quaternary alluvial deposits from the Rio Grande and fan gravels from eastern uplands overlain in some cases by eolian sands (Figure 4) and described by Cather and Colpitts (2005.) The Alpha site is located on Holocene Quaternary sand and gravel deposits (Qsg), which are located in the Rio Grande valley and active arroyos. The Beta and Creosote sites are placed on the unit Qae, which is composed of eolian sand and loessic silt deposits, from the upper Pleistocene to Holocene. The Nichole and Tripp sites are located on Holocene (Qf) mud and sand deposits from the floodplain of the Rio Grande.

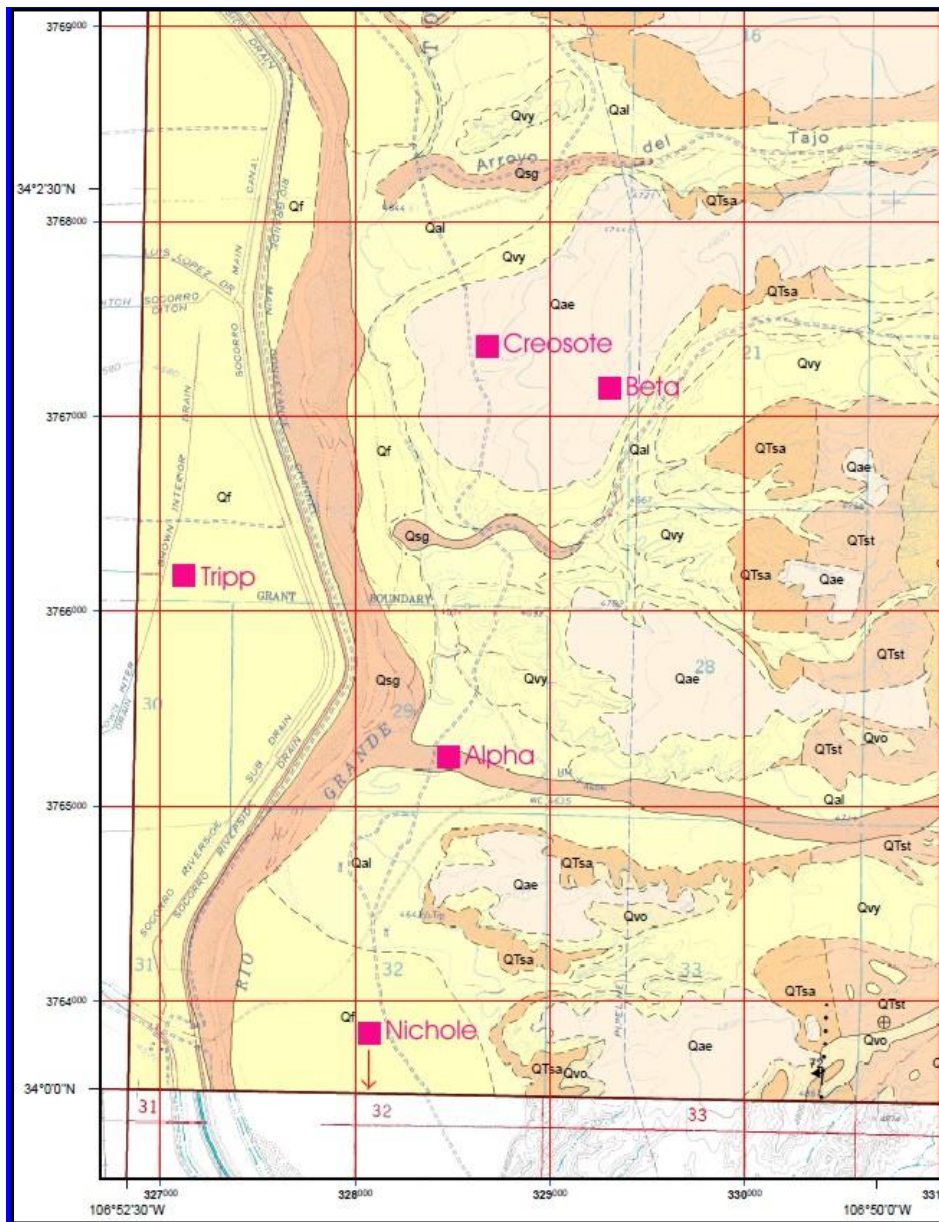


Figure 4. Geologic Map of study area. The study area is covered by young Cenozoic geologic units. *Qsg*: sand and gravel (Holocene); *Qal*: alluvium (Holocene); *Qf*: Mud and sand (Holocene); *Qae*: Eolian deposits; *Qpy*: younger piedmont alluvium (upper Pleistocene); *Qpo*: older piedmont alluvium (middle to lower Pleistocene); *Qtsa*: axial-river facies (Sierra Ladrones formation, SantaFe group); *Qtst*: transitional axial-piedmont facies (Sierra Ladrones formation, SantaFe group). Source: Cather and Colpitts, 2005.

2.1.2 Soils

The validation sites are located on deep to shallow soils on flood plains, bajadas, cuestas and fan terraces, according to the Soil Survey of Socorro County Area, New Mexico (1988). Figure 5 shows the spatial distribution of the soil units that correspond to the collection sites.

The Alpha site is located in the Arizo-Riverwash complex soil unit, which contains deep and well-drained soils that have accumulated in alluvial deposits. The Arizo soil is characterized by gravelly sandy loam in the upper 5 cm of the soil profile; the next 10 cm are composed of gravelly loamy coarse sand. The Riverwash soil unit consists of coarser soils, such as loose sand, pebbles, cobbles. The Beta and Creosote sites are placed on the Wink- Pajarito Complex soil unit, which is characterized by deep and well drained soils, formed on alluvial and eolian deposits, such as hummocky, sand-mantle plains, bajadas and sand terraces. The Wink soil is formed by fine sand in the upper 5 cm of the profile, underlain by 20 cm of sandy loam. The Pajarito unit is composed of loamy fine sand in the upper 5 cm and sandy loam in the next 15 cm.

The Nichole site is on a Typic Ustifluent soil unit, characterized by deep soils, where drainage varies from poor to good and is located in flood plains. Usually these soils are composed of fine sand in the upper 5 cm and are underlain by clay and silty clay loam in the next 15 cm; having at depth stratified layers of sand, loam and fine sandy loam. The Tripp site is located in the Popotosa clay loam soil unit, which is composed of deep and well drained soils that were formed on recent alluvial deposits (USDA, 1988).

This soil unit is composed of clay loam in the upper 30 cm, with loam and clay loam in the underlying 45 cm.

Geomorphic processes influence the formation of soils in the study sites, e.g. there are coarse textured soils with weak development on eolian deposits that overlying older alluvial deposits at Alpha, Beta and Creosote sites. These older alluvial deposits have stronger soil development. These characteristics influence several variables relevant for this study, such as soil water content, surface roughness, soil micro-topography and soil structure.

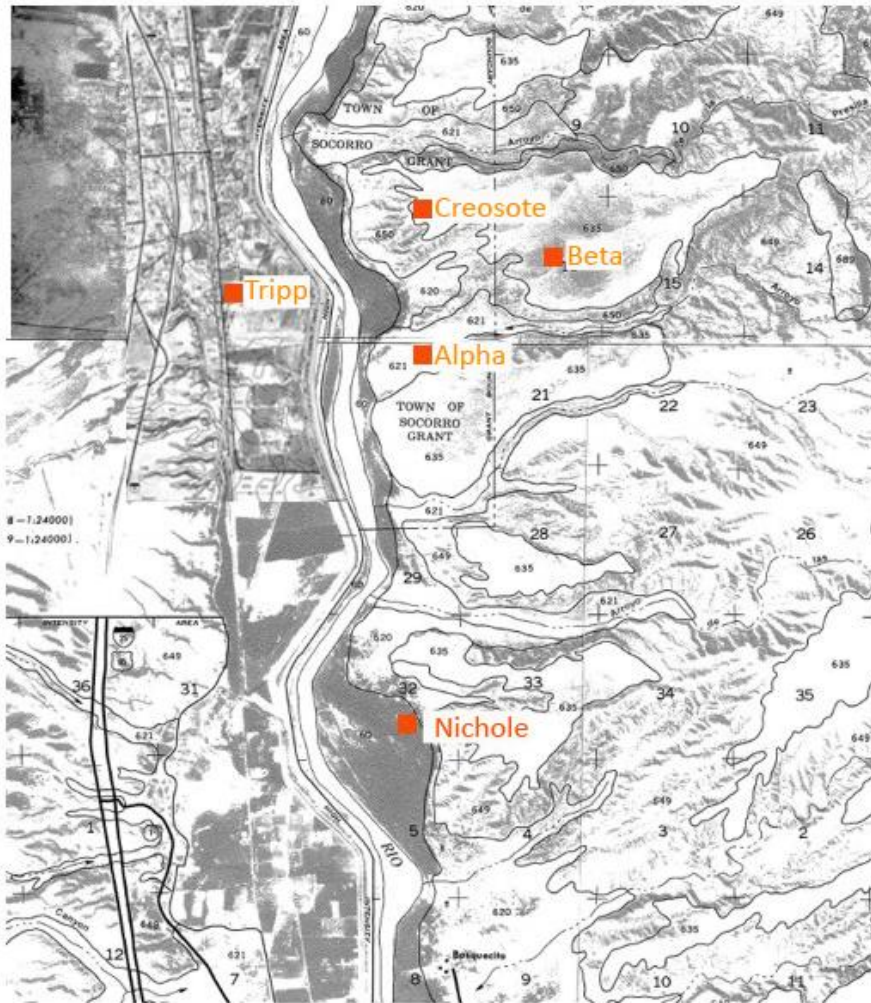


Figure 5. Soils map of study area. 621: Arizo-Riverwash complex; 635: Wink- Pajarito Complex; 60: Typic Ustifluent; 26: Popotosa clay loam. Other references can be obtained at USDA, 1988.

3 METHODS AND MATERIALS

3.1 Estimation of soil moisture data from RADARSAT-2 signal acquisition

RADARSAT-2 is an active radar sensor launched in December 2007. For acquiring data, it uses polarization in the C-band (5.3 GHz), which interacts with the surface depending on the dielectric properties of the soils and other characteristics, such as roughness, and vegetation coverage. Furthermore, the satellite has an enhanced characteristic called quad-polarization, which allows the combination of the different polarization channels, horizontal and vertical. This feature improves the measurement of several variables of the surface, including soil moisture.

Field sampling procedures were performed during hours when the RADARSAT-2 sensor was passing over the study area, in order to have representative data for comparing and correlating soil moisture values. Table 2 summarizes the acquisition days that were used in the present study and the characteristics of each image.

The estimation of soil moisture values by the radar sensor depends on the dielectric properties of the surface and its interaction with the radar signal emitted by the satellite. The dielectric constant of materials increases as soil moisture increases. Moreover, surface roughness and soil moisture content control the radar signal backscatter and therefore, the estimation of soil water content (Campbell, 2007; Sabins, 1978).

Because of the influence of these factors, several models have been developed in order to obtain the most accurate estimation of soil moisture, as described in chapter 1. The RADARSAT-2 soil moisture maps validated in this study were produced by the

MDA Company, using the Oh (2004) semiempirical model. This method is based on the estimation of the volumetric soil moisture M_v from dielectric coefficients (Oh, 2004). It uses the following parameters: 1) the incident angle of the radar signal θ , 2) the backscatter coefficients σ_{vv} (vertical-vertical), σ_{hh} (horizontal –horizontal), σ_{vh} (vertical–horizontal) and σ_{hv} (horizontal –vertical), and, 3) the surface roughness parameters κs , where κ is the wavelength and s is the root mean square (rms) height. In brief, the model uses these parameters for solving iteratively the unknowns M_v and s through the equations 1 and 2, using a root-finding numerical technique.

$$1 - \left(\frac{\theta}{90}\right)^{0.35} M_v^{-0.65} e^{-0.4} [ks(\theta, M_v, \sigma_{vh})]^{1.4} - \frac{\sigma_{hh}}{\sigma_{vv}} = 0 \quad (1)$$

$$ks(\theta, M_v, \sigma_{vh}) = \left[-3.125 \ln \left\{ 1 - \frac{\sigma_{vh}}{0.11 M_v^{0.7} (\cos \theta)^{2.2}} \right\} \right]^{0.556} \quad (2)$$

The Oh model (2004) was derived from the Oh model (2002), which uses 3 equations for solving M_v and s . These equations are solved for the backscatter coefficient σ_{vv} and σ_{hh} , by calculation of: 1) the cross-polarized vertical-horizontal coefficient σ_{vh} , 2) the co-polarized ratio $p \left(\frac{\sigma_{hh}^o}{\sigma_{vv}^o} \right)$, which express the relation between the co- polarized coefficients (horizontal-horizontal and vertical- vertical) and 3) the cross-polarized ratio $q \left(\frac{\sigma_{vh}^o}{\sigma_{vv}^o} \right)$, which express the relation between the cross- polarized coefficient vertical-horizontal and the co-polarized coefficient vertical- vertical. The calculations are made using the equations 3, 4 and 5, respectively.

Day (2008)	Orbit	Local time over-passing study area
June 12	Ascending	7 p.m.
June 14	Descending	7 a.m.
July 08	Descending	7 a.m.
August 01	Descending	7 a.m.
August 23	Ascending	7 p.m.
August 25	Descending	7 a.m.
September 16	Ascending	7 p.m.
September 18	Descending	7 a.m.
October 10	Ascending	7 p.m.
October 12	Descending	7 a.m.

Table 2: Characteristics of RADARSAT-2 images during the study time. This is part of the routine left and right looking capability (Morena et al, 2004). During the ascending orbit, made during afternoon hours in the study area, the image was taken using right looking orientation; whereas during the descending orbit in the morning it was used the left looking orientation. The fact that the satellite overpasses the study area under ascending and descending orbits, allows a more frequent monitoring and measurement of the soil moisture.

$$\sigma_{vh} = 0.11Mv^{0.7} (\cos \theta)^{2.2} [1 - \exp(-0.32 (ks)^{1.8})] \quad (3)$$

$$p = \frac{\sigma_{hh}^o}{\sigma_{vv}^o} = 1 - \left(\frac{2\theta}{\pi}\right)^{0.35} Mv^{-0.65} e^{-0.4(ks)^{1.4}} \quad (4)$$

$$q = \frac{\sigma_{vh}^o}{\sigma_{vv}^o} = 0.095 (0.13 + \sin 1.5 \theta)^{1.4} [1 - \exp(-1.3 (ks)^{0.9})] \quad (5)$$

The model can only be applied if the following conditions are met: $\sigma_{vh}^o < -9.6$ dB, $p < 1$, and $q < 0.11$. The model is only valid within the ranges $0.04 < M_v < 0.29$ and $0.13 < ks < 6.98$. According to Oh (2004), the parameter p is influenced by very dry conditions in the soil and very rough surfaces, therefore the data obtained under those conditions cannot be selected for applying the inversion model. The cross polarized ratio q is also highly sensitive to the roughness parameter ks . The incident angle θ is a factor that can control the effectiveness of the model. Oh (2004) states that the inverse method gives the best results if: $ks < 3.5$ and $M_v > [6.286 / \ln(\theta/90)]^{-1.538}$.

A second version of the RADARSAT-2 soil moisture maps was obtained by adding a volume correction to the Oh model (2004). The correction was proposed by Yamaguchi, et al. (2005) to approach cases of non-reflection symmetric scattering for decomposing the SAR images. The authors used a four-components scattering model, adding a helix scattering to the other three standard components: surface, double bounce and volumetric scattering. This helix component corresponds to the relation between co-polarized and cross-polarized backscatter coefficient asymmetry, it means $[S_{HH}S_{HV}^*] \neq 0$ and $[S_{VV}S_{HV}^*] \neq 0$. These characteristics are common in the “complicated geometric scattering structures” of urban areas.

Furthermore, Yamaguchi, et al. (2005) included asymmetric volume scattering covariance matrices in the decomposition process. The improvement of the matrix is based on the modification of the orientation angle distributions, which are originally uniform in a probability distribution function. The process approaches the asymmetric relations between S_{HH} and S_{VV} , expressing the characteristic asymmetric distribution that occurs over vegetated areas. Depending on the characteristics of the surface area, using symmetric or asymmetric approaches will allow the best fit of the data. In the specific case of this study, the asymmetric volumetric correction could allow complicated geometric scattering structures, such as the branches of bushes or trees.

3.2 Field sampling

3.2.1 Gravimetric Water Content (GWC)

Table 3 lists the dates when field gravimetric water content (GWC) values were obtained in coincidence with the RADARSAT-2 mission on the five validation sites. Approximately 6,000 GWC samples were collected during 19 days. Due to technical and logistical challenges, not all five sites were sampled on all dates.

Day	Alpha	Beta	Creosote	Nichole	Tripp
June 12	✓			✓	✓
June 14			✓		
July 08	✓			✓	✓
August 01	✓	✓	✓	✓	✓
August 23	✓	✓	✓	✓	✓
August 25	✓	✓	✓	✓	✓
September 16	✓			✓	✓
September 18	✓	✓	✓	✓	
October 10	✓	✓	✓	✓	✓
October 12	✓		✓	✓	✓
Total	9	5	7	9	8

Table 3: Collection dates in coincidence with RADARSAT-2 in five study sites

Each site consists of 16 sampling points located a 100x100 m² plot. The distance between adjacent points is 20 meters (Figure 6). Every point was sampled from 0 to 10 cm; samples were taken at one cm depth increments 0-1, 1-2, 2-3, 3-4, and 4-5 cm, plus a bulk sample from 5-10 cm. Between 200 to 400 g of soil were extracted from each depth range and placed in plastic bags.

The aim of the small depth increments was to identify the depth of penetration of the radar signal into the soil profile. Previous studies (e.g. Moran et al., 2000; Schmutge, 1998; Ulaby et al., 1996) have validated remote sensing data by sampling over depth intervals of several centimetres, usually from a bulk sample from 0-5 cm. However, the precise depth of penetration of the radar signal has not yet been defined. Consequently whether the remote sensed values from RADARSAT-2 accurately represent the ground measured values is still unknown.

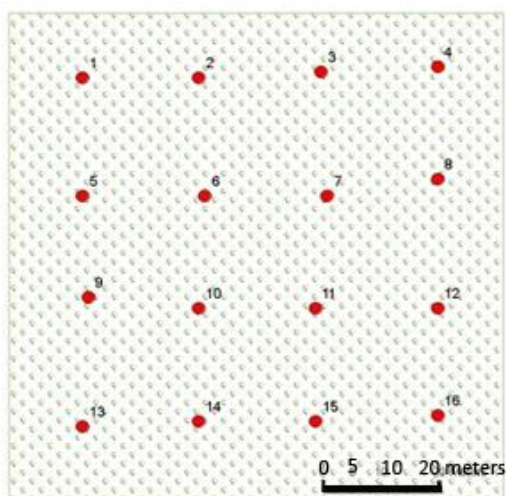


Figure 6. Diagram of collection points into a study site.

3.2.2 Soil profiles

One soil pit, with approximate dimensions 1 x 1 x 1.5 m deep, was dug near every validation site. Soil horizons were defined using the USDA-NRCS method, which uses the characterization of soil properties, such as moist and dry colour, structure, wet consistence, texture, clay films, percentage of roots and pores and carbonate content.

3.2.3 Soil bulk density

In order to convert GWC to Volumetric Water Content (VWC) values, soil bulk density sampling was carried out in each study site. Two different methods were used to measure soil bulk density values: 1) sampling with a soil ring of known volume and oven-dry samples, and 2) the bulk density-paraffin method. For the first method, samples were collected at: 1) eight points at each site at two depths: from 0 to 5 cm and 5 to 10 cm.; 2) For sampling at greater depths, metal ring samples were taken from different depths in the soil profile, corresponding to changes in soil horizonation. The sampling was performed using a metal ring of known volume value (98.17 cm^3). The volume of soil in the metal cylinder was extracted, placed in a plastic bag and sent to the lab for subsequent procedures and calculations explained in the next section. A total of 77 samples were collected and analysed. For carrying out the bulk density-paraffin method, soil peds were extracted from each soil horizon in each soil pit. A total of 35 samples were extracted and analysed using this method.

3.3 Lab procedures and calculations.

3.3.1 Gravimetric water content.

The weight of each wet soil sample was recorded. Then, the samples were dried at room temperature and oven-dried at 25-30 °C. Samples were dried until the water evaporated, indicated by no more change in weight.

Gravimetric water content (GWC) was calculated by the equation

$$GWC = \frac{(M_w - M_d)}{(M_d - M_{pb})} \quad (6)$$

where M_w is mass of wet soil, M_d is mass dry soil, and M_{pb} is mass of the plastic bag that contains the sample.

Subsequently, the GWC values of every depth were averaged over the 16 sampling points that compose each site. Therefore, six GWC mean values were calculated for each sampling date in every site.

3.3.2 Soil bulk density calculation.

Metal ring soil bulk density

A soil sample was weighed, to obtain the wet soil mass. It was then oven-dried at approximately 25-30 °C, until all the water was evaporated. Sample density was calculated using the relation between the mass of the dry soil and the volume it occupied.

$$\rho_b = \frac{M_d}{V_r} \quad (7)$$

where ρ_b is soil bulk density and V_r is the volume of soil in the metal ring.

Soil bulk density with paraffin method

An undisturbed soil ped was separated from the sample and oven dried for 24 hours at 30°C. Then, the weight of the soil clod was measured. Next, the clod was covered with paraffin, suspended in water and weighed. Finally, the paraffin was removed, and the clod was weighed in air. The clod without paraffin was sieved (2 mm) and the gravel particle size (>2mm) were removed and weighed (Blake 1965, modified by Singer 1986).

The soil bulk density ρ_b was calculated through the relation

$$\rho_b = \frac{[(PW \text{ in air}) - (PW \text{ in water})]}{\left[\left(W\left(\frac{1}{0.9}\right)\right) - (G \ 2.65)\right]} \quad (8)$$

where PW is the weight of the ped plus the paraffin, W is the weight of the paraffin, and G is the weight of the particles >2 mm. 0.9 is an average density value for paraffin, whereas 2.65 gr/cm³ is the density for a rock.

3.3.3 Volumetric Water Content

GWC were converted to VWC using the soil bulk density values obtained through the lab procedures described in section 3.3.2. The conversion is performed via the relation

$$VWC = GWC \ \rho_b \quad (9)$$

where GWC is the Gravimetric Water Content and ρ_b is soil bulk density.

3.3.4 Soil particle size

The particle size analysis (PSA) used in this research follows the standard procedures provided by Smith (1998). Initially, a representative 30 g sample was selected from each soil depth. After, it was weighed and oven-dried for 24 hours at 30°C, the sample was placed in a 125 ml erlenmeyer flask (previously weighed), and 30 ml of deionized water and 50 ml of Sodium- pyrophosphate were added. Then, the flask was weighted again and placed in a shaker for 4 hours.

The final solution was wet sieved (63 μ m) to extract the sand- sized grains, while the clay and silt particles were collected in a flask. The sand was oven dried and weighed, whereas the solution containing the clay and silt particles was decanted after settling for 7 hours and 40 minutes. Finally, 25 ml of particle sized clay was pipetted from the flask, oven dried and weighed, in order to obtain the particle- size distribution of the soil.

3.3.5 Carbonate content calculation

The calcium carbonate content of the soil samples was measured using the Chittick Apparatus method (Dreimanis, 1962; modified by Machette, 1986, and Association of Official Analytical Chemist, 1950). Initially, the samples were oven-dried and crushed until the soil particles passed a 200 mesh sieve (0.075 mm). Then, an individual sample was placed into a flask and connected to the Chittick apparatus, where 6 N of hydrochloric acid were added, in order to digest the carbonate. The process produced a certain volume of CO₂ gas that displaced a volume of air into the apparatus.

That volume represented the carbonate content in the sample, which is corrected for temperature and pressure conditions, and for the sample weight.

3.4 Post-processing RADARSAT-2 soil moisture maps

All RADARSAT-2 soil moisture maps were processed using the software ArcGIS 9.2, in order to obtain data from the validation sites of the study. First, the pixels covering the area of each validation site were extracted from every image (Figure 7). The edges of each area around the 16 sampling points were defined based on a distance of 15 meters from the most external points of each site (Figure 8). The mean, standard deviation, minimum, and maximum values of the VWC values were calculated for the pixels that cover each site. The same statistical values were calculated at a smaller scale, by extracting the pixels that covered an area of 10x10 m around each sampling point (Figure 9). Considering the VWC values of the pixels covering the area around the 16 sampling points and VWC of the pixels covering the area around each point, the accuracy and correlation of the RADARSAT-2 maps and field measurements can be determined at two scales: plot and point scale.

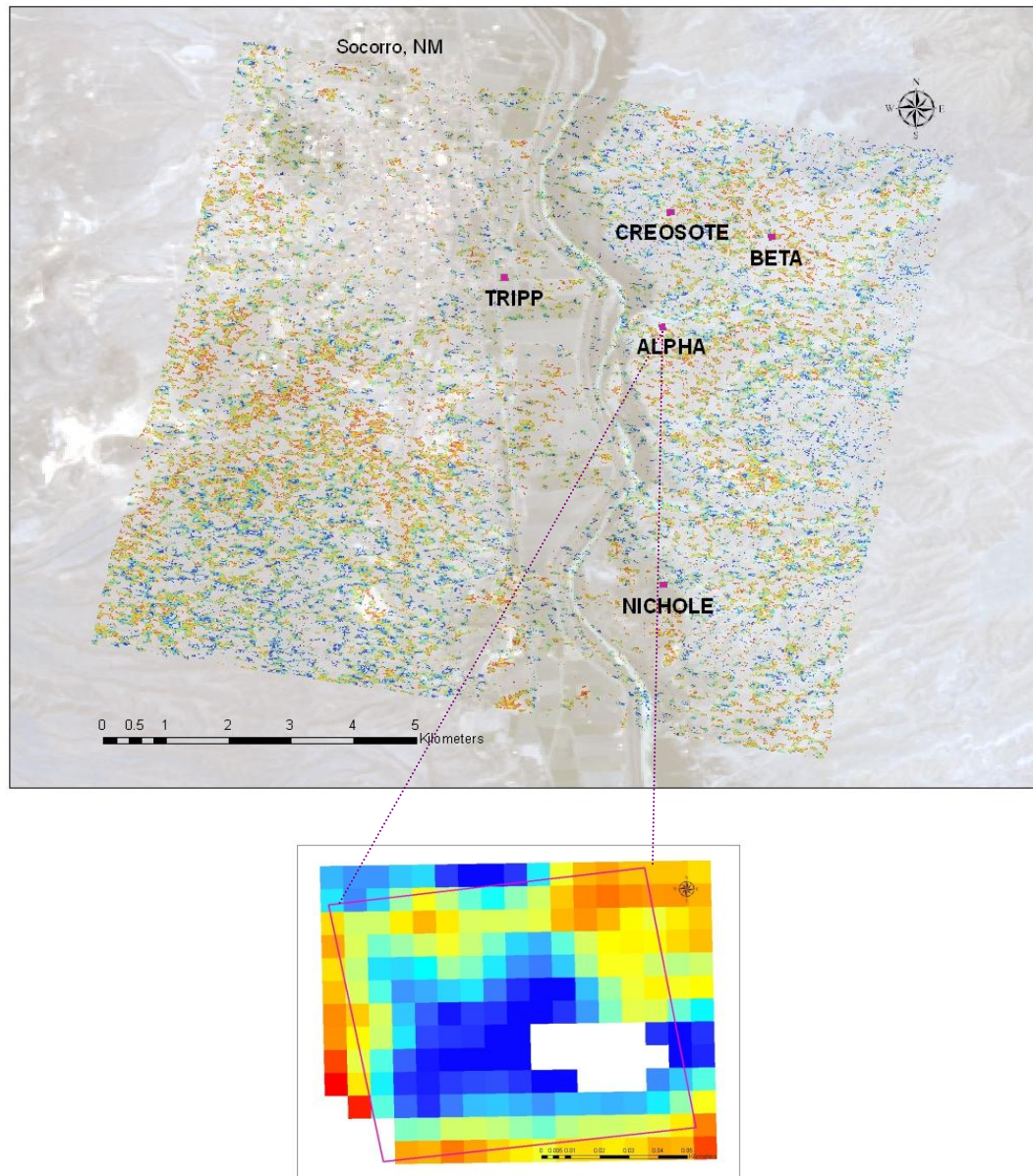


Figure 7. : Extraction of pixels covering each collection site. Pixels vary from red (dry conditions 4% VWC) to blue (wet conditions 28% VWC).

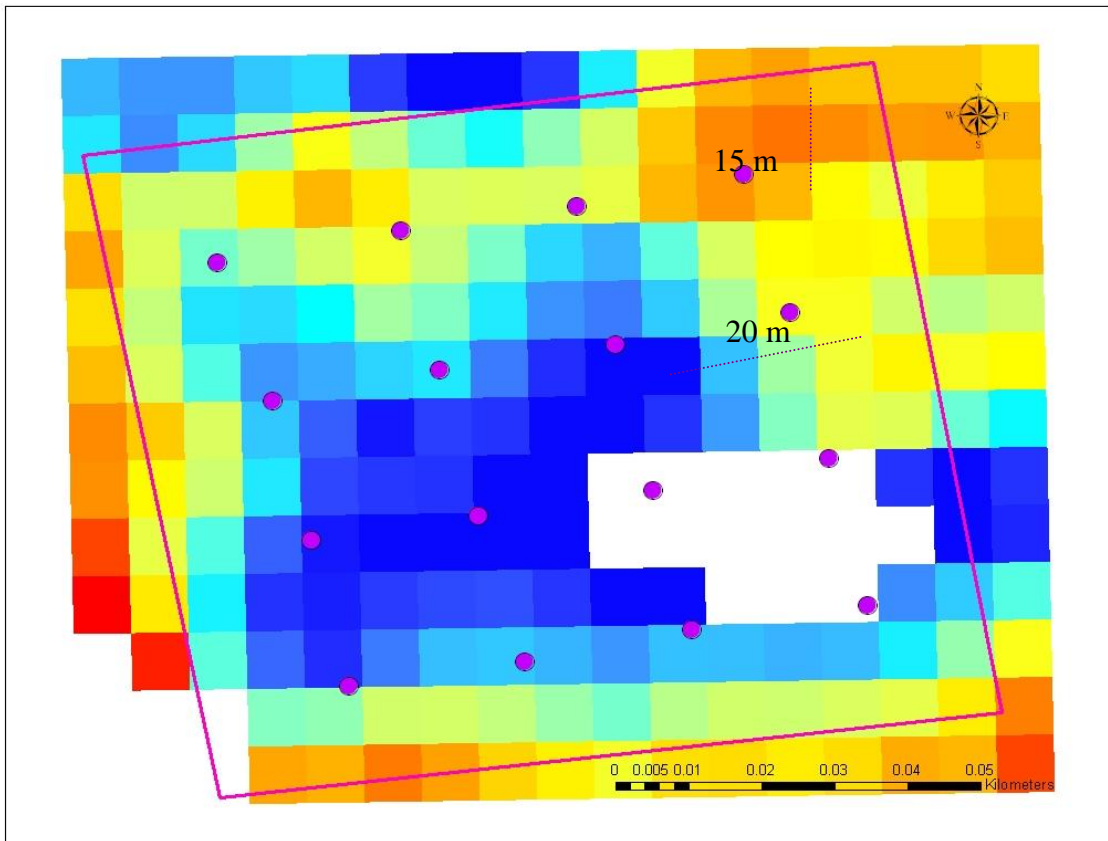


Figure 8. Dimensions of each area extracted from RADARSAT-2 soil moisture maps. Pixels vary from red (dry conditions 4% VWC) to blue (wet conditions 28% VWC).

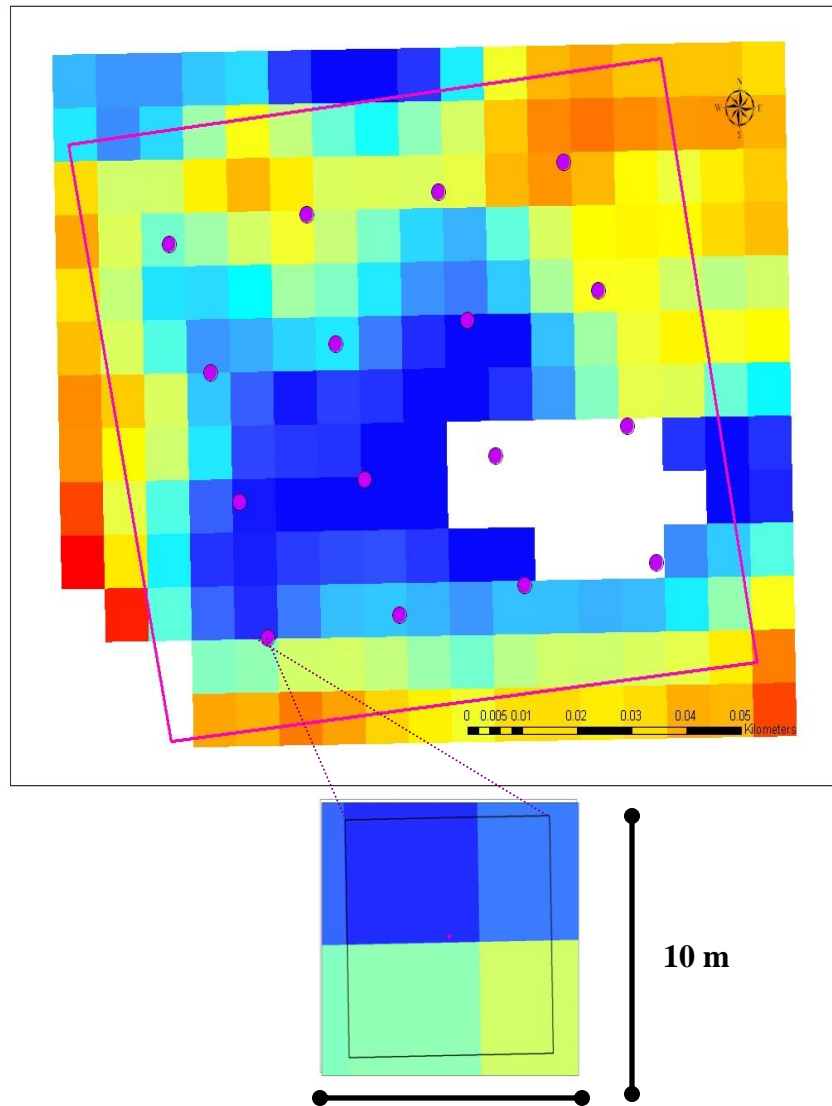


Figure 9. Extraction of pixels covering an area of 10x10 m around each point. Pixels vary from red (dry conditions 4% VWC) to blue (wet conditions 28% VWC). The area around the sampling point may be covered by 4 or 6 pixels.

3.5 Comparison of field measurements and RADARSAT-2

Accuracy of the soil moisture maps produced by RADARSAT-2 was evaluated by comparing the VWC values obtained from them with the values of GWC and VWC measured in the field. The comparison is based on correlation coefficients and linear regression equations between the variables. All calculations were made through the statistical software SAS.

- For each site (Alpha, Beta, Creosote, Nichole and Tripp) the correlation was calculated between the mean VWC from RADARSAT-2 maps and the mean field measured GWC and VWC at each depth interval (0-1, 1-2, 2-3, 3-4, 4-5, 5-10 cm) using all sampling days for the site. (Figure 10). The sites Alpha, Beta, Creosote, Nichole and Tripp were sampled respectively on 9, 5, 7, 9 and 8 sampling days (Table 3).
- For each site (Alpha, Beta, Creosote, Nichole and Tripp) the correlation was calculated between the mean VWC from RADARSAT-2 maps with asymmetric volumetric correction and the mean field measured GWC and VWC at each depth interval (0-1, 1-2, 2-3, 3-4, 4-5, 5-10 cm) using all sampling days for the site.
- For each site, correlations were calculated between the GWC and VWC at each sampling point and at each depth interval (0-1, 1-2, 2-3, 3-4, 4-5, 5-10 cm) and the VWC of each of the closest pixels of the RADARSAT-2 maps (Figure 11).
- For each site, correlations were calculated between the GWC and VWC at each point and at each depth interval (0-1, 1-2, 2-3, 3-4, 4-5, 5-10 cm) and the VWC of

each of the closest pixels of the RADARSAT-2 maps with asymmetric volumetric correction.

- For each sampling date, the correlation between the mean VWC of RADARSAT-2 maps and GWC and VWC of the five sites (Alpha, Beta, Creosote, Nichole, Tripp) at each depth interval (0-1, 1-2, 2-3, 3-4, 4-5, 5-10 cm) was calculated (Figure 12).
- For each sampling date, the correlation between the mean VWC of RADARSAT-2 maps with asymmetric correction and GWC and VWC of the five sites (Alpha, Beta, Creosote, Nichole, Tripp) at each depth interval (0-1, 1-2, 2-3, 3-4, 4-5, 5-10 cm) was calculated.

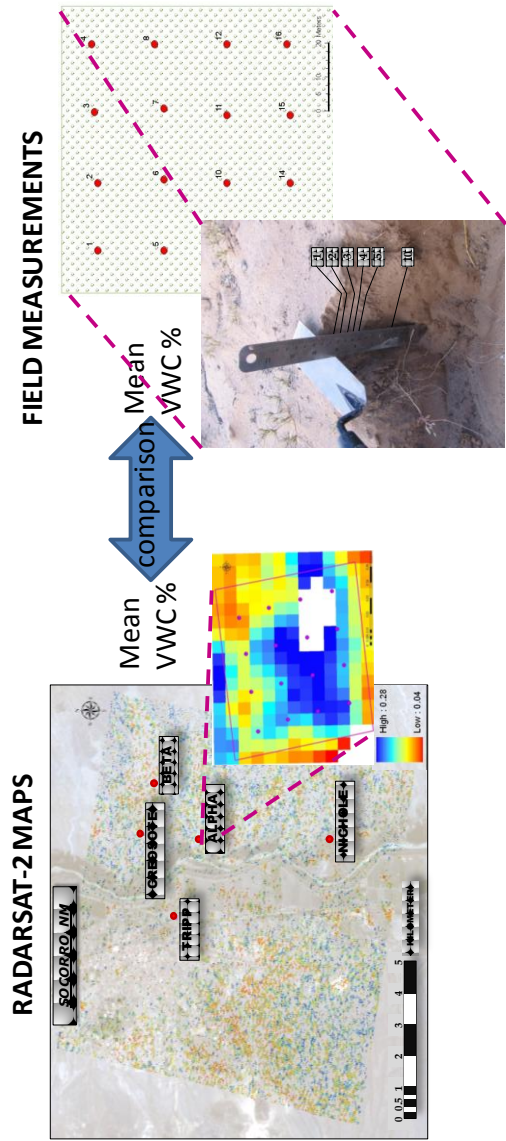


Figure 10. Comparison between mean VWC % from RADARSAT-2 maps and mean VWC % of the entire site at each site

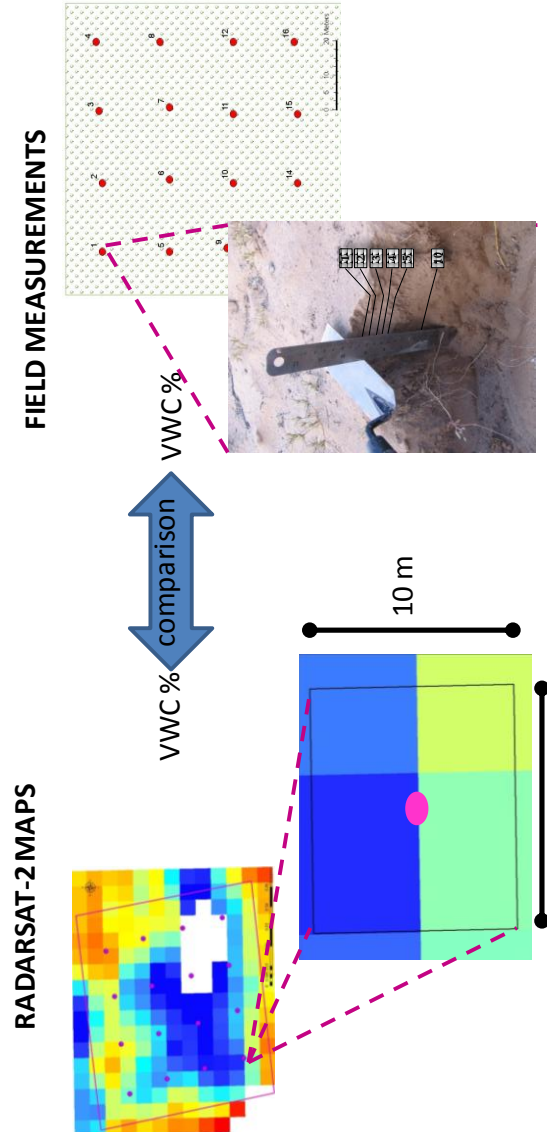


Figure 11. Comparison between VWC % from RADARSAT-2 maps and VWC % of each sampling point at each site

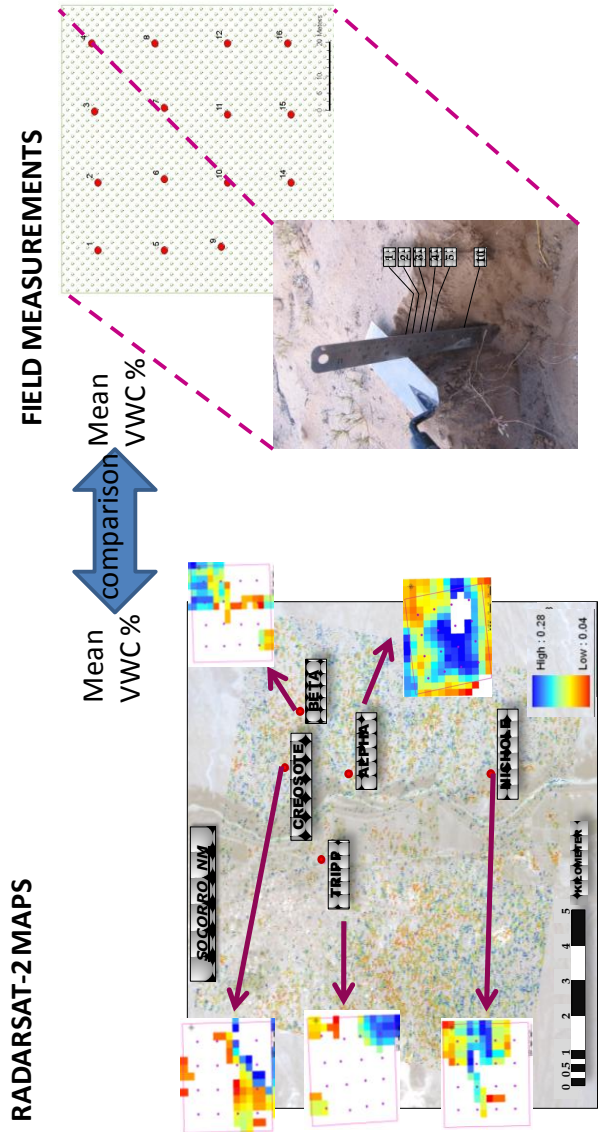


Figure 12. Comparison between mean VWC % from RADARSAT-2 maps and mean VWC % of the five sampling sites at each day

4 RESULTS AND DISCUSSIONS

4.1 Field observations

4.1.1 General characteristics of soils

The soil horizon characteristics for each site, including bulk density, particle size and carbonate content are summarized in Table 4. The soil particle size of each horizon of each soil at the five sites is shown in Figure 13. The Alpha site exhibits weak development of A and B horizons, with a shallow C horizon; all 3 horizon are sandy and have a calcium carbonate content from 8 to 13%. The Beta site shows a compound soil profile, with a weak soil developed in recent eolian sand overlying three B horizons with low CaCO₃ content (~0 to 5%). The Creosote site also has a compound soil profile with a recent soil forming in sand dunes overlying A and B horizons with calcium carbonate content that increases with depth, from 3.31 in the upper horizons, to 32.21 between 32 and 80 cm (K horizon). Both the Beta and Creosote sites show relatively homogeneous sandy loam and loamy sand textures throughout the profile.

In contrast, the Nichole site shows more heterogeneity in the soil particle size distribution with depth. Soils at this site are formed by alternating layers of loamy sand and sand, characteristic of the flood plain area where this site is located. Four sequences of A and C horizons were described, all of them with relatively low carbonate content between 4 and 8%. The Tripp site has a thick A horizon with a high humus content, characteristic of irrigated fields in this area, followed by a transitional AB horizon. From

there to the deepest layers of the soil profile, four C horizons were identified, belonging to four sedimentary stratigraphic units.

The data obtained in this study is consistent with the information obtained from the USDA report (1988). Soils at the Alpha, Beta and Creosote sites have coarser particle size in the upper cm of the profile (i.e. sand, loamy sand) and the Tripp site contains fine particle size in the soil profile. The Nichole site does not follow exactly the same pattern described for the Typic Ustifluvents, but in general has a similar pattern of intercalation of layers with fine and coarse particle size.

Analysis of 8 of the 16 sampling points in each site show low variability of soil bulk density (ρ_b), except at the Nichole site and in the upper 5 cm at the Tripp site (Table 5). The general trend is that the highest bulk soil densities are in the Beta and Creosote sites, whereas the lowest bulk soil density is in the Tripp site. The Nichole site shows the highest average soil bulk density with depth of the soil profile in the soil pit (Table 5, column 3), and the Tripp site has the lowest bulk density of all the soil profiles. This may be due to the high clay content of the Nichole site, which increases the bulk density of the soil profile. The Tripp site has a lower ρ_b due to the high amount of organic matter, despite the soils in this site have a fine texture.

ALPHA				
Horizon	Depth (cm)	ρ_b (g/cm ³)	Particle size	Carbonate content %
Avk	0-5	1.58	sandy loam	8.07
Bwk	5 -15	1.55	sandy loam	8.73
Bwk	15-20	1.42	sandy loam	10.93
Bwk	20-25	1.48	sandy loam	12.60
Ck	30-50	1.42	sandy loam	10.49
Ck	50-70	1.42	sandy loam/loam	10.35
Ck	70-90	1.29	sandy loam	8.39

BETA				
Horizon	Depth (cm)	ρ_b (g/cm ³)	Particle size	Carbonate content %
C	0-5	1.11	sand	0.78
2Bwk	5 -10	1.48	loamy sand	1.63
2Bk1	10 -35	1.56	sandy loam	4.73
2Bk2	35-70	1.67	sandy loam	2.69
2C	70-100	1.66	loamy sand	3.60

CREOSOTE				
Horizon	Depth (cm)	ρ_b (g/cm ³)	Particle size	Carbonate content %
Ck	0-2	1.50	sandy loam	3.31
2Avk	2- 5	1.40	sandy loam	2.54
2Bk	5 -20	1.42	sandy loam	5.22
2Bk	20-32	1.59	silt loam	7.27
2K	32-80	1.68	clay loam	32.21

Table 4: Soil horizons characteristics at the Alpha, Beta, Creosote, Nichole and Tripp sites. **A**: Mineral horizon formed at surface; **B**: Subsurface mineral horizon, accumulation of clays, iron minerals, etc; **C**: Mineral horizon with little pedogenesis; **v**: vesicular; **k**: carbonate accumulation; **w**: weak accumulation of materials; **h**: humus/organic matter accumulation; **g**: strong gleyed.

NICHOLE				
Horizon	Depth (cm)	ρ_b (g/cm ³)	Particle size	Carbonate content %
Ak	0-7	1.40	silt loam	8.11
Ck	7- 15	1.39	sandy loam	4.09
2Ak/2Ck	15- 27	1.49	loam/sand	6.27
3Ak	27-32	1.45	sandy loam	7.15
3Ck	32- 44	1.39	silt loam	4.38
4Ak	44-47	1.34	sandy loam	6.63
Ack	47-52	1.36	sand	3.88

TRIPP				
Horizon	Depth (cm)	ρ_b (g/cm ³)	Particle size	Carbonate content
Ah	0-5	1.50	clay loam	3.89
Ah	5 10	1.61	clay loam	1.63
Ah	10 15	1.60	sandy clay loam	4.80
Ah	15 20	1.50	silty clay loam	4.51
Ah	20-30	1.51	silty clay loam	5.15
Ah	30-46	1.55	silty clay loam	5.17
AB	46-50	1.46	silty loam	5.87
2C1	50-70	1.25	silty loam	4.68
3C2	70-90	1.80	clay	6.62
4C2g	90-100	1.44	sandy loam	4.91
5C4	104-120	-	sand	0.64

Table 4: Soil horizons characteristics at the Alpha, Beta, Creosote, Nichole and Tripp sites. A: Mineral horizon formed at surface; B: Subsurface mineral horizon, accumulation of clays, iron minerals, etc; C: Mineral horizon with little pedogenesis; v: vesicular; k: carbonate accumulation; w: weak accumulation of materials; h: humus/organic matter accumulation; g: strong gleyed.

Mean			
SITE	ρ points 0-5 cm	ρ points 5-10 cm	ρ pit all depth
ALPHA	1.60	1.53	1.52
BETA	1.64	1.63	1.59
CRESOTE	1.63	ND	1.54
NICHOLE	1.46	1.54	1.63
TRIPP	1.10	1.40	1.42

Standard deviation			
SITE	ρ points 0-5 cm	ρ points 5-10 cm	ρ pit all depth
ALPHA	0.06	0.07	0.07
BETA	0.04	0.06	0.06
CRESOTE	0.10	ND	0.07
NICHOLE	0.16	0.11	0.69
TRIPP	0.45	0.17	0.08

Variability coefficient			
SITE	ρ points 0-5 cm	ρ points 5-10 cm	ρ pit all depth
ALPHA	0.04	0.05	0.04
BETA	0.02	0.03	0.04
CRESOTE	0.06	ND	0.04
NICHOLE	0.11	0.07	0.43
TRIPP	0.41	0.12	0.06

Table 5: Bulk densities in the study area. First and second columns show the mean of the bulk density values (ρ_b) for the 8 points sampled at each site, at depths 0-5 and 5-10 cm, respectively. The third column shows the mean of the bulk density values (ρ_b) of the soil horizons identified at each soil pit at each site.

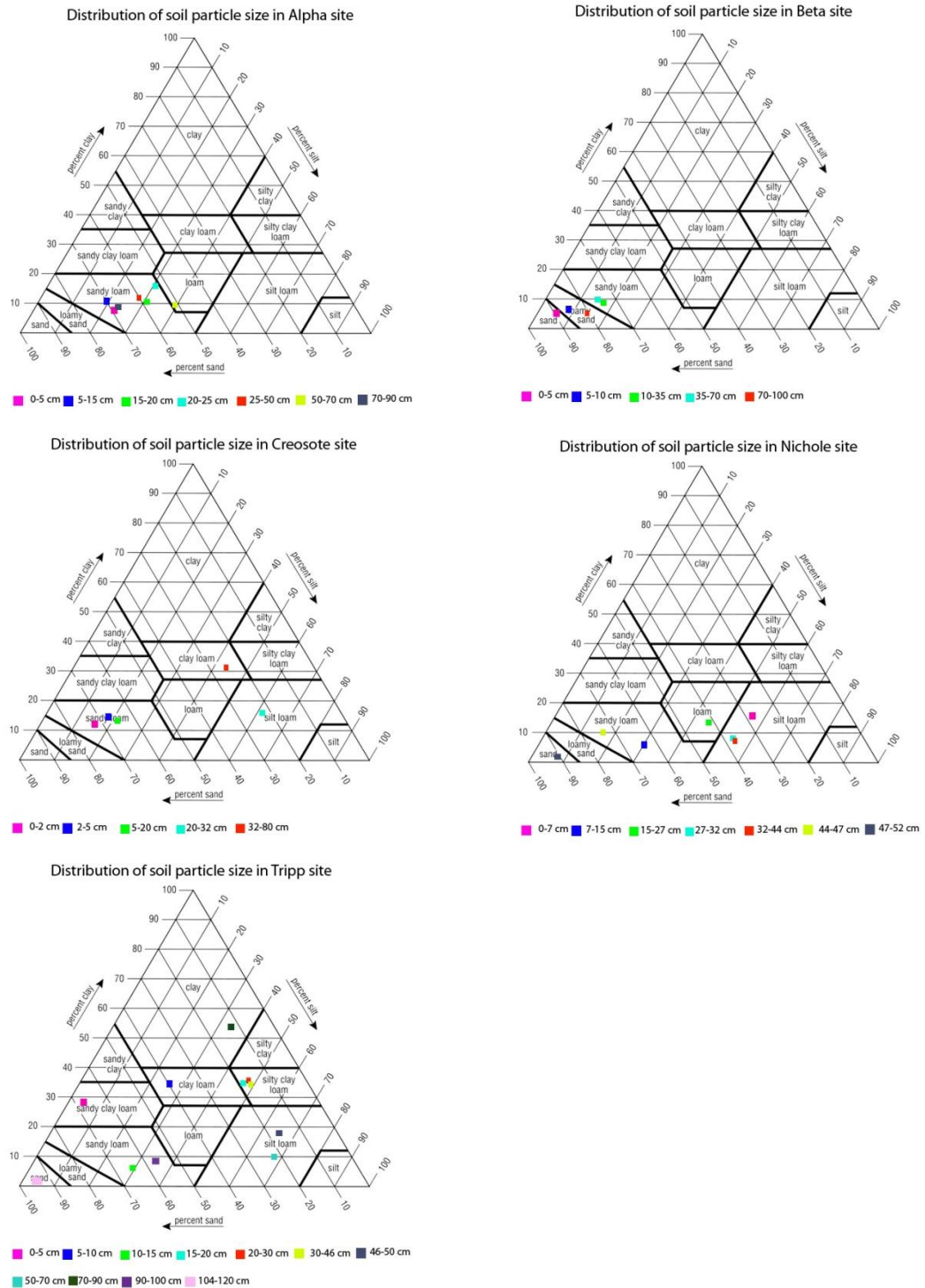


Figure 13. Soil particle size classification for the five sampling sites.

4.1.2 Soil moisture

Soil moisture (GWC and VWC) measured in the field showed different conditions between the 5 study sites during the 10 sampling days (see Figure 14 to Figure 18 for GWC and Figure 19 to Figure 23). The patterns in the soil moisture distribution of the sites are quite similar for GWC and VWC, as expected. RADARSAT-2 soil moisture is expressed as VWC. Therefore, all references to field measurements and comparisons among RADARSAT-2 and ground soil moisture measurements are made using VWC. The Beta site has the lowest soil moisture content followed closely by the Creosote and Alpha sites. The Tripp and Nichole sites are significantly moister than the other sites, with Nichole being the one with the largest variability in water content in the study area. In general deeper soil layers had a higher moisture content and greater variability in moisture content; except when precipitation occurred close to the sampling time, as on July 8, when the upper cm of all soils are moister.

Rain events previous to sampling (~7 days) increase the soil moisture. For example, during July 08 and August 23, soil moisture increases significantly compared to days without considerable preceding precipitation, e.g. September 18 (Figure 24 through Figure 28). During moist conditions, soil moisture is more homogeneously distributed among all the sites and all the soil profiles (Figure 29). When dry conditions apply over the study area, there is more variability in the soil moisture along the points that represent

each site and across the soil profile. The upper soil cm are significantly dryer than the 5-10 cm depth.

The Nichole site exhibits the highest soil moisture levels, but also the highest variability between the 16 sampling points, due to the high variability of soil texture; the values range from ~0 to 60%. The Tripp site follows Nichole with a larger percentage of soil moisture, however, the volumetric water content along the entire site is more homogeneous than at the Nichole site, with values between 3 and 35 %. The Alpha site exhibits drier conditions than the Nichole and Tripp sites, ranging between ~0 and 20%, with a low variability along the site. The Beta and Creosote sites are the driest of the study area, with values between ~0 and 8%; water content variability is low in both sites, although less evident at the Creosote site. The comparison between VWC (%) on moderate moist (August 23) and dry days (September 18) in the study area is shown in Figure 29.

The results of this study (i.e: GWC, VWC) are consistent with previous work by Canton et al. (2004), and Gomez-Plaza et al. (2001), that in semiarid environments soil moisture is function of the amount of precipitation, the soil particle size and the soil's depth. Gomez-Plaza et al. (2001) also stated that soil moisture under densely vegetated areas is higher than under bare areas, which occurs in the Alpha site for the current research. However, this is not the case in areas like the Creosote and Beta sites, covered with creosote bushes or seasonal vegetation, respectively. Vegetation is not the only factor that controls the distribution of soil moisture in the study site. It seems highly related to the soil particle size covering the surface, as determined by Yair (1987). This

author states that the coarser textured soils allow deeper water infiltration, therefore have higher soil moisture than finer textured soils. In this study, the Nichole and Tripp sites are influenced by seepage from below and irrigation, respectively. The fine particle size of the soils at those sites allows a higher water retention and increases the soil moisture in the surface cm of soils, comparing with sites with coarse particle size (Alpha, Beta, Creosote), which are drier in the upper cm of the profile and are moister with depth.

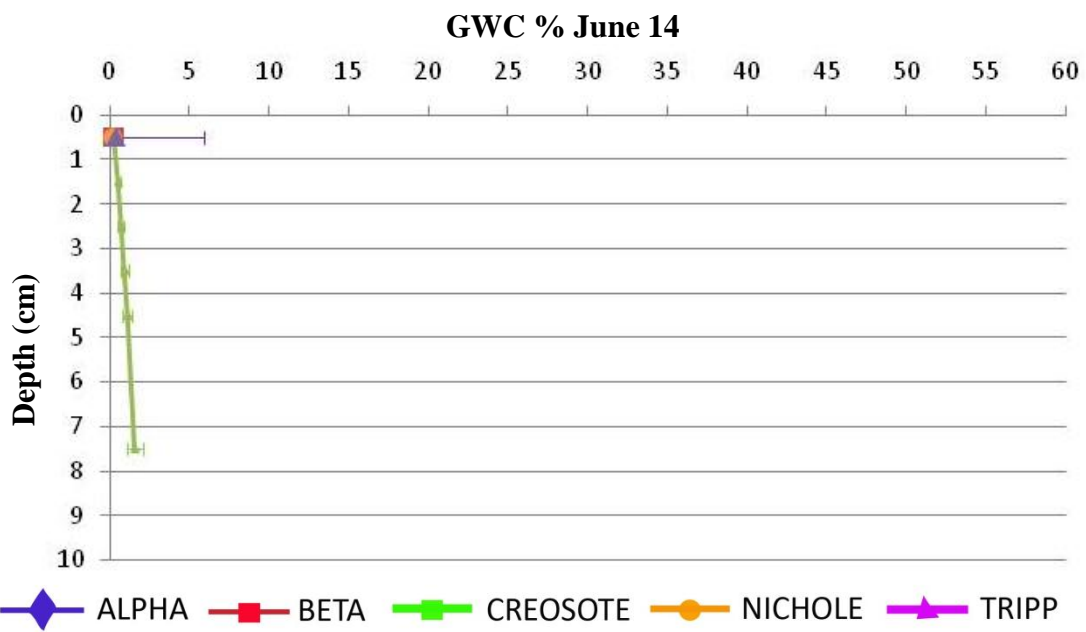
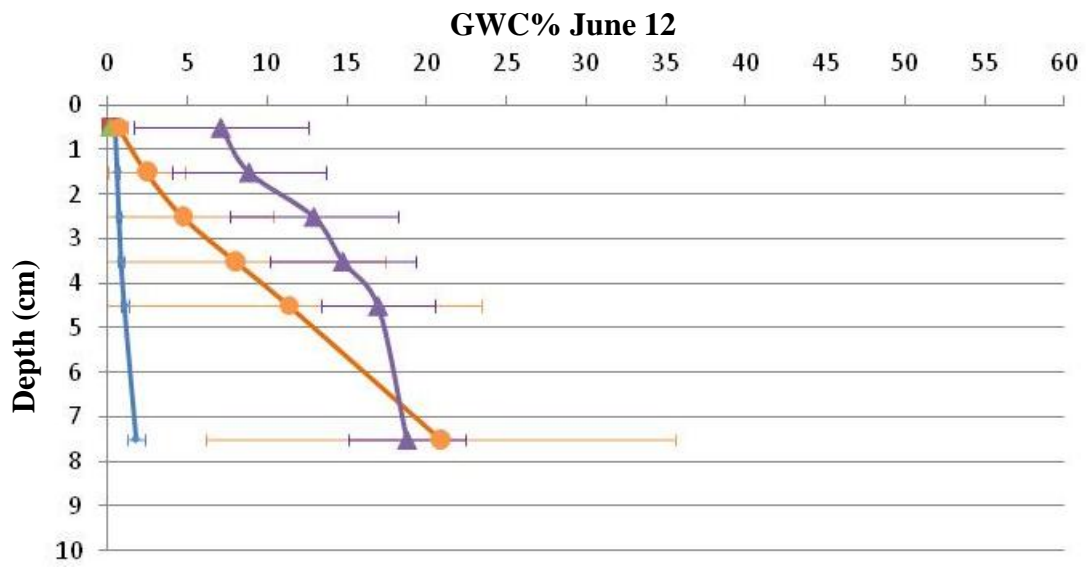


Figure 14. Distribution of GWC in the 5 sites at: a) June 12; b) June 14. For June 14 there was sampling just Creosote site.

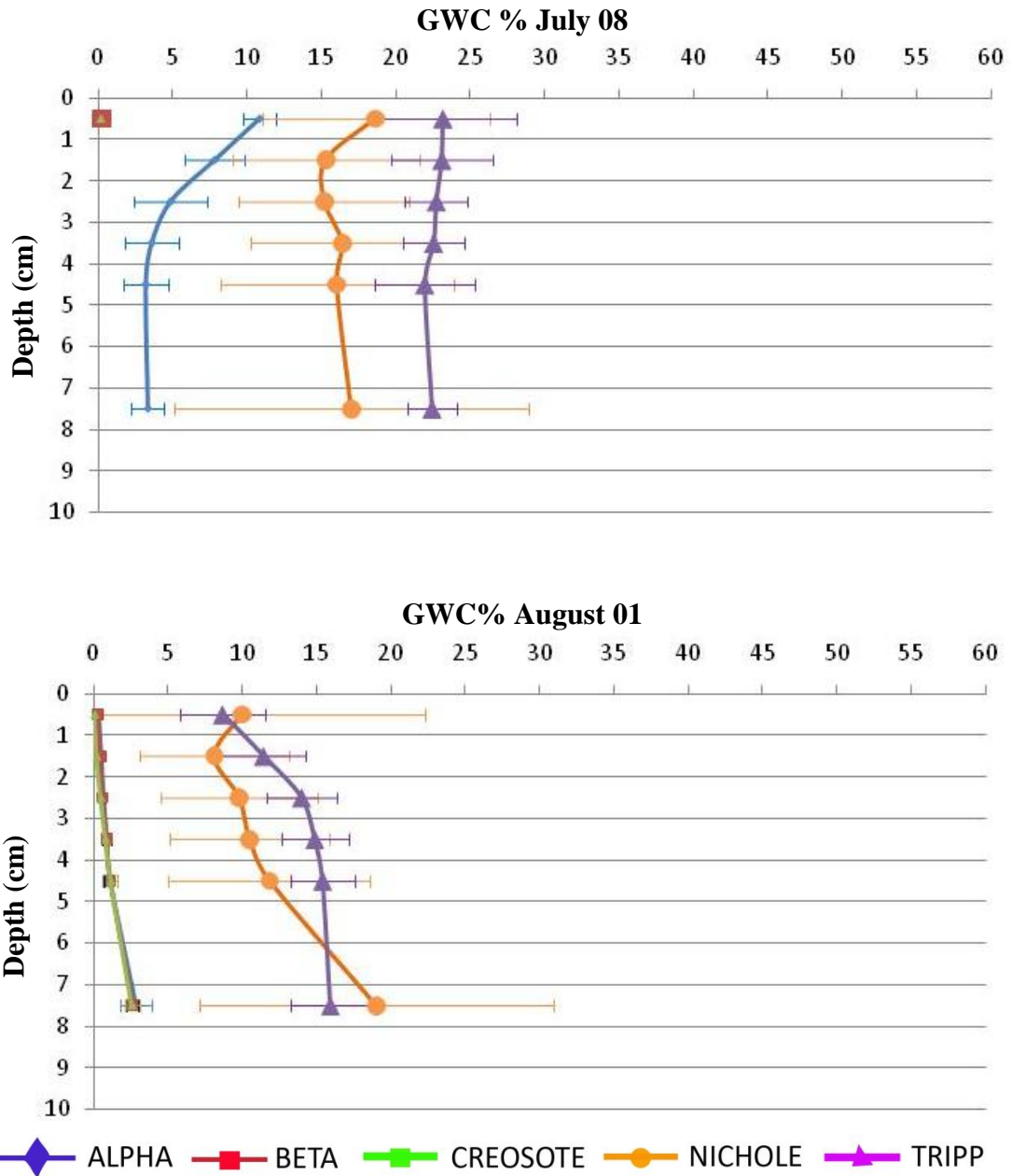


Figure 15. Distribution of GWC in the 5 sites at: a) July 08; b) August 01

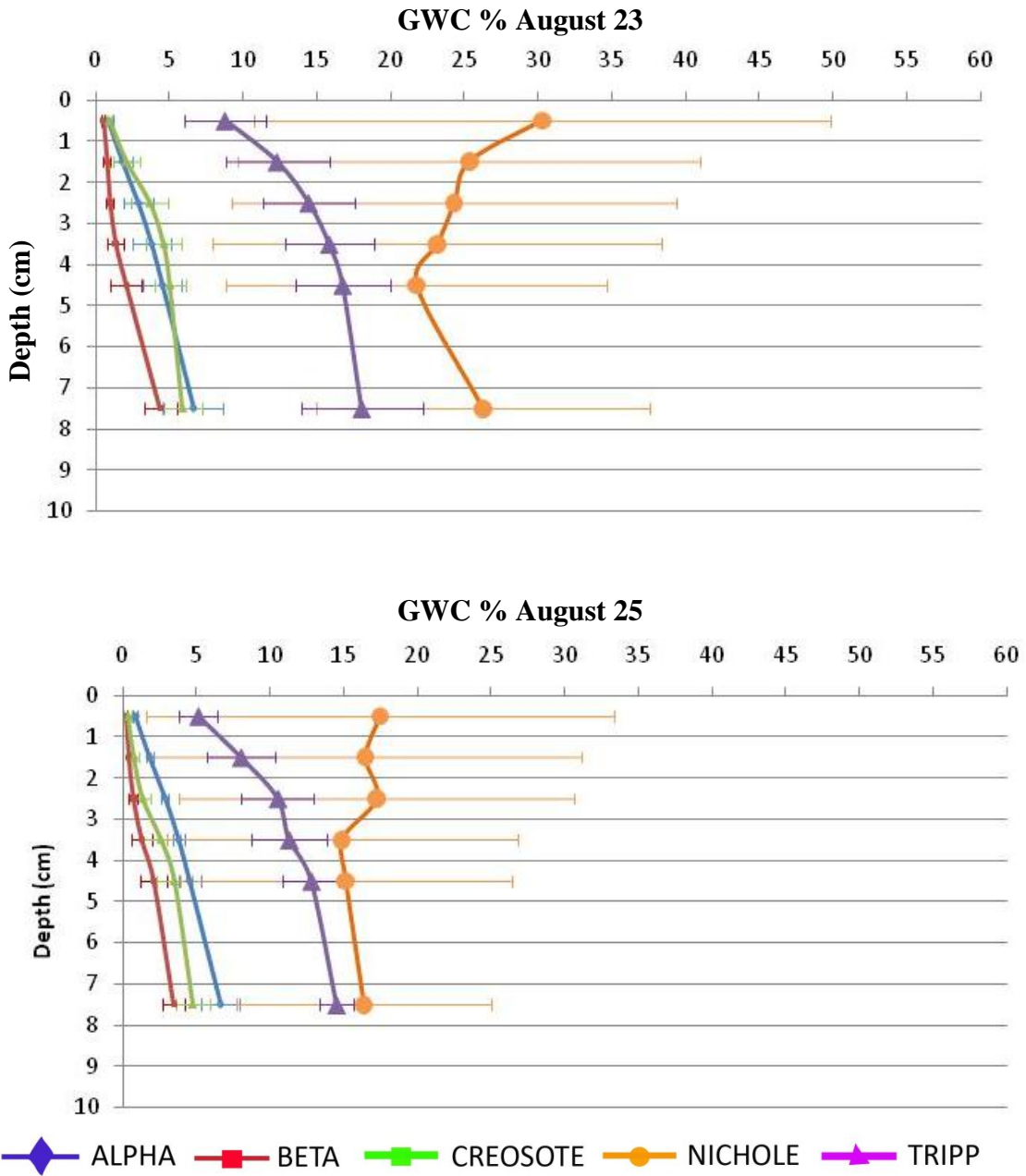


Figure 16. Distribution of GWC in the 5 sites at: a) August 23; b) August 25

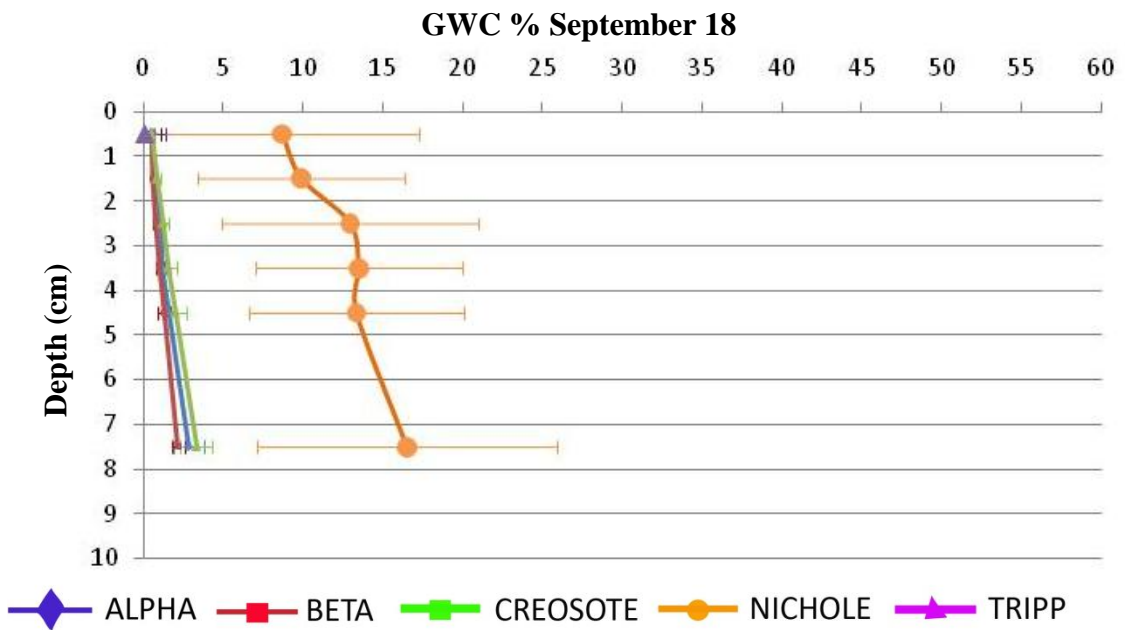
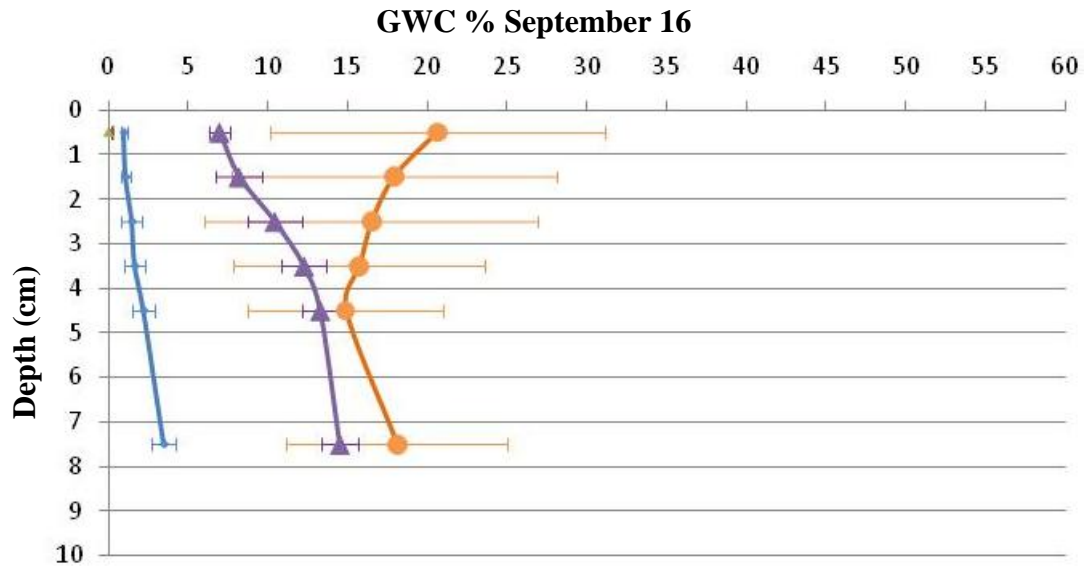


Figure 17 Distribution of GWC in the 5 sites at: a) September 16; b) September 18

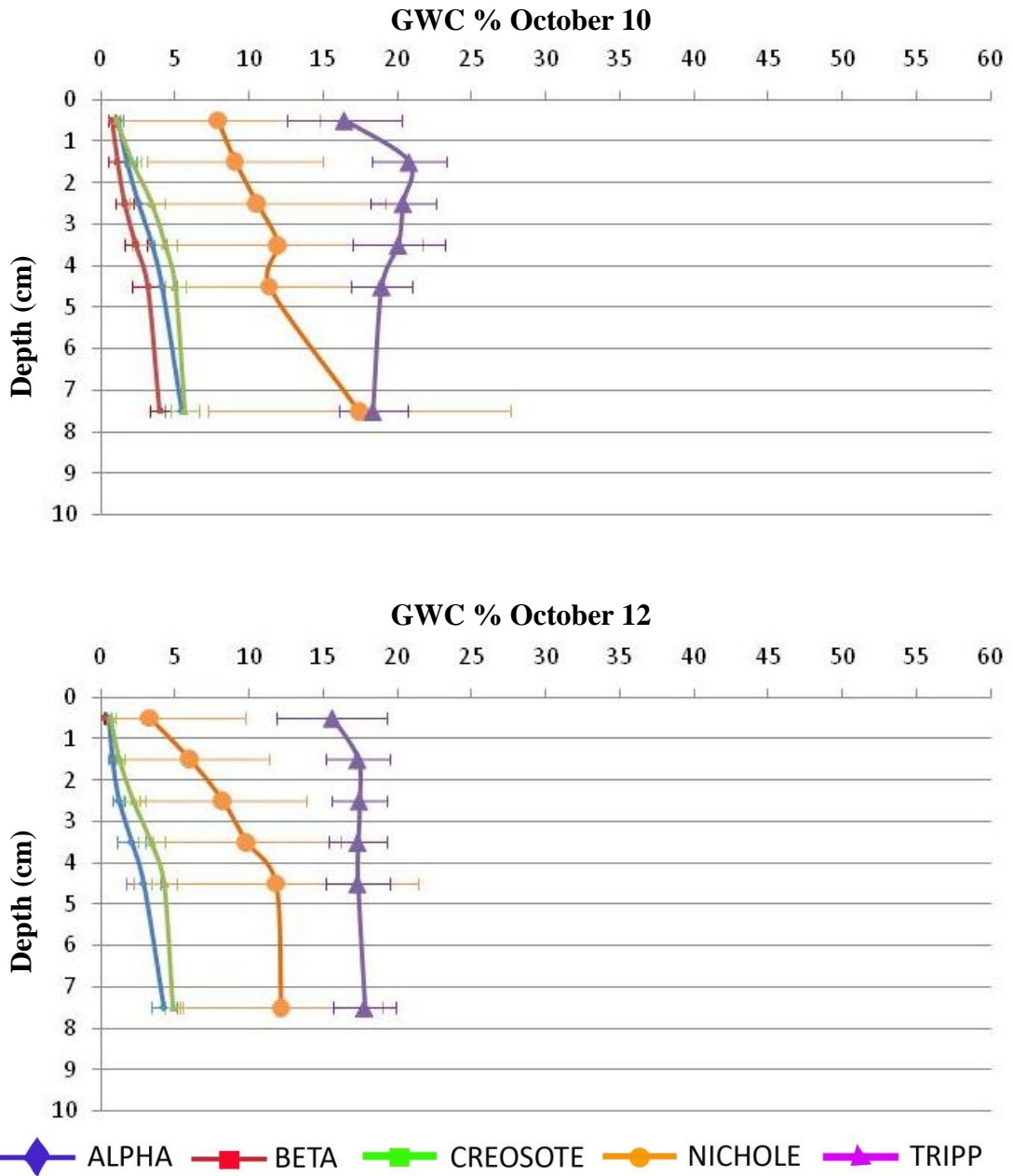
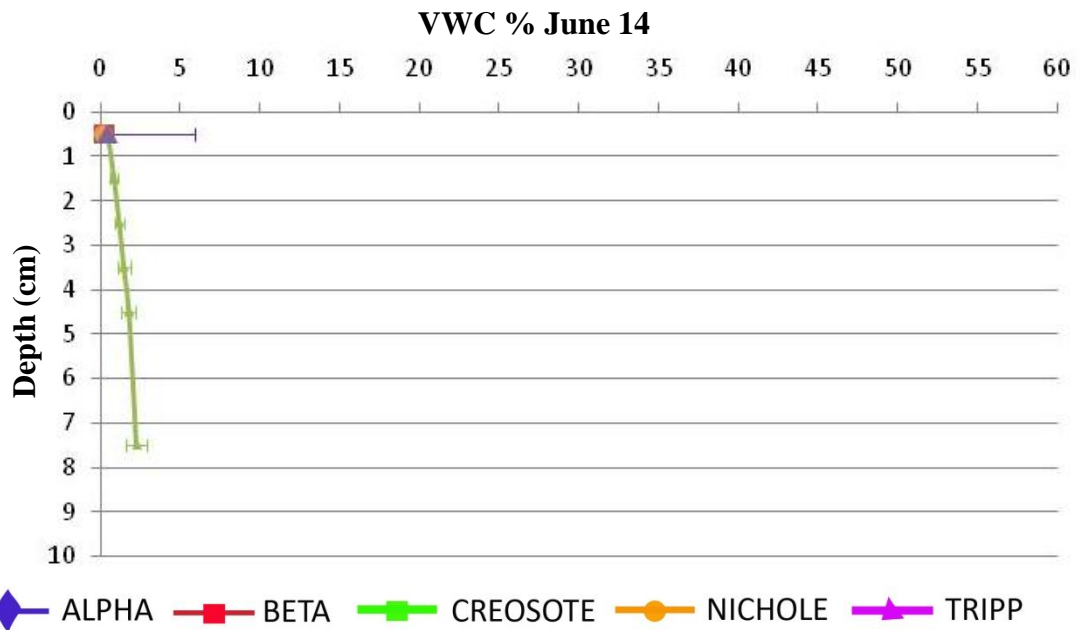
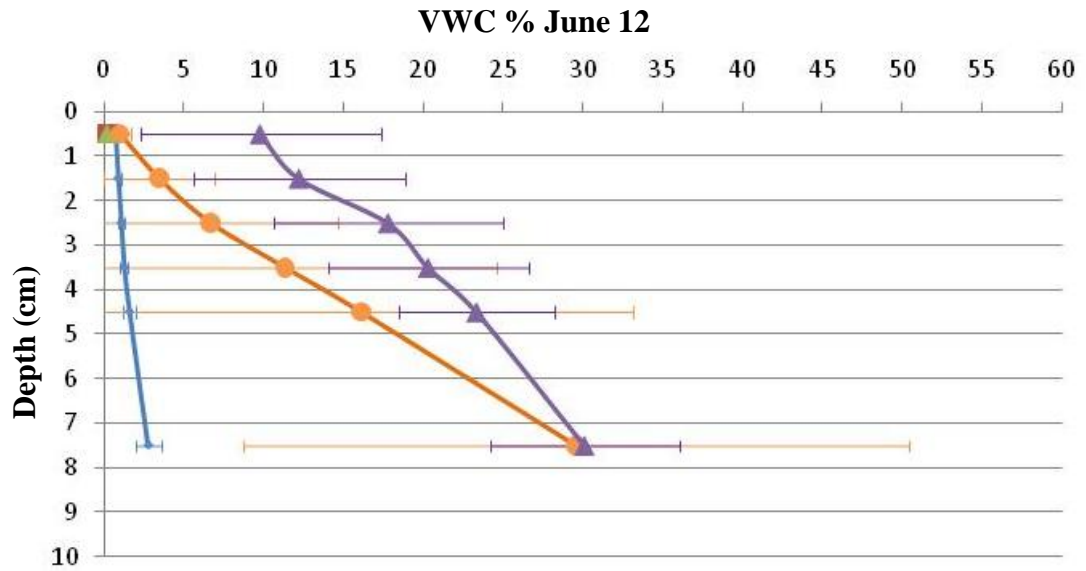


Figure 18. Distribution of GWC in the 5 sites at a) October 10; b) October 10



◆ ALPHA
 ■ BETA
 ■ CREOSOTE
 ● NICHOLE
 ▲ TRIPP

Figure 19. Distribution of VWC in the 5 sites at: a) June 12; b) June 14

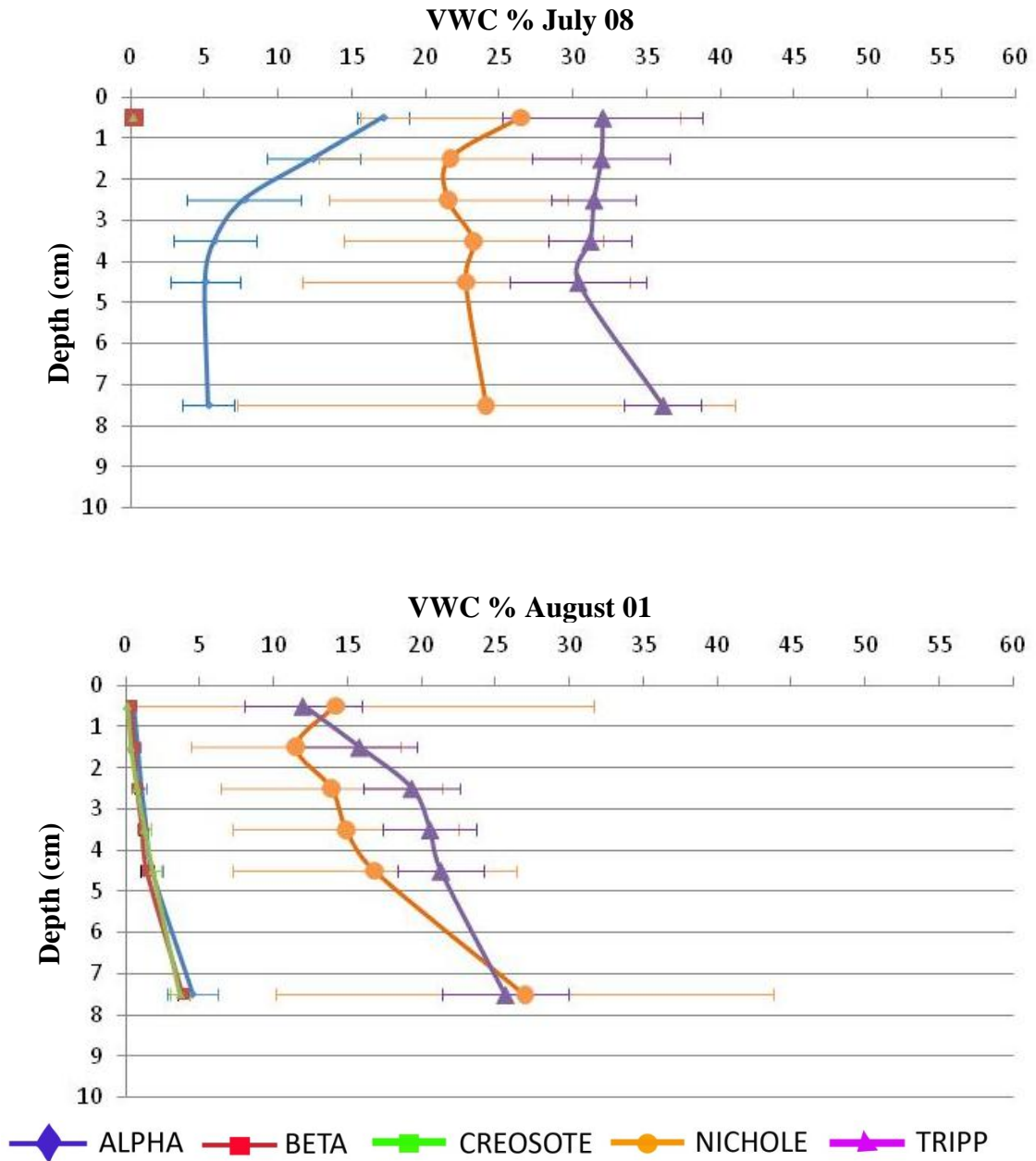


Figure 20. Distribution of VWC in the 5 sites at: a) July 08; b) August 01

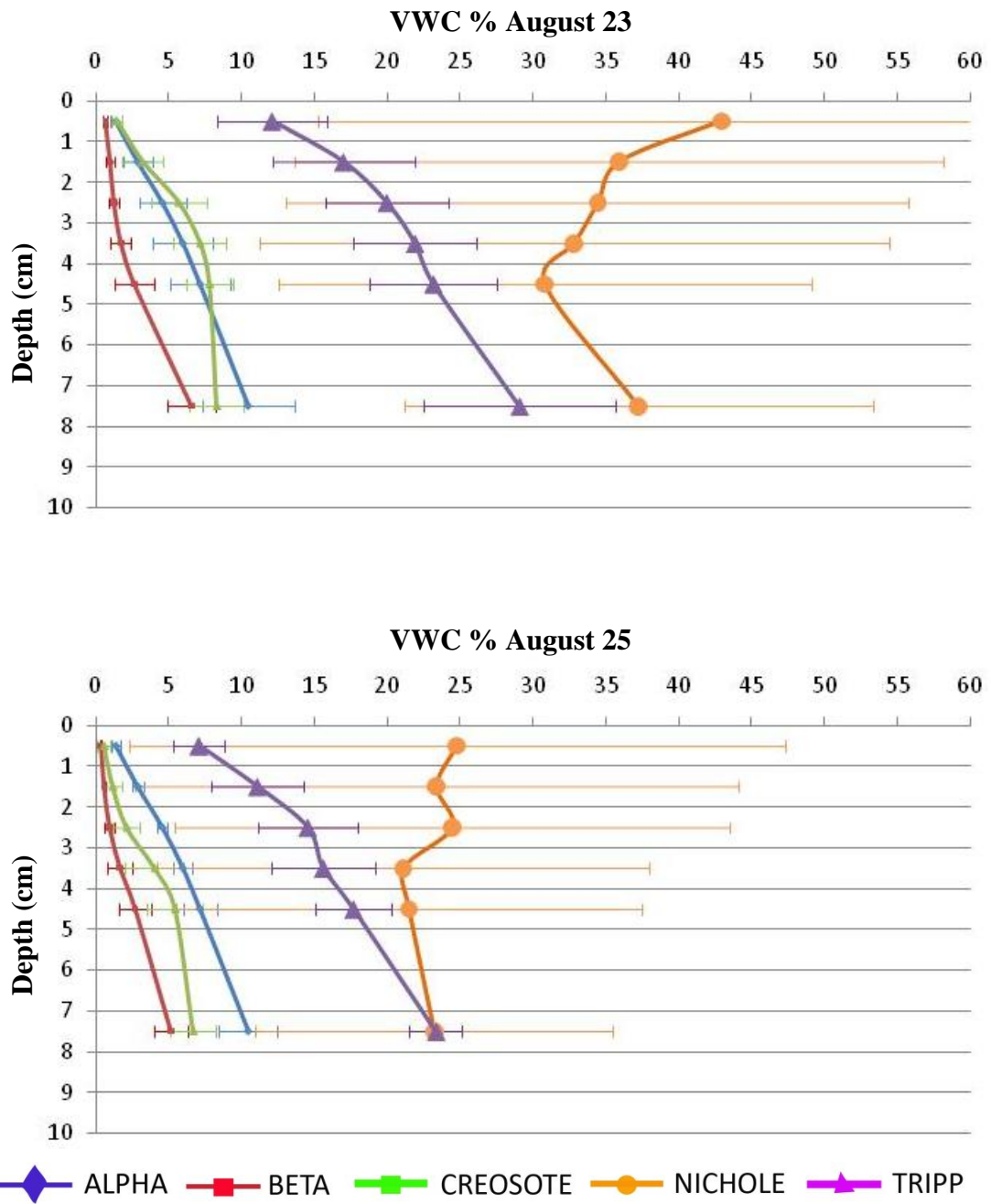


Figure 21. Distribution of VWC in the 5 sites at: a) August 23; b) August 25

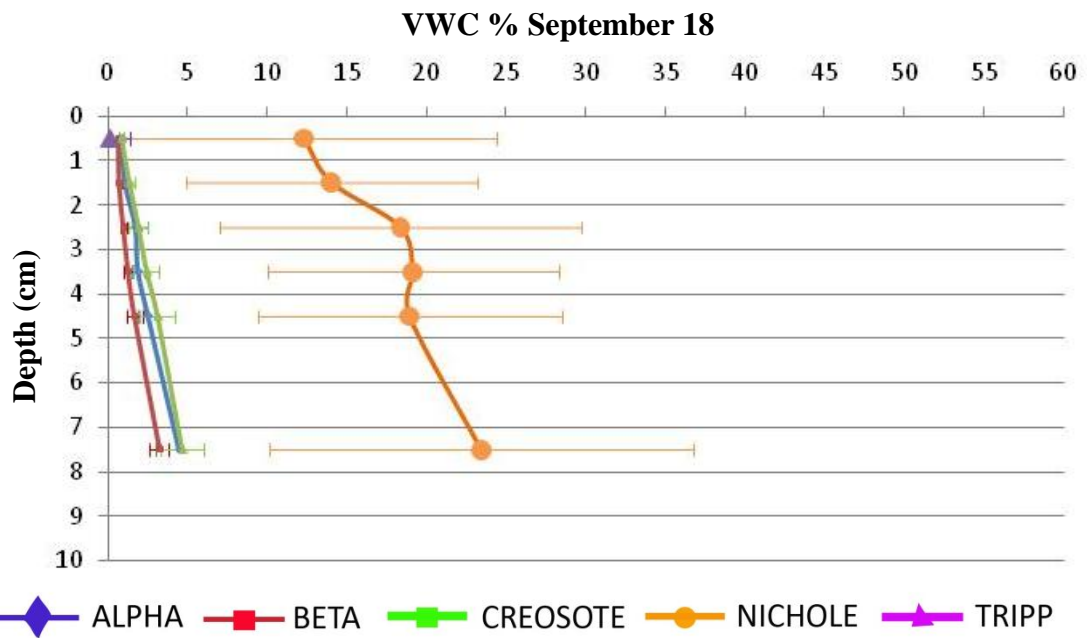
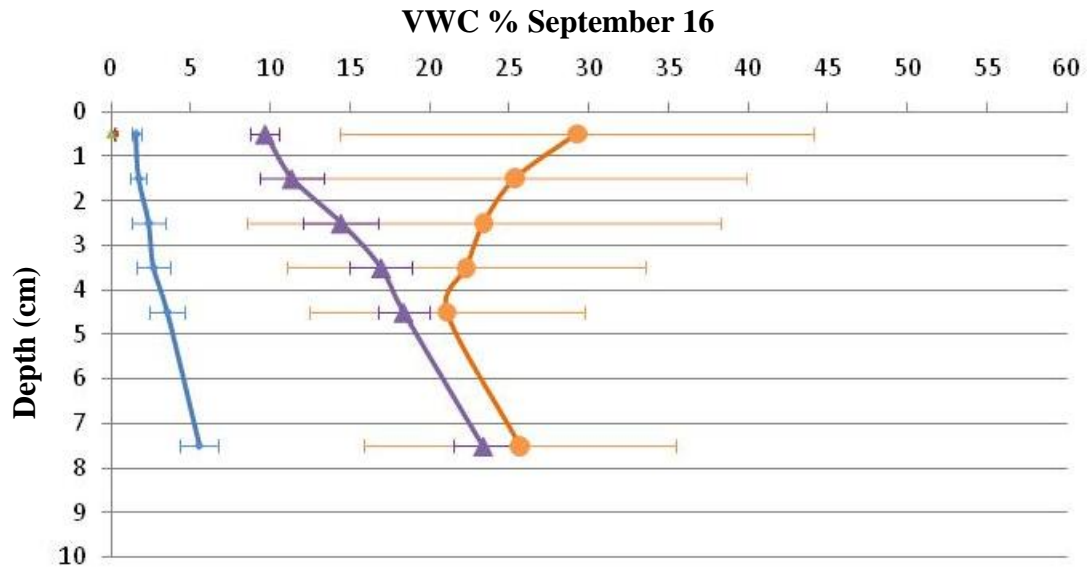


Figure 22 Distribution of VWC in the 5 sites at: a) September 16; b) September 18

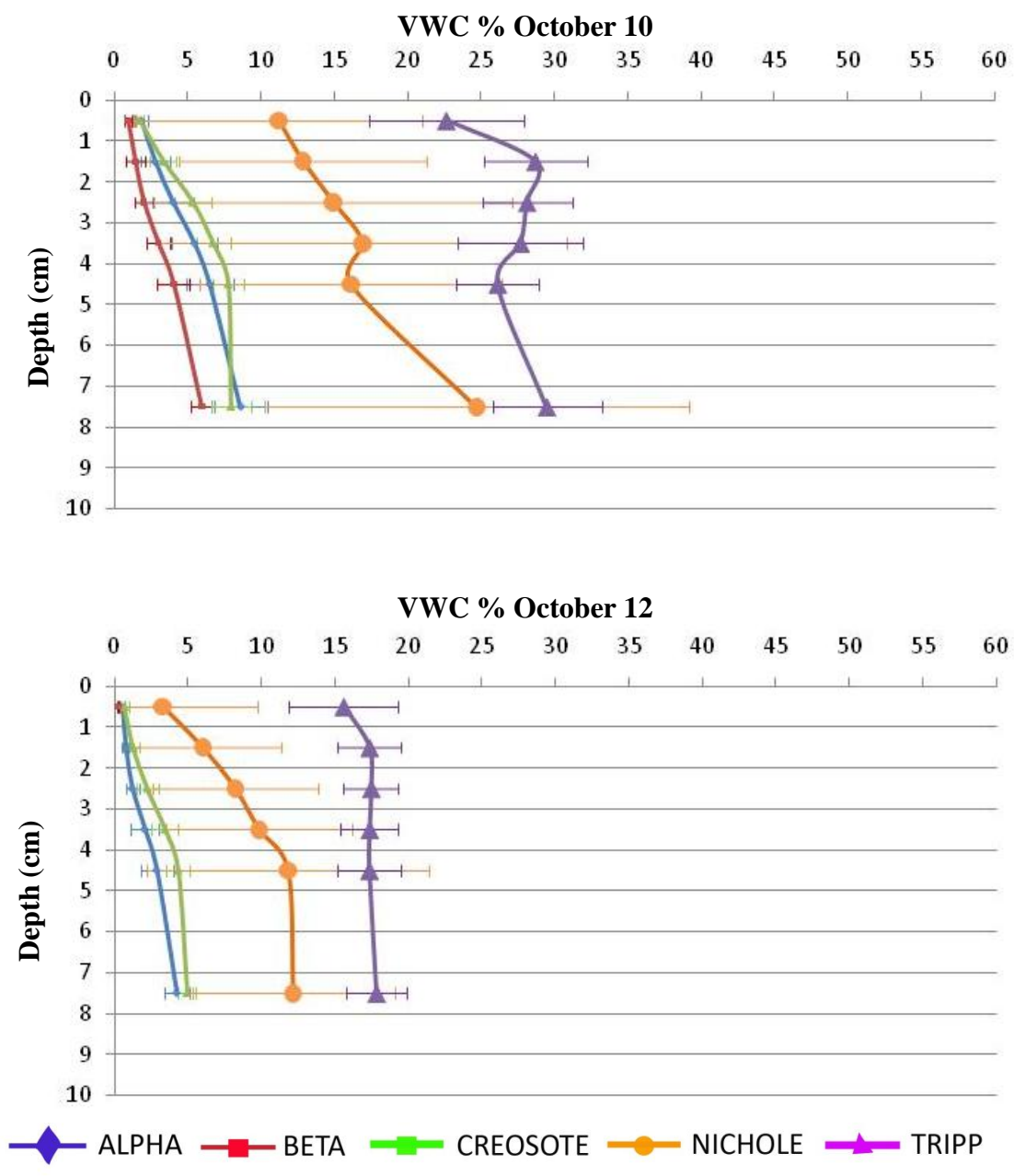


Figure 23. Distribution of VWC in the 5 sites at a) October 10; b) October 12

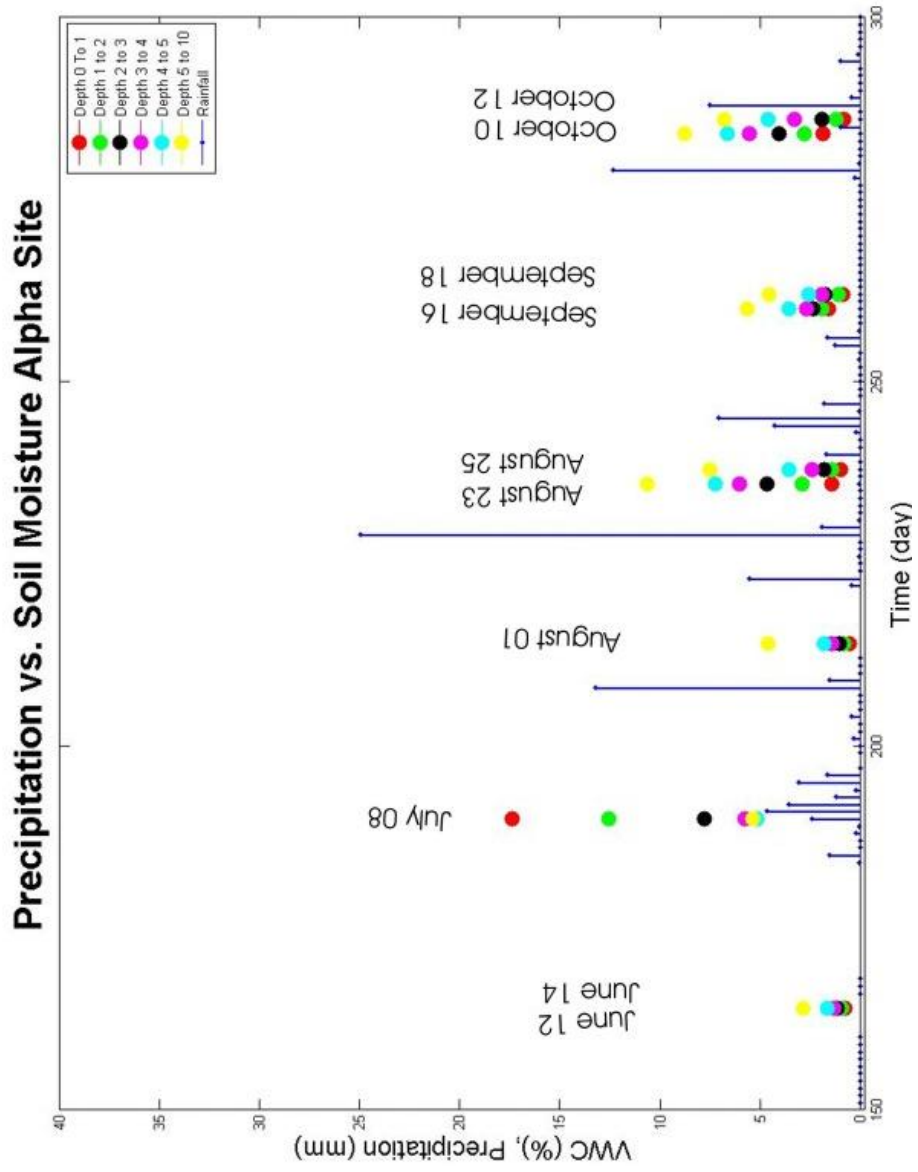


Figure 24. Precipitation events and VWC % field measurements for the Alpha site.

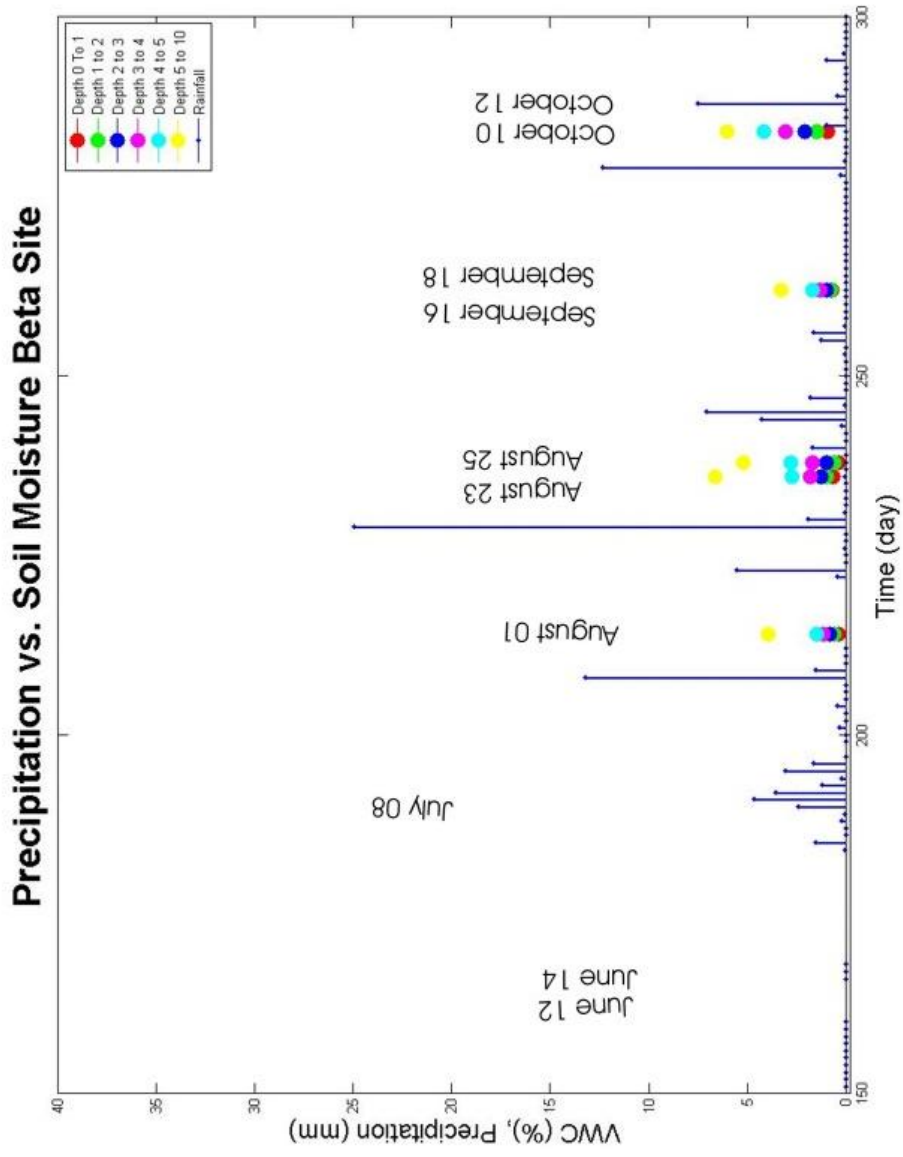


Figure 25. Precipitation events and VWC % field measurements for the Beta site

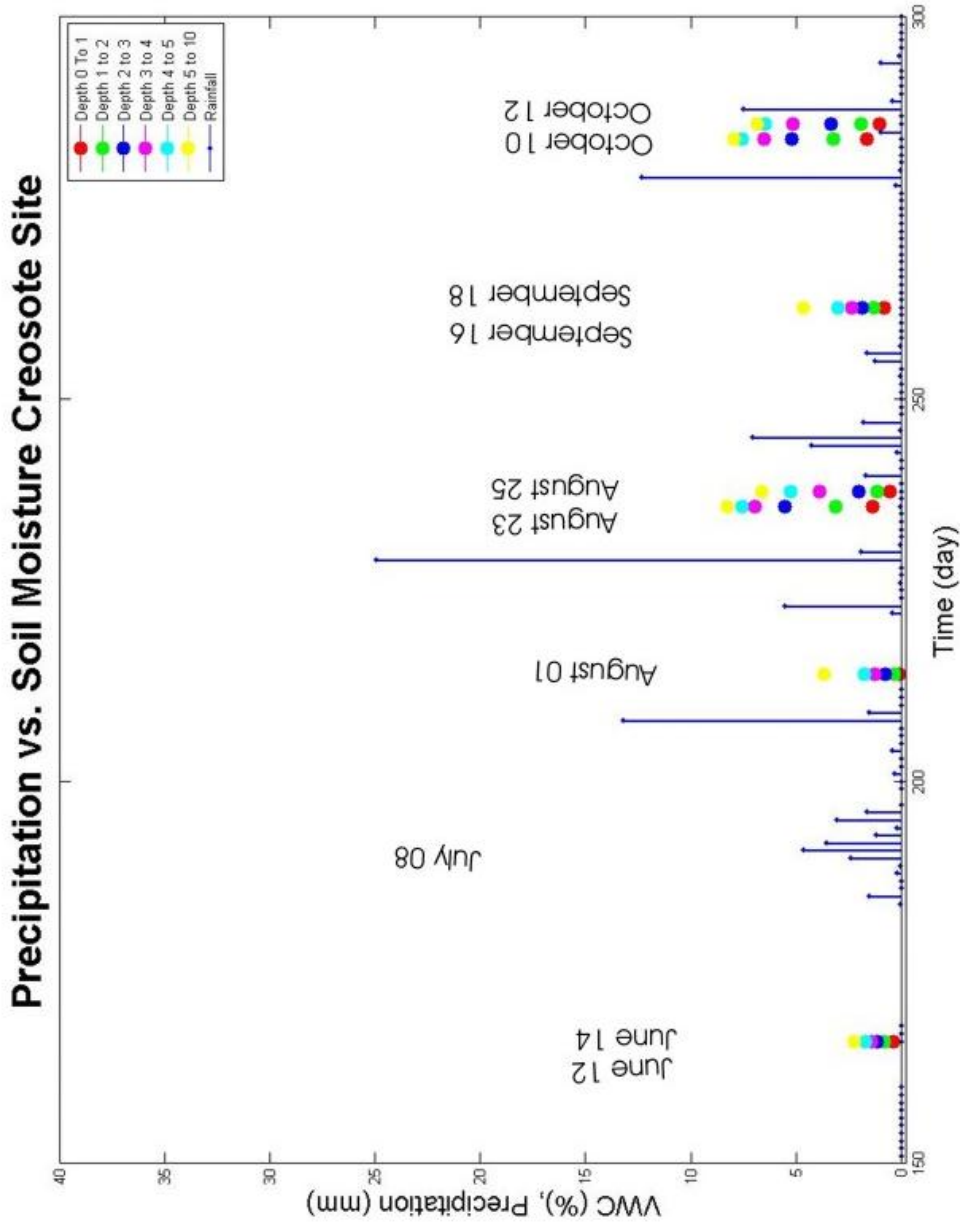


Figure 26. Precipitation events and VWC % field measurements for the Creosote site

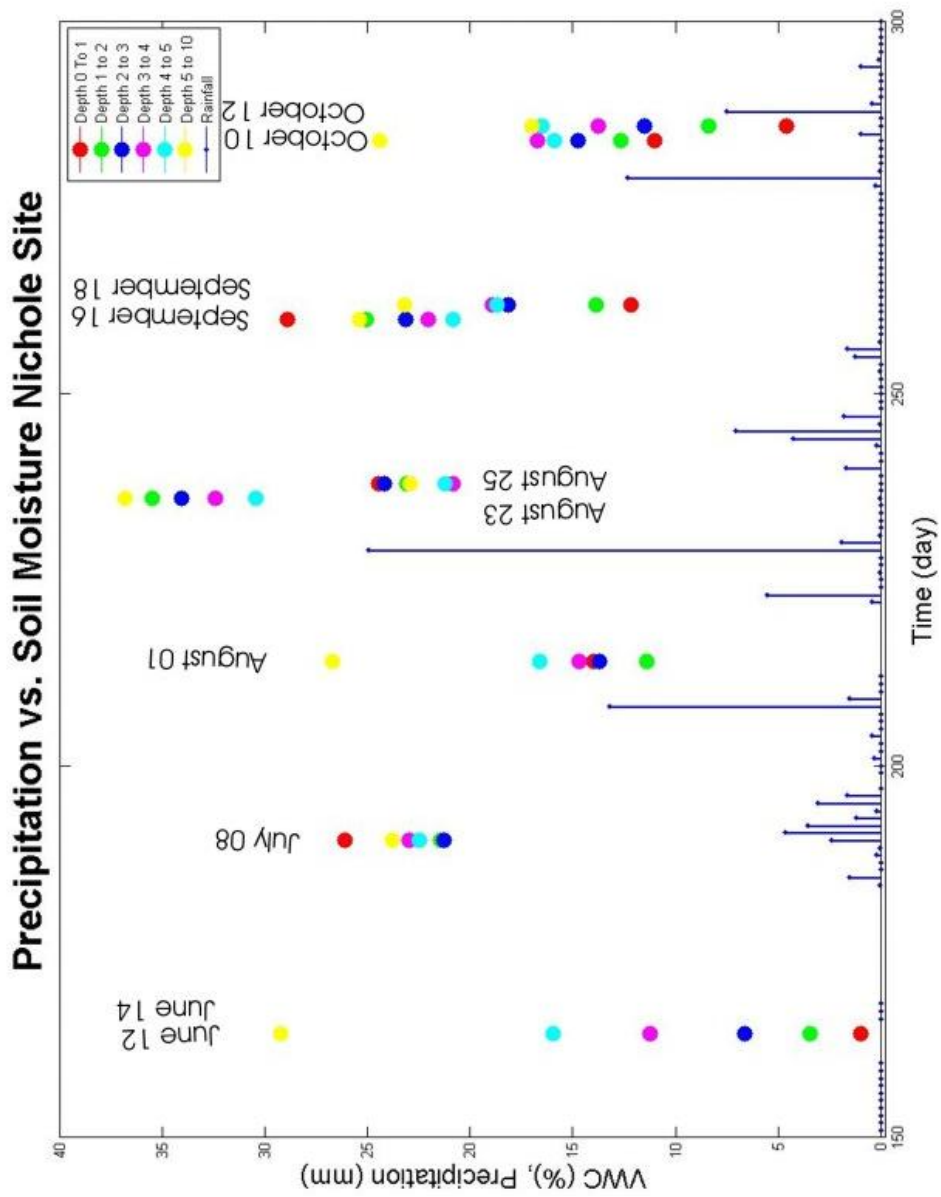


Figure 27. Precipitation events and VWC % field measurements for the Nichole site

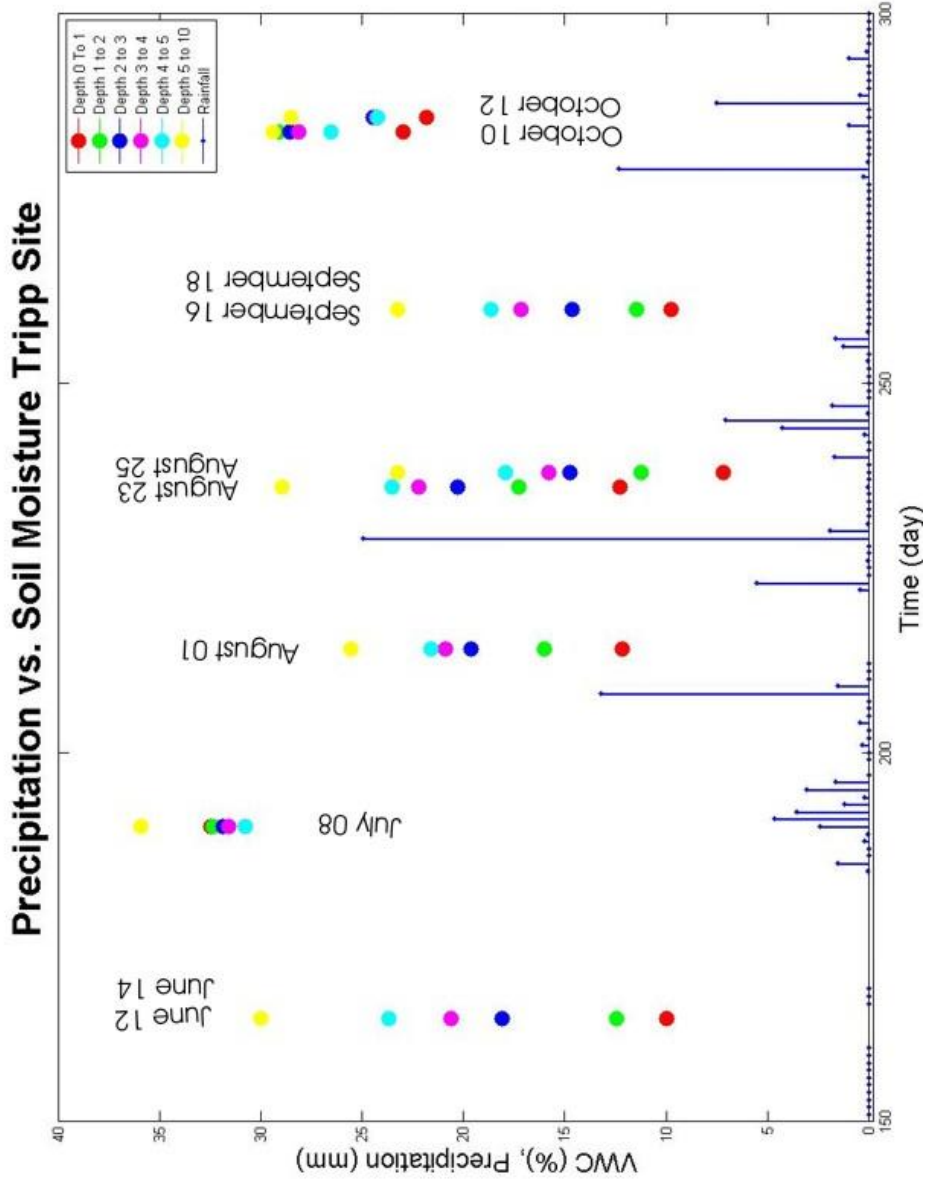


Figure 28. Precipitation events and VWC % field measurements for the Tripp site

August 23 (moist conditions)

September 18 (dry conditions)

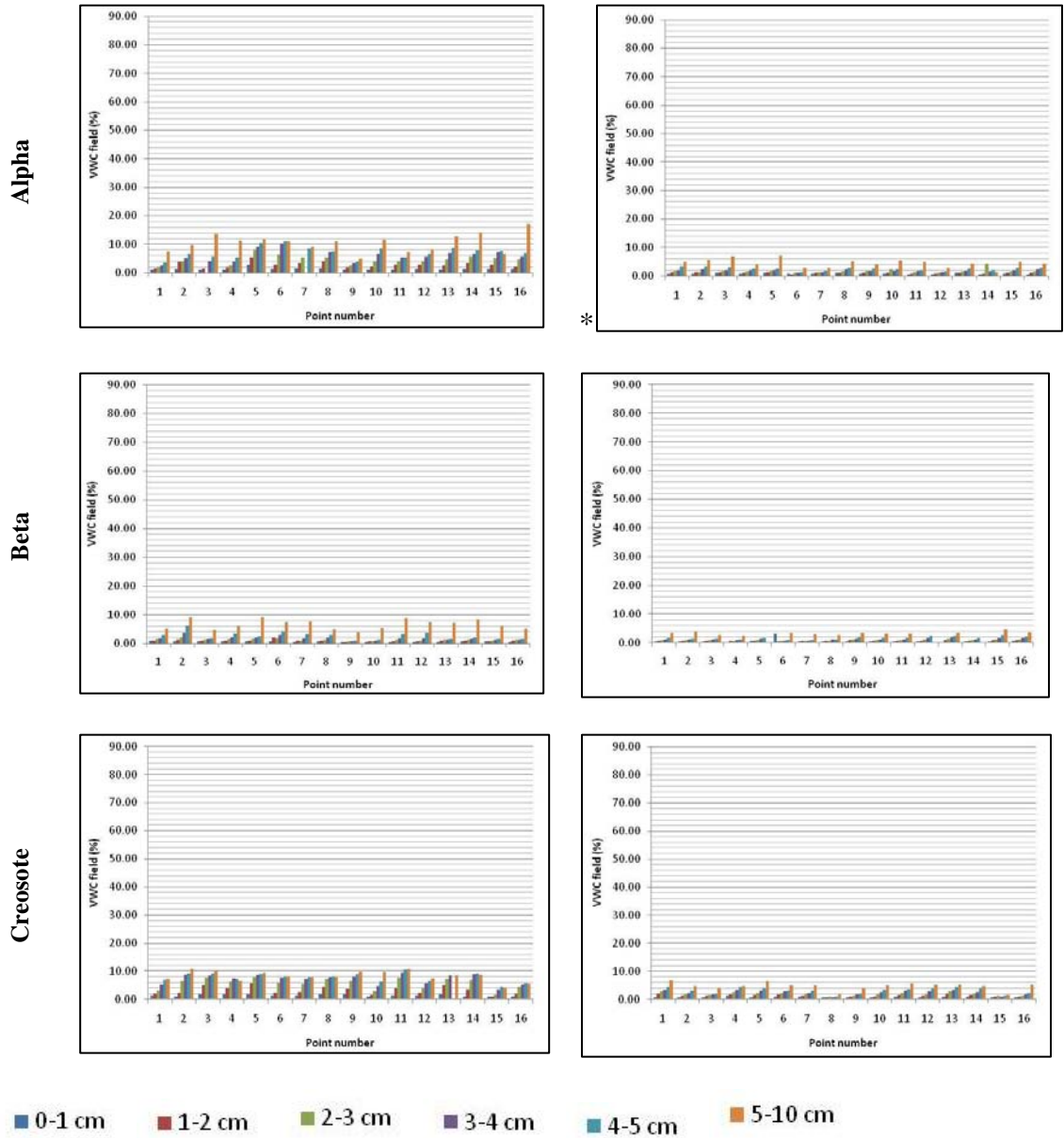


Figure 29. Comparison of VWC (%) between moist and dry conditions.

August 23 (moist conditions)

September 18 (dry conditions)

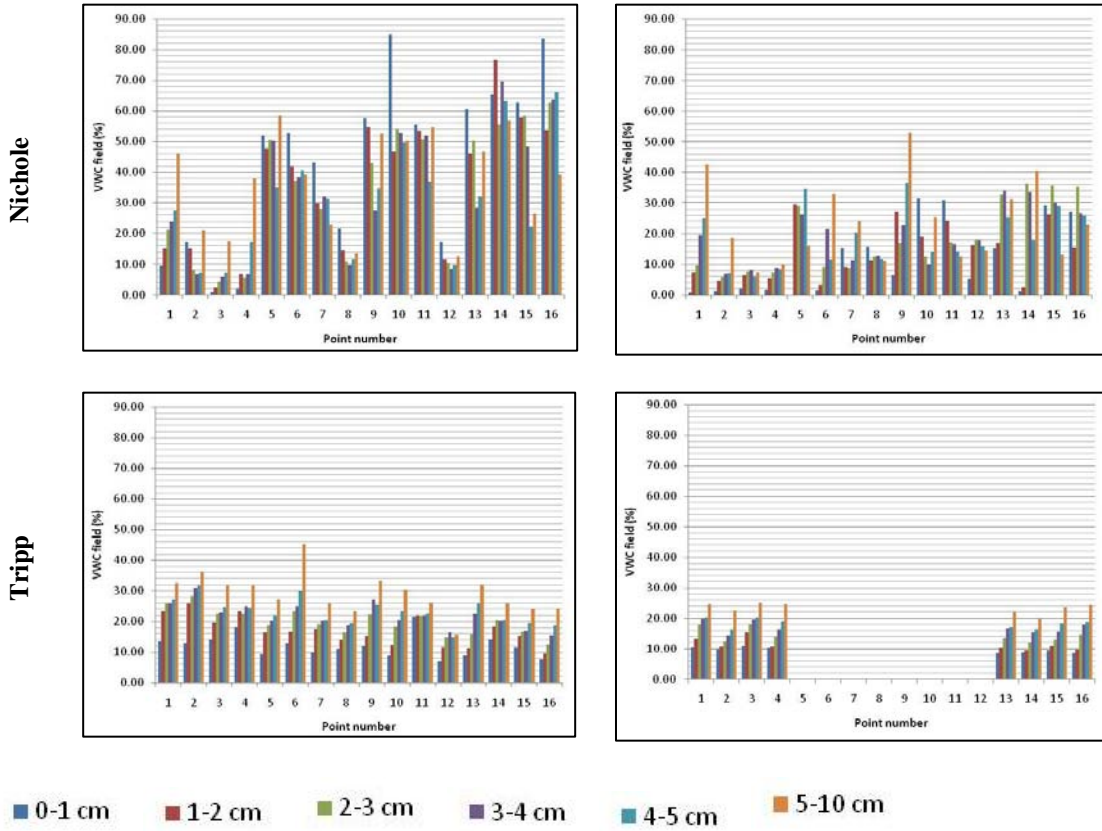


Figure 29. Comparison of VWC (%) between moist and dry conditions

4.2 RADARSAT-2 soil moisture maps

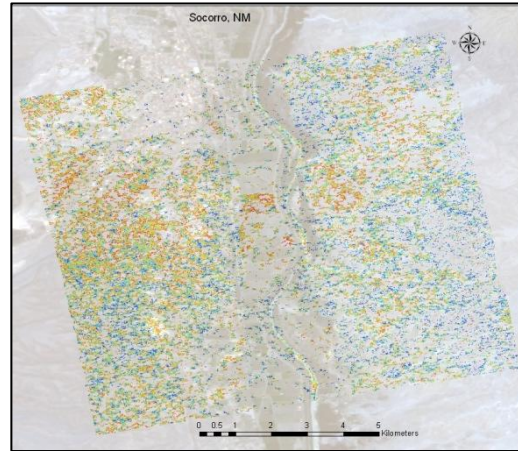
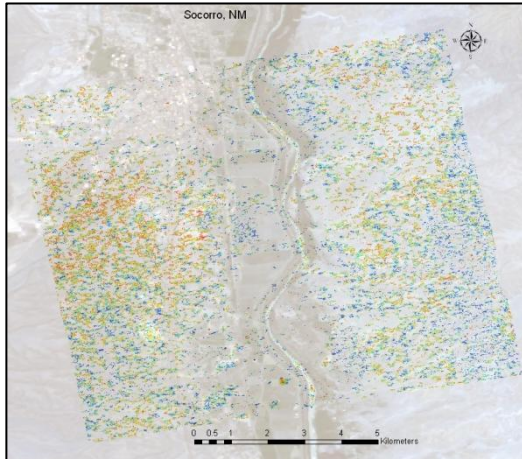
4.2.1 Coverage of RADARSAT-2 soil moisture maps obtained with Oh model.

Ten RADARSAT-2 soil moisture maps were generated for 10x10 km² area that covers the five sites of the validation study. The soil moisture maps were generated using the Oh (2004) model (see Figure 30 for four examples of maps for representative days). The maps showed significant spatial and temporal changes in the area covered. Spatially, the areas closer to the Rio Grande had less coverage than the areas further away from the river valley, probably because of moister conditions and denser vegetation in the valley. The coverage also changed temporally with precipitation events that increase the soil moisture. The factors cited above may increase Mv beyond the range required for optimum performance of the Oh model. During moderately dry and moist conditions, the coverage was slightly higher (19 to 22% of the entire area) than during extremely moist or dry conditions (17%).

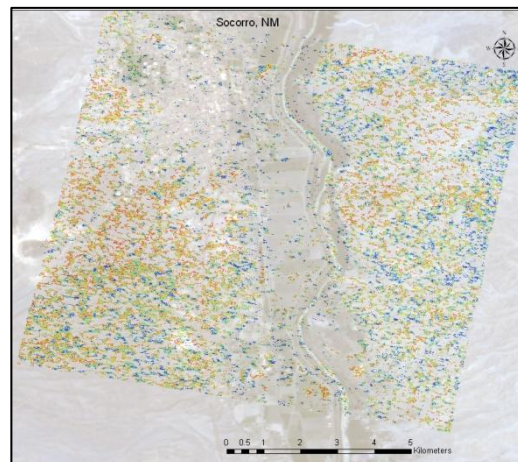
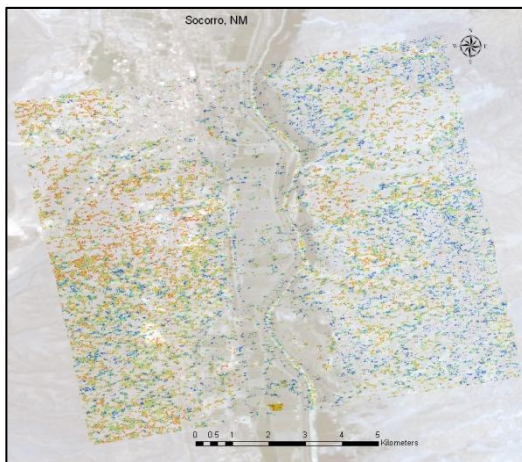
On a smaller scale, the maps showed variable coverage at each of the five sites. The Alpha site had medium to high coverage in almost all the dates (between 40 and 60%), compared to the other sites (Table 6). The percent coverage seems to be primarily related to the vegetation conditions of the sites, which impacts the performance of the Oh model. Low coverage could be expected in dry sites such as Alpha, Beta and Creosote, because VWC is usually lower than the minimum 4% volumetric water content required by the model. However, during days with precipitation, such as July 08, the coverage should be higher, since VWC in the top soil had increased. In these conditions, the Alpha site showed a high coverage by the sensor, while the Beta and Creosote sites had lower

coverage (around 30 % in both sites). This indicates that the Oh model performs better where there is low surface roughness and a bare surface, such as at the Alpha site.

The Nichole and Tripp sites, which have moister conditions, especially at depth, should have high coverage; however, the Nichole site had very low coverage, compared to the other sites. Poor coverage was the result of the high soil moisture, which exceed the maximum value allowed by the inversion method. The Tripp site had medium to poor coverage, despite its ideal surface conditions (flat and homogeneous vegetation cover).



Extremely wet: July 08. Coverage: 16.9% Wet: October 10. Coverage: 19.4%



Extremely dry: Septemb. 18. Coverage: 17.2% Dry: August 01. Coverage: 22.9%

Figure 30. Comparison of maps with different moisture conditions. Soil moisture VWC ranges from 4% (red) to 28% (blue). During extremely wet (July 08) or extremely dry (September 18) conditions, the percent coverage is less than during days with moderate moisture conditions (October 10 or August 01).

COVERAGE %					
Date	Alpha	Beta	Creosote	Nichole	Tripp
June 12	35	56	44	15	0
June 14	62	16	43	43	42
July 08	92	31	30	33	17
August 01	56	34	43	51	49
August 23	17	7	11	0	10
August 25	17	18	40	37	6
September 16	42	20	37	0	22
September 18	13	12	31	3	28
October 10	61	9	25	0	30
October 12	24	15	17	14	11
Average	42	22	32	20	22

Table 6: Percentage of coverage of each site by day in RADARSAT-2 maps

The smallest study scale of the present research is at each of the sampling points of the sites (area of 10x10 m²). The percentage of the area around the 16 points that was covered by the RADARSAT-2 maps' pixels is similar to the percent coverage of the site (see Table 6). At the Alpha site the total area of the 16 points is almost completely covered by the sensor, whereas the Nichole site showed low coverage by the satellite maps.

Comparison of individual sampling points does not suggest a pattern for coverage at the Alpha, Beta and Creosote sites. For example, at the Alpha site almost all the points were covered homogeneously, but point 4 and 13, which have, on average, high (70%) and low coverage (17.5%) in the 10 days, respectively. These points have similar physical characteristics (i.e: flat and bare surfaces). Similarly, points 12 and 3 at the Beta site, which have similar surface conditions, were poorly (6.7%) and highly (30%) covered, respectively.

The Nichole site showed a spatial pattern of point coverage: points closer to the river have less coverage than those further away. This is possibly due to the high soil moisture content in soils closer to the river, which reduces the response of the target to the radar signal and does not fit the conditions for the model. Furthermore, the points in the southern part of the Nichole site showed a low percent coverage, probably related to the effect of high moisture and high vegetation cover. The Tripp site showed homogeneous, but low coverage in all the points. At the Tripp site the coverage reduction does not seem related to any particular characteristic of the surface.

The results of this section show the temporal and spatial variation of percent coverage in the study area, at both site and point scales. Temporally, there was higher coverage during days with moist conditions (recent precipitation in the area) than during days with dry conditions. However, if the moisture conditions were extreme, either moist, (e.g. July 08), or dry (e.g. September 18), the general coverage of the sites was reduced significantly. Spatially, the coverage percentage varied depending on the particular surface features of each site. When a smaller scale was evaluated (sampling point), the results indicate that there was not an specific pattern for having more or less coverage over a point, by the sensor.

4.2.2 Coverage of RADARSAT-2 soil moisture maps with asymmetric volumetric correction

The RADARSAT-2 soil moisture maps generated by using the asymmetric volumetric correction in the satellite images had a higher percent coverage. The coverage on the entire area increased, as much as 70%, as occurred in July 08 (Figure 31). An upscale factor of three was applied to the data in the inversion process of the radar images; therefore, each block of 3x3 pixels in the maps has the same value of VWC. Spatially, there was a pattern similar to the previous soil moisture maps, the areas closer to the river were less covered than areas further from the river. However, there was more coverage during the summer (55-70%) than during the fall (50%), except for July 08, when the coverage was reduced slightly (51%) compared with the other summer dates.

At the site scale, RADARSAT-2 maps with the asymmetric correction showed an increase in the percent cover (Table 7). Nevertheless, the general pattern remained the same or very similar to the maps with just the Oh model. There was no temporal pattern (rainfall events) to increase the coverage of the sites. The maximum values of coverage at each site do not coincide with the days with the best conditions for coverage, such as can be expected on July 08. The Creosote site exhibited the highest coverage of the sites, with a maximum of 95%, followed by the Tripp and Alpha sites, with maximums of 93 and 100% respectively. The percent cover of the Beta site increased significantly compared with the non-corrected version of the maps; this site had a maximum of 94% cover. On the other hand, the Nichole site still showed low coverage, despite the

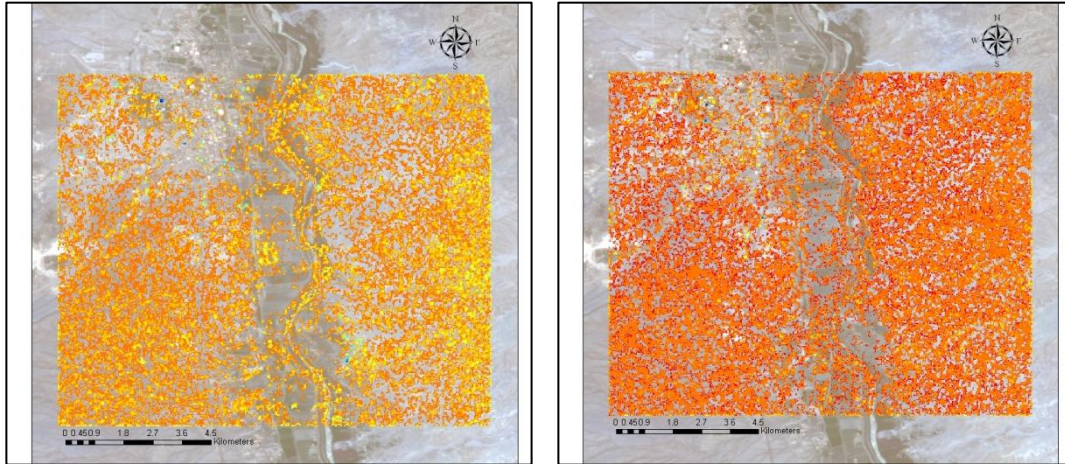
percentage increased, it was very low compared with the increase in the other sites and still had days with no cover at all.

At the sampling point scale, the percentage of area around all the 16 points that was covered by the maps was similar to the entire site scale. The Creosote site exhibited the highest coverage of the 16 points of the area, followed by the Tripp and Alpha sites. The 16 points at the Beta site also had high coverage in the corrected version of the maps, whereas the Nichole site showed significantly low percentage coverage.

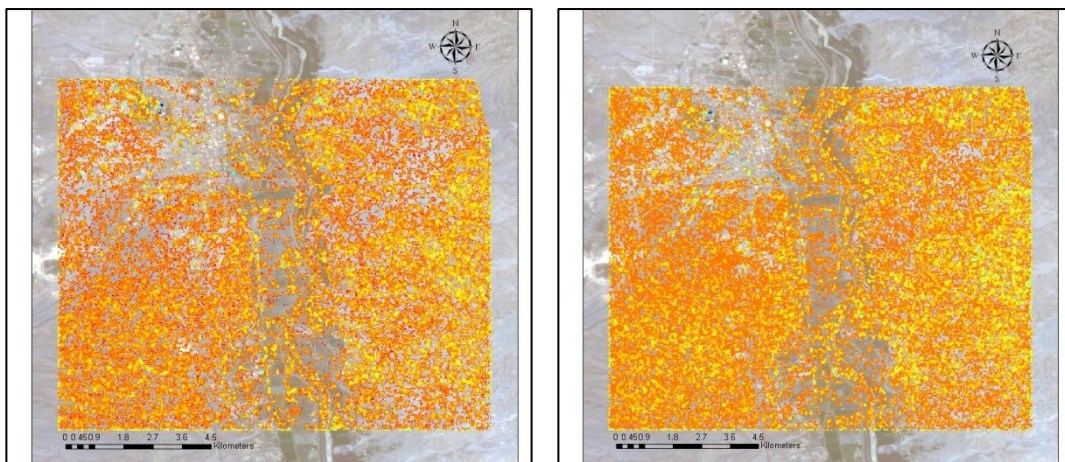
At higher detail, a comparison of each sampling point in each site, the situation is similar to a coarser scale. The corrected maps showed a higher percent and more homogeneous cover than the non-corrected maps. There are no indications of a specific surface characteristic determining when a point was covered by the sensor. The exception to this pattern is the Nichole site, where the points closer to the river and in the southern area of the site had less coverage than the other points. This is the same pattern observed in the previous version of the RADARSAT-2 maps, so the behaviour of the surface conditions to the radar signal seem to be consistent.

The last results suggest that several factors could influence the percent cover of the RADARSAT-2 soil moisture maps with the asymmetric volumetric correction: 1) the higher coverage could be closely related to the upscaling of the data by a factor of 3, which can add extra data pixels to areas where there was a gap in the information in the previous maps. 2) As the asymmetric volumetric correction takes into account the vegetation influence in the scatter coefficients, areas with homogeneous vegetation such as the Creosote or Tripp sites had higher coverage. However, this does not seem to be the

only factor that influenced the map's coverage. Extremely high or low soil moisture, as occurred at the Nichole and Beta sites, respectively, influence the percent coverage. At the Nichole site, the VWC was above the range of the inverse method applied on the data; whereas at the Beta site the moisture conditions were below the VWC required for the application of the Oh model.



Extremely wet: July 08. Coverage: 51.3% *Wet: October 10. Coverage: 49.1%*



Extremely dry: Septemb. 18. Coverage: 48.8% *Dry: August 01. Coverage: 69.0%*

Figure 31. Comparison of maps with different moisture conditions in RADARSAT-2 soil moisture maps with asymmetric volumetric correction. Soil moisture VWC ranges from 4% (red) to 28% (blue).

COVERAGE %					
Date	Alpha	Beta	Creosote	Nichole	Tripp
June 12	66	94	91	28	10
June 14	80	70	77	69	93
July 08	100	59	92	65	50
August 01	79	42	86	80	83
August 23	60	76	57	14	68
August 25	29	89	90	65	74
September 16	84	76	91	9	74
September 18	30	32	95	0	78
October 10	92	55	80	0	81
October 12	79	84	86	23	93
Average	70	68	85	35	70

Table 7. Percentage of coverage of each site by day in RADARSAT-2 maps with asymmetric volumetric correction.

4.2.3 Soil moisture values obtained through RADARSAT-2

Soil moisture values (VWC (%)) were extracted from the area that surrounded the 16 sampling points at the Alpha, Beta, Creosote, Nichole and Tripp sites. The mean VWC (%) of each site for each of the 10 dates is shown in Figure 32 for the first version of the soil moisture maps and in Figure 33 for the maps with asymmetric volumetric correction.

The Volumetric Water Content (%) in the first version of the soil moisture maps ranged between 5 and 15%, except for some days with moist conditions when VWC increases to ~20% (July 08). However, there were high values of VWC (%) in days with dryer conditions, such as August 01, when the sensor could be overestimating the real soil moisture conditions. There were other days when the sensor did not recover data from the Nichole site (September 16 and October 10) and the Tripp site (June 12). In general, the Creosote site exhibited the highest soil moisture values, with an average of 13% for the 10 days. The Nichole, Tripp and Alpha sites followed this trend, with 12, 11 and 10% respectively. The Beta site had the lowest average moisture content, with 8%.

Soil moisture values measured by the sensor increased significantly when the asymmetric volumetric correction was applied. VWC (%) ranged between 8 and 20%, with extreme values going up to 30%. There were extremely high VWC values during days with moist conditions (July 08) for the Alpha site, however, the other sites did not show a similar increase. As with the first version of the maps, the sensor estimated high soil moisture values for days under moderately dry conditions (e.g. August 01). The

Creosote site showed the highest soil moisture, but also the highest variability, with an average of 17%. The other sites had lower soil moisture values, with average VWC for the 10 days, between 10 and 11%.

The results in section 4.2 show that the coverage of the RADARSAT-2 maps is highly influenced by the surface features that affect the conditions required for using the Oh model. These surface characteristics vary spatial and temporally in the study area. Under moist conditions, (summer season) there is higher coverage, at site and point scales. However, the primary factors that influence signal retrieval are high surface roughness, vegetation density, and soil type. Under dry conditions (August 01) or under extremely dry (September 18) or moist (July 08) conditions, the coverage decreases over the entire study area, at site and point scale. Mean soil moisture values measured by the sensor in the five sites ranged between 5 and 15%; the Creosote and Beta sites had the highest and lowest values, respectively.

When the asymmetric volumetric correction is applied to the RADARSAT-2 maps, the percent cover increases significantly at all scales. Nevertheless, areas with relatively homogeneous vegetation (Creosote and Tripp) and good surface conditions (Alpha) for signal retrieval have higher coverage than areas without these features. Mean values of the corrected soil moisture increased significantly, compared with the previous version of the maps, as shown in Table 8 (VWC between 8 and 20%). The Creosote and Beta sites remained as the sites with the highest and lowest soil moisture values, respectively.

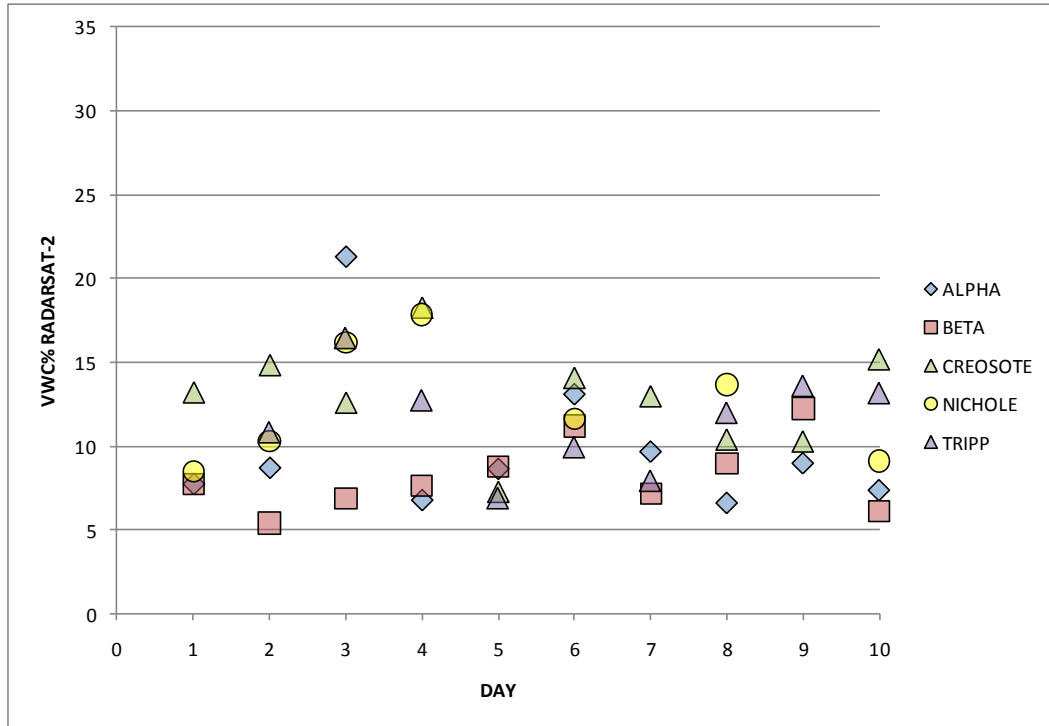


Figure 32. Mean of VWC % from RADARSAT-2 maps, in the 5 sites at the 10 study dates. Days: **1:**June 12; **2:** June 14; **3:** July 08; **4:** August 01; **5:** August 23; **6:** August 25; **7:** September 16; **8:** September 18; **9:** October 10; **10:** October 12.

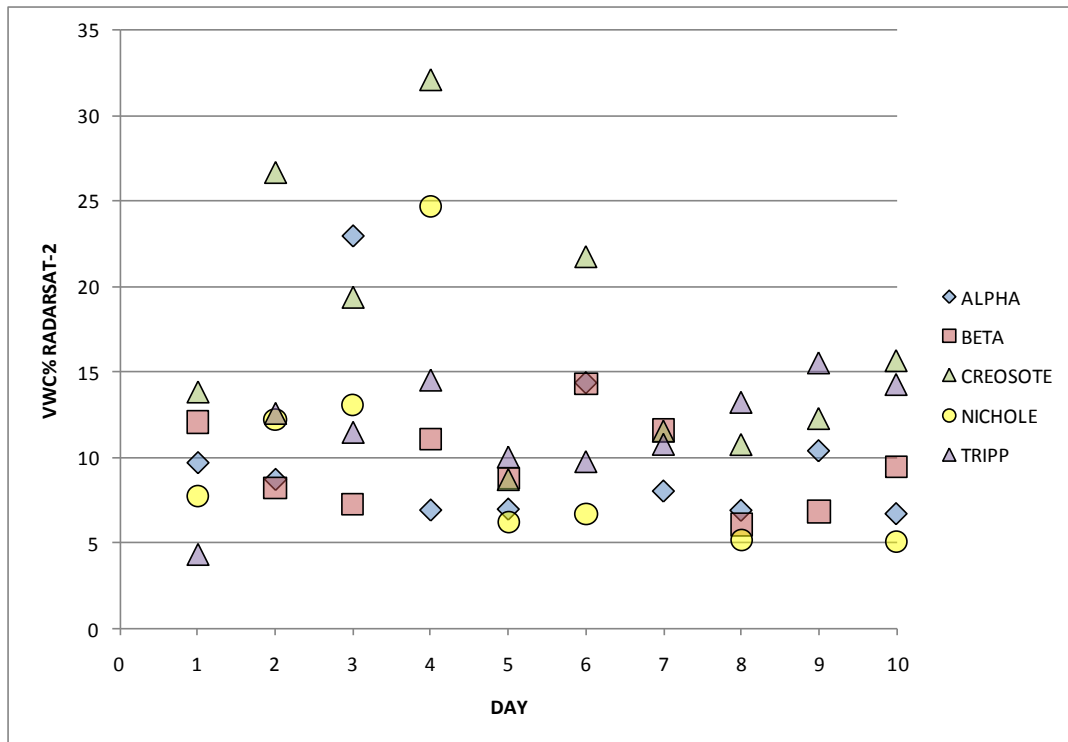


Figure 33. Mean of VWC % from RADARSAT-2 maps with asymmetric volumetric correction, in the 5 sites at the 10 study dates. Days: **1:** June 12; **2:** June 14; **3:** July 08; **4:** August 01; **5:** August 23; **6:** August 25; **7:** September 16; **8:** September 18; **9:** October 10; **10:** October 12

PERCENT COVER %										
Date	Alpha		Beta		Creosote		Nichole		Tripp	
	1	2	1	2	1	2	1	2	1	2
June 12	35	66	56	94	44	91	15	28	0	10
June 14	62	80	16	70	43	77	43	69	42	93
July 08	92	100	31	59	30	92	33	65	17	50
August 01	56	79	34	42	43	86	51	80	49	83
August 23	17	60	7	76	11	57	0	14	10	68
August 25	17	29	18	89	40	90	37	65	6	74
September 16	42	84	20	76	37	91	0	9	22	74
September 18	13	30	12	32	31	95	3	0	28	78
October 10	61	92	9	55	25	80	0	0	30	81
October 12	24	79	15	84	17	86	14	23	11	93
Average	42	70	22	68	32	85	20	35	22	70

Table 8. Comparison of the percent coverage between the first version of the soil moisture maps (1) and the RADARSAT-2 maps with asymmetric correction (2).

4.3 Comparison and analysis of soil moisture field measurements and RADARSAT-2 soil moisture maps

The three most relevant correlation parameters evaluated are: 1) Pearson R, 2) the probability of the correlation $Pr>F$, and 3) R^2 . Pearson R shows the correlation between both variables, the RADARSAT-2 and field soil moisture values. R ranges from -1 (perfect negative correlation) through 0 (no correlation) to $+1$ (perfect positive correlation). $Pr>F$ represents the significance of that correlation and which is the probability of obtaining a better correlation trend between the variables. The correlation is significant if the value of $Pr>F$ is less than 0.05 (5%). Finally, R^2 indicates the proportion of variance in one of the variables that can be explained by the variation in the other variable, and is evaluated between 0 and 1 (Cody and Smith, 1997).

4.3.1 Correlation between soil moisture values from field and RADARSAT- 2 soil moisture maps.

Mean soil moisture values from RADARSAT-2 maps were compared with field samples VWC (%) for the 10 sampling days at each site (see Table 9). The results show that the correlation of the VWC (%) at the Alpha site is high and significant in the upper 3 cm, with values of R-Pearson and R^2 close to 1, and $Pr < 0.05$. The Tripp site exhibits high correlation in the upper 4 cm of the soil profile, its significance is high, but lower than the Alpha site. The correlations at both sites are positive, meaning that as VWC from the field increases, VWC from the RADARSAT-2 maps also increases. The Alpha site has the ideal physical conditions for obtaining a high correlation of the RADARSAT-2 soil moisture maps, i.e. bare and smooth surface and the range of VWC between 4 and 29%. The Tripp site has a low percentage of the sensor coverage in almost all the days of the experiment, and even though the correlation coefficients are high and significant, the RADARSAT-2 soil moisture maps should be used with caution in sites with similar conditions.

The Creosote site exhibits high but negative R-Pearson coefficients with moderate significance. This negative correlation indicates that the estimated soil moisture decreases as the soil moisture in field increases. These results suggest that vegetation has a large influence in the estimation of soil moisture by the radar. The Beta and Nichole sites show poor correlation and significance between the satellite maps and the field measurement values. The reasons for the poor agreement in those sites seem to be related to the surface

conditions, characterised by medium to high vegetation density and the moisture conditions of the soils (low in Beta and high in Nichole, respectively).

Another aspect that has to be considered is the accuracy of the sensor; for example RADARSAT-2 overestimates the field VWC, especially under dry conditions at the Alpha site (Figure 34). The soil moisture measured in the field varies between ~0 to 5% for depth 0 to 1 cm, whereas the RADARSAT-2 maps ranges between 5 and 15%. For the values obtained in July 08 (the moistest point in the plot), the sensor estimated VWC values similar to the field measurements (~20%) In the Creosote and Beta sites the overestimation is higher than at the Alpha site, up to one order of magnitude (see Figure 35 and Figure 36). The RADARSAT-2 maps calculated VWC values between 5 and 15%, while the field measurements show soils with almost zero water content. In contrast, at the Nichole site the RADARSAT-2 soil moisture maps tend to underestimate the high and variable soil moisture values obtained at field (Figure 37). The Nichole site has mean VWC values up to 40%, but the sensor estimates are usually below 30%. The Tripp site exhibits relatively better accuracy, compared with the other sites, but RADARSAT-2 still overestimates the water content (Figure 38).

At a smaller scale, comparison of VWC (%) from the map's pixels and the field measurements show a general poor agreement at any of the depths of the soil profile. There are a few isolated points that show good correlation between both measurements. However, the significance of that correlation is low and there is not spatial continuity of the agreement. RADARSAT-2 maps also overestimates the VWC measured in field when the conditions are dry, and the sensor underestimates VWC when conditions are moist.

Correlation between the mean VWC (%) from each of the RADARSAT-2 maps and the mean VWC (%) of the field measurements for the five sampling sites was determined. Two dates, August 01 and Aug 25, were chosen for performing the correlation. The data shows low correlation coefficients Person R and $P < F$, meaning that there is poor correlation in space between the two types of soil moisture measurements.

Accuracy of the RADARSAT-2 maps and correlation with field soil moisture values are strongly influenced by the moisture and surface conditions of the terrain: 1) volumetric soil moisture, 2) surface roughness, 3) vegetation density, 4) vegetation homogeneity, 5) soil type/particle size. When these factors are the optimum for radar signal retrieval and application of the Oh model, the coverage and correlation with field measurements of the RADARSAT-2 soil moisture maps is high. When the terrain has a combination of features that do not fit into the conditions for using the model, or for optimal signal retrieval, there is not correlation between the soil moisture values and the RADARSAT-2 soil moisture maps estimates, as is common at the Beta, Creosote and Nichole sites.

These results are in agreement with previous studies, using other sensors such as: RADARSAT-1, ERS, and ENVISAR, where poor agreement was found between field data and C-band sensors estimations (D'Urso and Mincapalli, 2006). Surface roughness, vegetation, and volumetric soil moisture have been identified as the main factors affecting the retrieval and accuracy of estimation of the soil moisture by the sensor (i.e. Baghdadi and Zribi, 2006; Yang et al., 2006). The influence of temporally stable patterns of roughness (Alvarez-Mozos, et al., 2009) and soil moisture (Wagner et al., 2008) have

been also identified as factors controlling the temporal stability of soil moisture and its accurate retrieval from SAR sensors. This could explain the high correlation at the sites with ideal surface condition, such as the Alpha and Tripp sites, and the poor correlation of the RADARSAT-2 maps at sites with variable surface conditions, such as the flood plains at the Nichole site or the sand dunes at the Beta site.

ALPHA					
Depth (cm)	Days	Pearson R	R_square	Pr>F	coeff_var
0 to 1	9	0.91	0.83	0.0006	20.40
1 to 2	9	0.91	0.82	0.0008	21.22
2 to 3	9	0.81	0.65	0.0084	29.37
3 to 4	9	0.51	0.26	0.1630	43.00
4 to 5	9	0.27	0.07	0.4786	48.02
5 to 10	9	0.02	0.00	0.9655	49.90

BETA					
Depth (cm)	Days	Pearson R	R_square	Pr>F	coeff_var
0 to 1	5	0.42	0.18	0.4785	20.33
1 to 2	5	0.56	0.31	0.3314	18.66
2 to 3	5	0.72	0.52	0.1692	15.54
3 to 4	5	0.84	0.70	0.0782	12.34
4 to 5	5	0.88	0.78	0.0486	10.63
5 to 10	5	0.46	0.21	0.4396	19.96

CREOSOTE					
Depth (cm)	Days	Pearson R	R_square	Pr>F	coeff_var
0 to 1	7	-0.79	0.63	0.0338	19.48
1 to 2	7	-0.80	0.64	0.0302	19.07
2 to 3	7	-0.77	0.60	0.0407	20.16
3 to 4	7	-0.69	0.47	0.0871	23.12
4 to 5	7	-0.60	0.36	0.1563	25.56
5 to 10	7	-0.62	0.38	0.1397	25.09

Table 9. Statistical parameters calculated between mean VWC % from RADARSAT-2 maps and mean VWC % of 5 sites.

NICHOLE					
Depth (cm)	Days	Pearson R	R_square	Pr>F	coeff_var
0 to 1	6	0.62	0.38	0.1932	25.88
1 to 2	6	0.47	0.22	0.3439	28.94
2 to 3	6	0.45	0.21	0.3669	29.27
3 to 4	6	0.50	0.25	0.3147	28.48
4 to 5	6	0.37	0.14	0.4677	30.48
5 to 10	6	0.22	0.05	0.6800	32.06

TRIPP					
Depth (cm)	Days	Pearson R	R_square	Pr>F	coeff_var
0 to 1	8	0.83	0.69	0.0204	17.87
1 to 2	8	0.81	0.65	0.0279	18.95
2 to 3	8	0.81	0.66	0.0273	18.88
3 to 4	8	0.76	0.58	0.0454	20.75
4 to 5	8	0.74	0.54	0.0597	21.81
5 to 10	8	0.67	0.44	0.1030	24.02

Table 9. Statistical parameters calculated between mean VWC % from RADARSAT-2 maps and mean VWC % of 5 sites

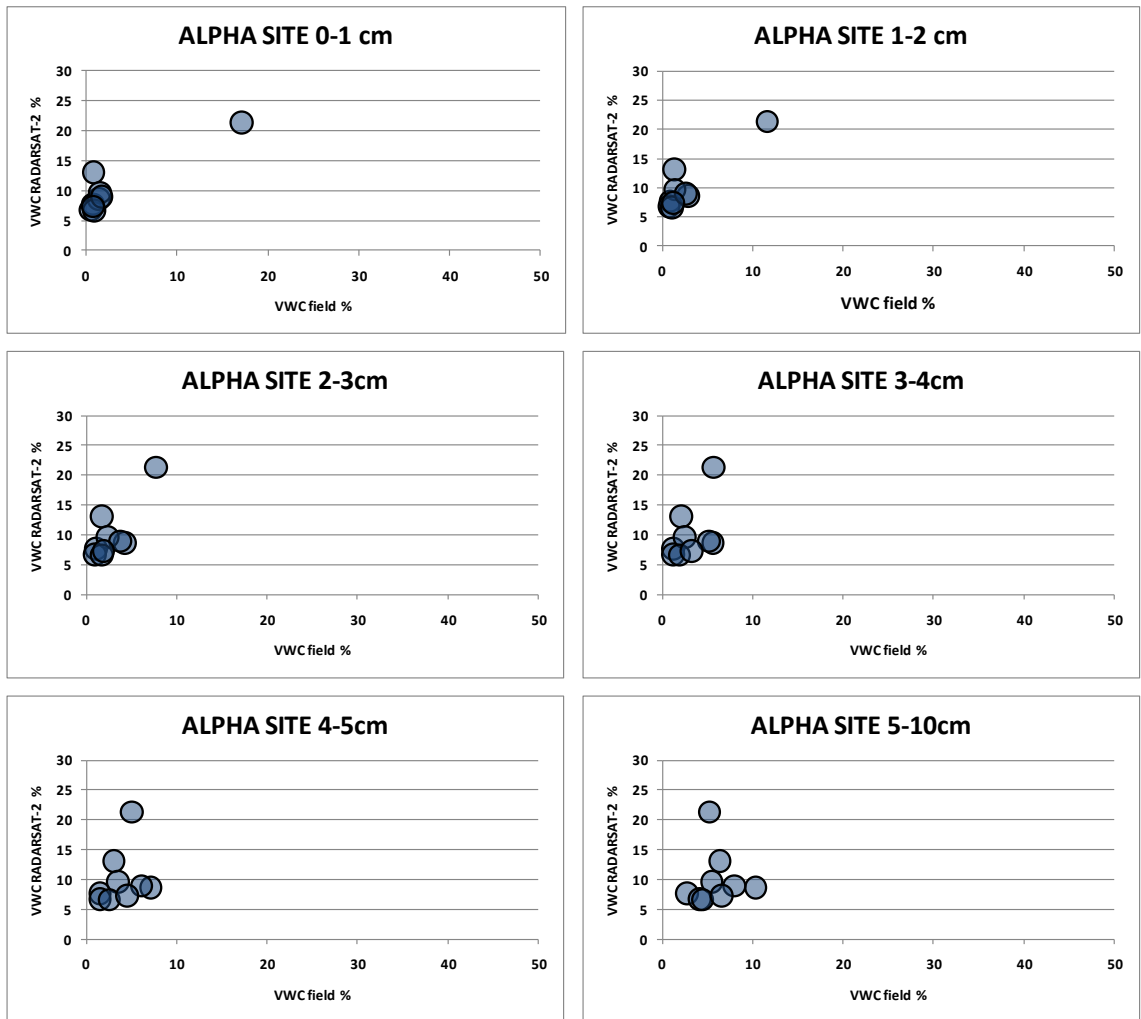


Figure 34. VWC % RADARSAT-2 maps vs. VWC% field values Alpha site

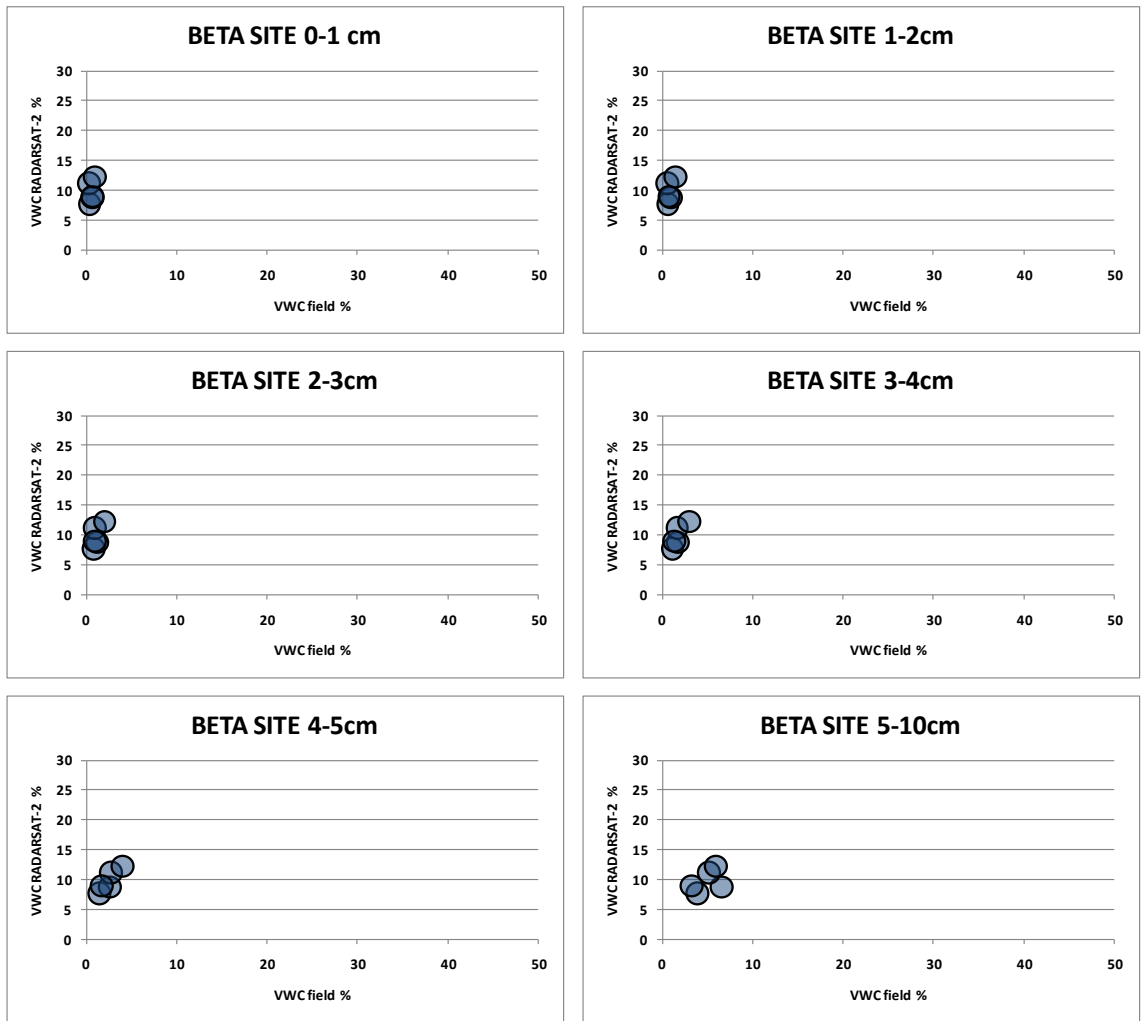


Figure 35. VWC % RADARSAT-2 maps vs. VWC% field values Beta site

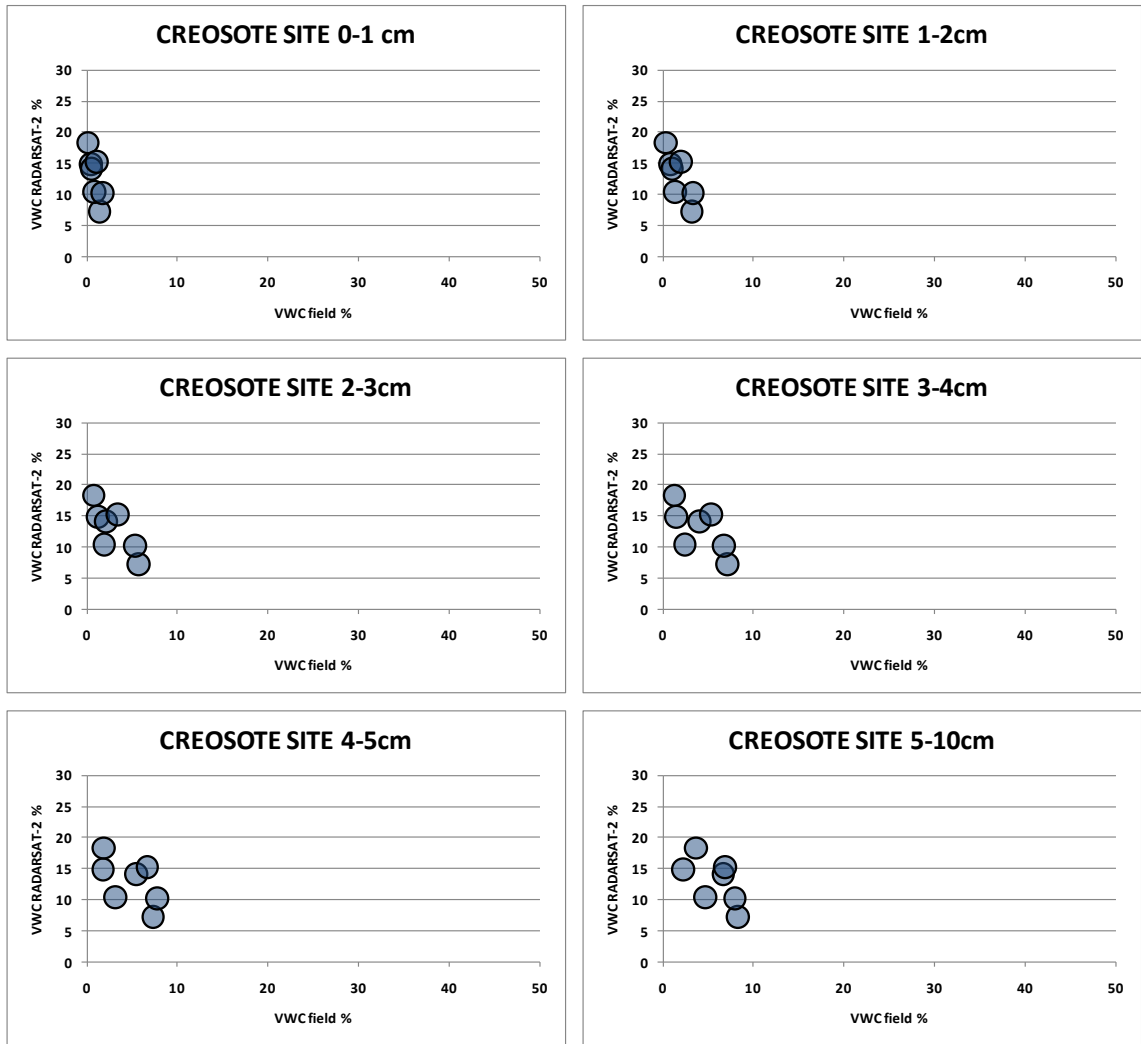


Figure 36. VWC % RADARSAT-2 maps vs. VWC% field values Creosote site

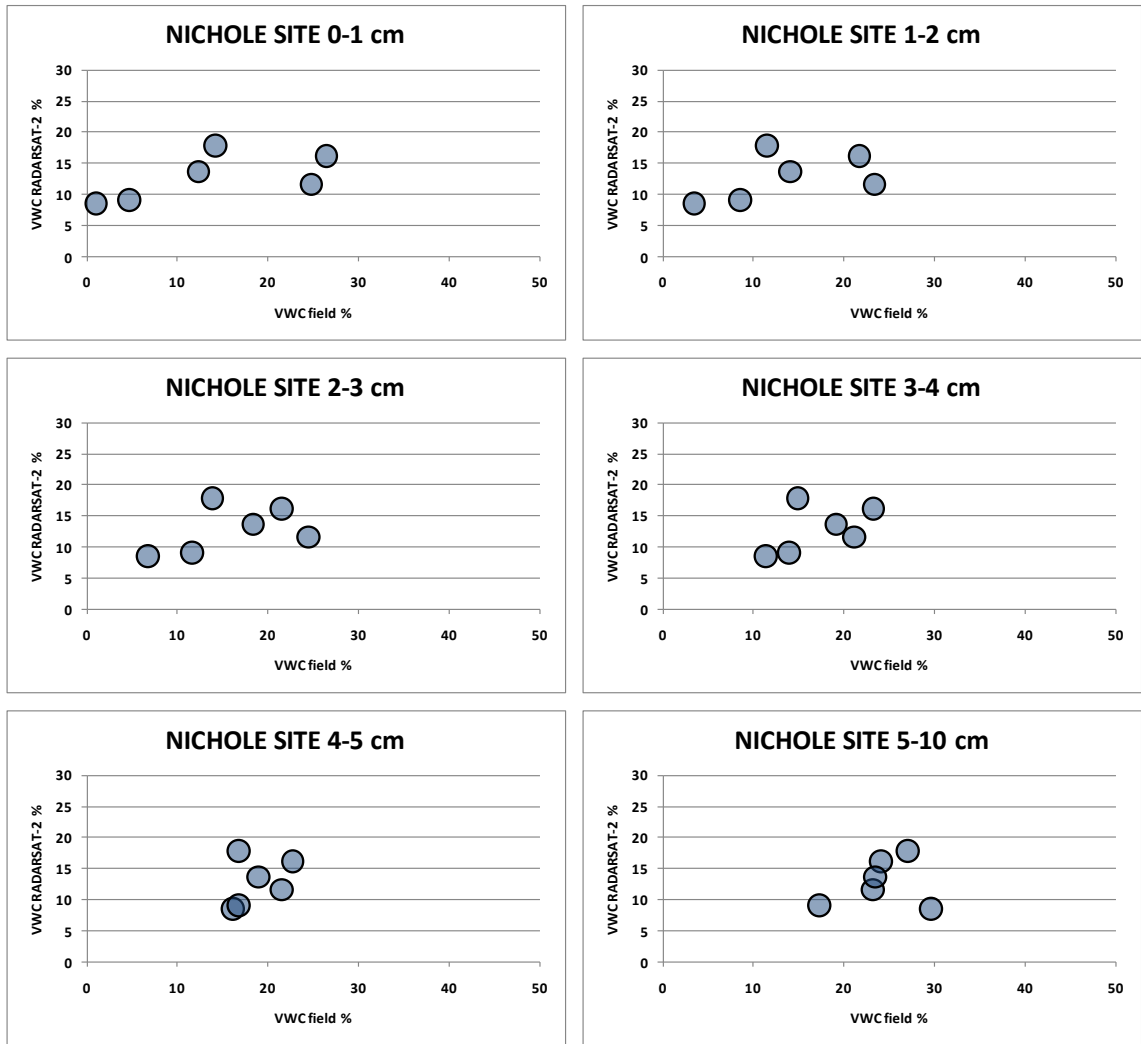


Figure 37. VWC % RADARSAT-2 maps vs. VWC% field values Nichole site

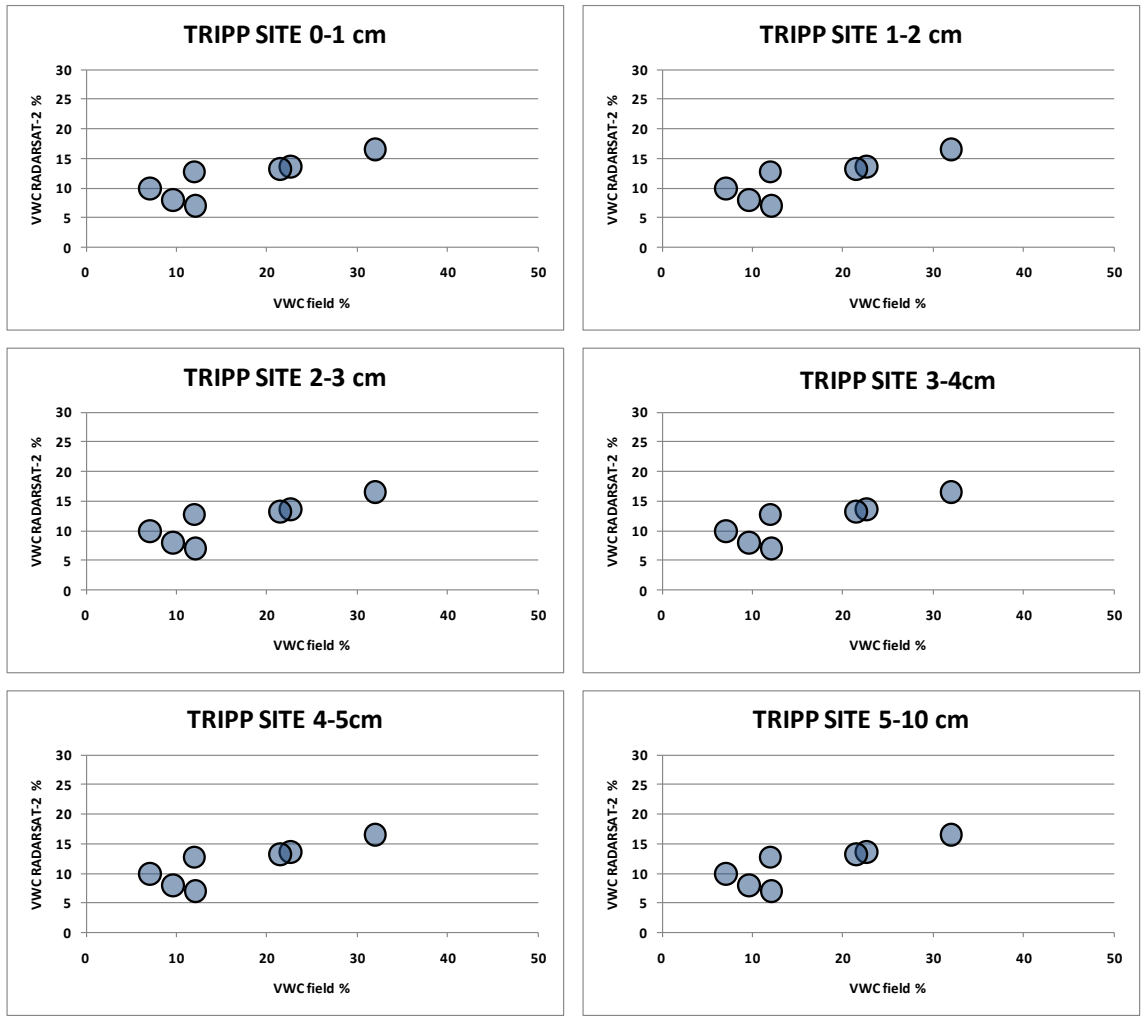


Figure 38. VWC % RADARSAT-2 maps vs. VWC% field values Tripp site

4.3.2 Correlation between soil moisture values from field and RADARSAT- 2 maps with asymmetric volumetric correction.

The mean values of VWC (%) from the RADARSAT-2 maps with asymmetric volumetric correction were compared with the mean field VWC (%) for the 10 sampling days (Table 10). The temporal trends in the correlation at the five sites are displayed in Figure 39 to Figure 43. At the Alpha site the correlation coefficients R and R^2 and the significance $Pr>F$ remains high in the upper 3 cm, compared to the non-corrected maps, but the magnitude of the parameters was reduced slightly. The Creosote site has a high but negative correlation between both measurements in the upper 3 cm, with $Pr<0.05$. Both sites, Alpha and Creosote sites keep the same correlation tendency observed in the previous version of RADARSAT-2 maps. However, the other sites have changes in the correlation patterns. The Beta site varied from low (previous version) to high and negative correlation (corrected maps), and it has low significance ($Pr>0.05$). At the Nichole site, the correlations decreased even lower (values close to 0). Similarly, at the Tripp site the correlation coefficients and significance decreased significantly, compared to the high correlation in the previous version of the maps.

The corrected RADARSAT-2 soil moisture maps have a similar accuracy as the original version of the maps. Overestimation of the field VWC (%) at the Alpha, Beta and Creosote sites is shown in Figure 39 through Figure 41. At the Tripp site the overestimation is smaller than in the previous sites (Figure 42), whereas underestimation of the field VWC (%) occurs at the Nichole site (Figure 43).

At the point scale, field VWC (%) at each of the 16 points in each plot and VWC (%) from each pixel of the RADARSAT-2 maps show poor agreement. As with the non-corrected version, there are some isolated points with high correlation coefficients, but low significance or non-spatial continuity of the agreement.

The correlation in space between the mean VWC (%) from the RADARSAT-2 maps and the field measurements of the five sites exhibit low values for R , R^2 and the significance of the correlations. Three dates, August 01, August 23 and Aug 25, were chosen for performing the comparison. Results demonstrated that there is a poor correlation in space between the soil moisture measurements from the sensor and the field.

The results show that despite of the increase in coverage, the correlation in time of the corrected maps with field VWC measurements did not improve. Correlation tendencies remained similar at the Alpha site (high correlation in upper 3 cm) and the Creosote site (high but negative correlation in 3 upper cm). However the correlation decreased at sites with heterogeneous or grass vegetation.

This response could be related to the structure and aim of the algorithm proposed by Yamaguchi et al. (2005). The algorithm considers the solution for decomposition of scattering in complicated geometric structures. It is probable that the structure of the vegetation covering the Beta, Nichole and Tripp sites does not fit into the conditions of the model. The authors developed the algorithm for dealing with urban structures and crops close to a town. The structure, density and homogeneity of the crops could be more similar to the vegetation at the Creosote site, than to the heterogeneous vegetation at the

Beta and Nichole sites and the grasses at the Tripp site. The heterogeneity of the area covered by each pixel can also affect the soil moisture retrieval, as reported by Loew (2008).

ALPHA					
Depth (cm)	Days	Pearson R	R_square	Pr>F	coeff_var
0 to 1	9	0.88	0.78	0.0015	25.76
1 to 2	9	0.87	0.75	0.0025	27.49
2 to 3	9	0.74	0.54	0.0238	37.36
3 to 4	9	0.42	0.18	0.2625	50.11
4 to 5	9	0.16	0.03	0.6811	54.46
5 to 10	9	-0.11	0.01	0.7857	54.86

BETA					
Depth (cm)	Days	Pearson R	R_square	Pr>F	coeff_var
0 to 1	5	-0.87	0.76	0.0539	20.13
1 to 2	5	-0.63	0.39	0.2583	32.05
2 to 3	5	-0.51	0.26	0.3769	35.29
3 to 4	5	-0.32	0.10	0.6030	38.98
4 to 5	5	-0.15	0.02	0.8059	40.62
5 to 10	5	0.08	0.01	0.9018	40.98

CREOSOTE					
Depth (cm)	Days	Pearson R	R_square	Pr>F	coeff_var
0 to 1	7	-0.87	0.75	0.0116	26.35
1 to 2	7	-0.82	0.67	0.0235	30.13
2 to 3	7	-0.79	0.63	0.0336	32.23
3 to 4	7	-0.76	0.57	0.0488	34.52
4 to 5	7	-0.72	0.52	0.0661	36.48
5 to 10	7	-0.72	0.53	0.0653	36.40

Table 10. : Statistical parameters calculated between mean VWC % from corrected RADARSAT-2 maps and mean field VWC % of 5 sites

NICHOLE					
Depth (cm)	Days	Pearson R	R_square	Pr>F	coeff_var
0 to 1	7	-0.02	0.00	0.9588	79.11
1 to 2	7	-0.15	0.02	0.7411	78.18
2 to 3	7	-0.20	0.04	0.6729	77.59
3 to 4	7	-0.21	0.04	0.6533	77.39
4 to 5	7	-0.24	0.06	0.5997	76.76
5 to 10	7	0.09	0.01	0.8550	78.84

TRIPP					
Depth (cm)	Days	Pearson R	R_square	Pr>F	coeff_var
0 to 1	8	0.46	0.21	0.2518	30.48
1 to 2	8	0.55	0.31	0.1547	28.58
2 to 3	8	0.47	0.22	0.2426	30.34
3 to 4	8	0.39	0.15	0.3409	31.62
4 to 5	8	0.19	0.04	0.6502	33.69
5 to 10	8	-0.04	0.00	0.9168	34.29

Table 10: Statistical parameters calculated between mean VWC % from corrected RADARSAT-2 maps and mean field VWC % of 5 sites

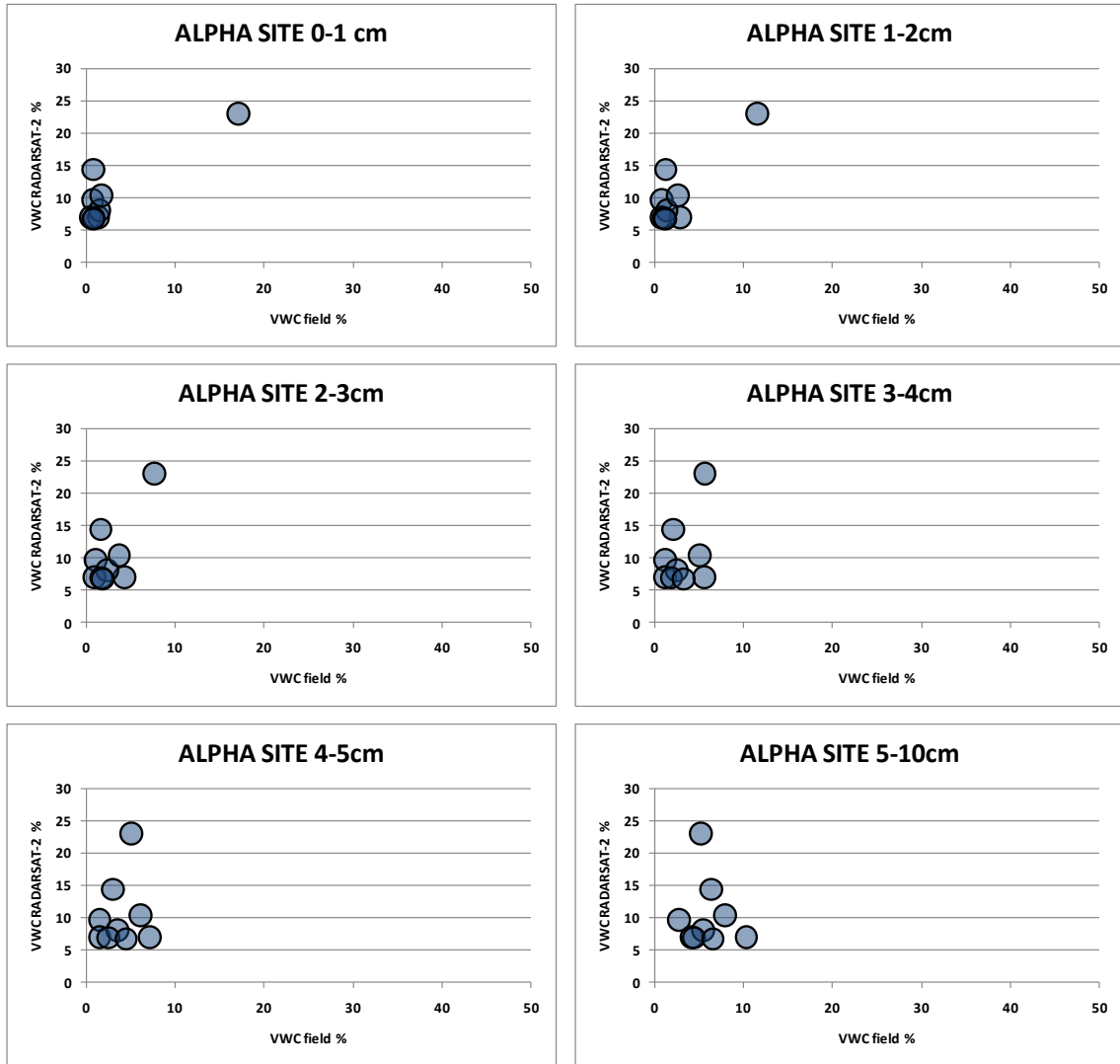


Figure 39. VWC % corrected RADARSAT-2 maps vs. VWC% field values Alpha site

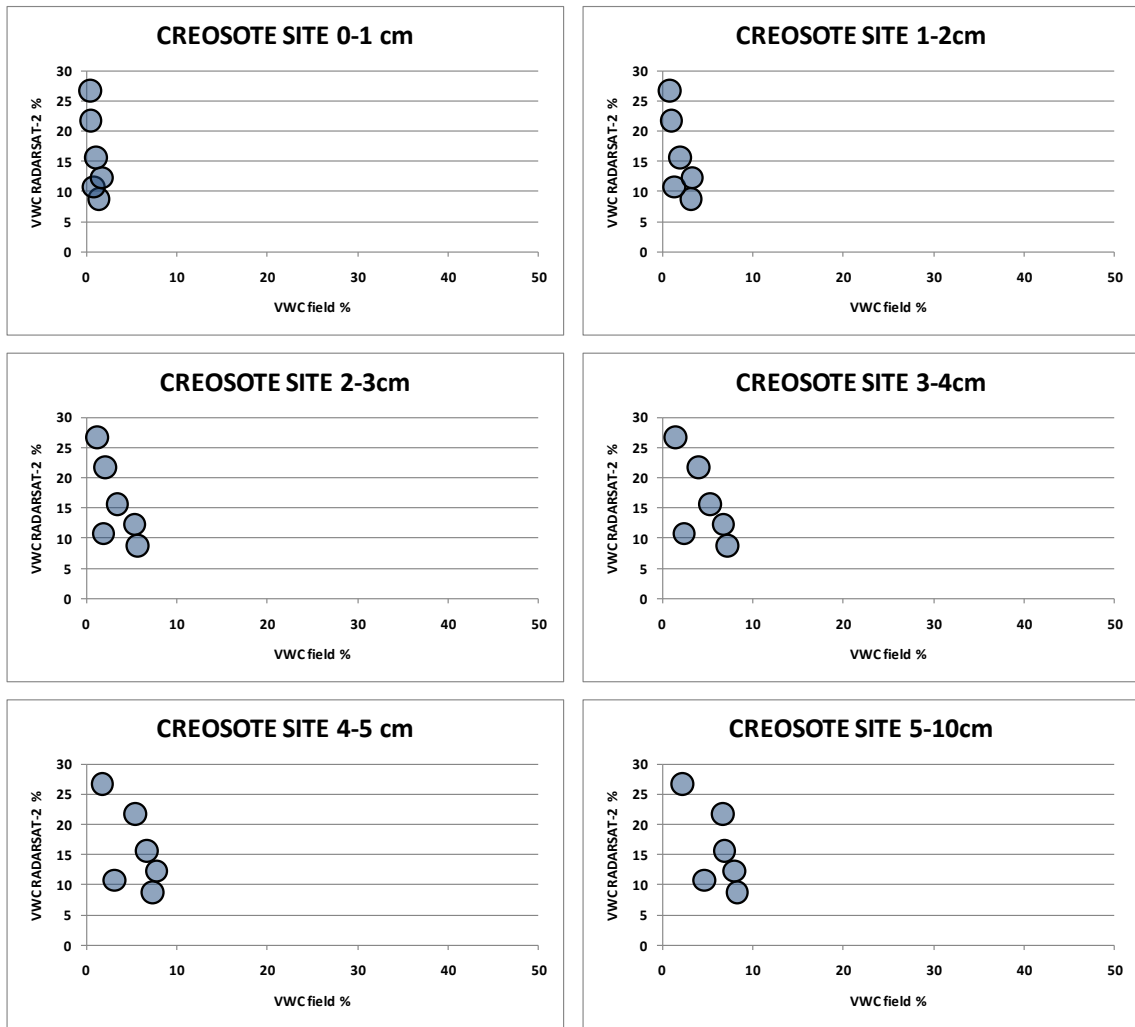


Figure 41. VWC % corrected RADARSAT-2 maps vs. VWC% field values Creosote site

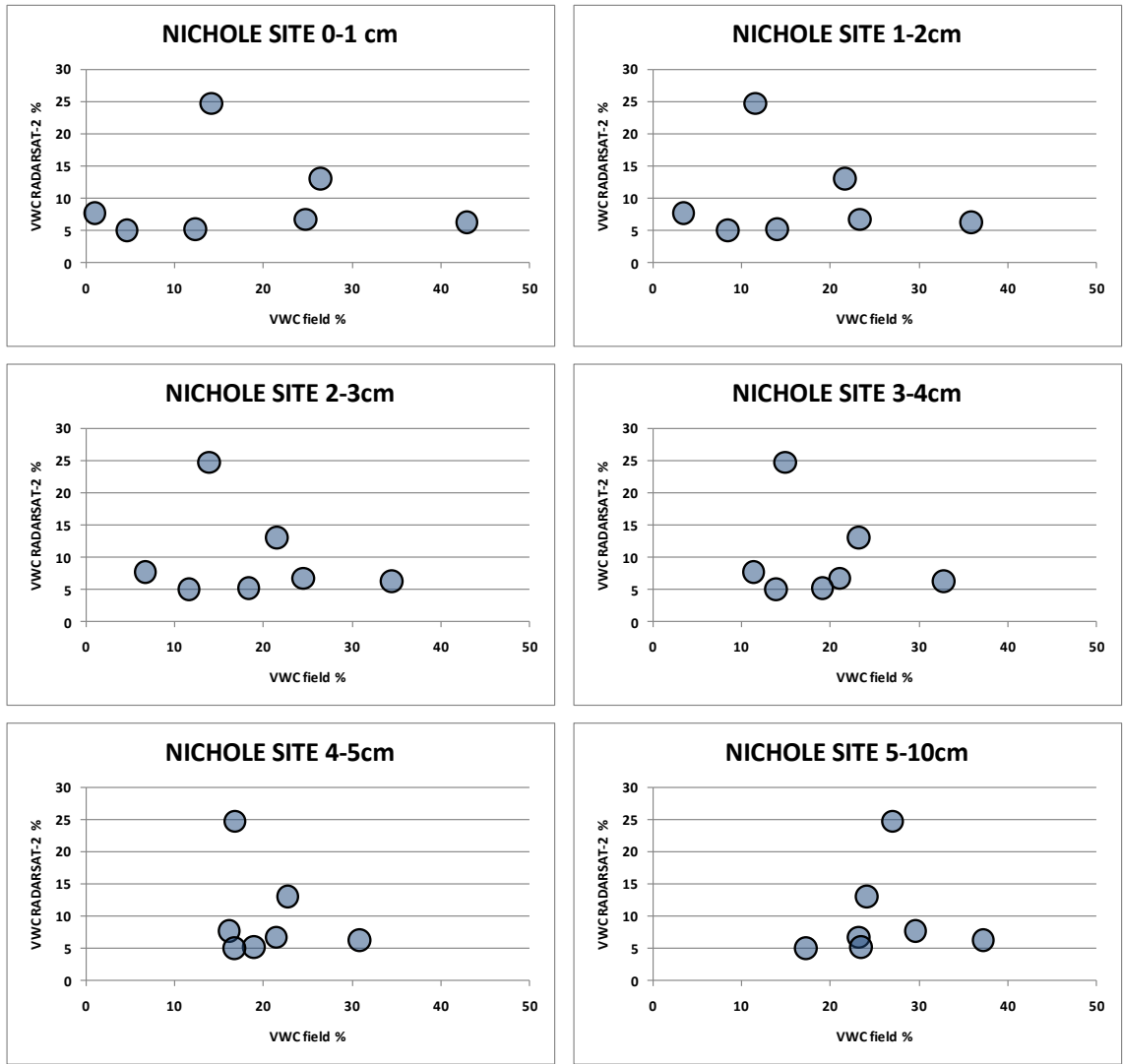


Figure 42. VWC % corrected RADARSAT-2 maps vs. VWC% field values Nichole site

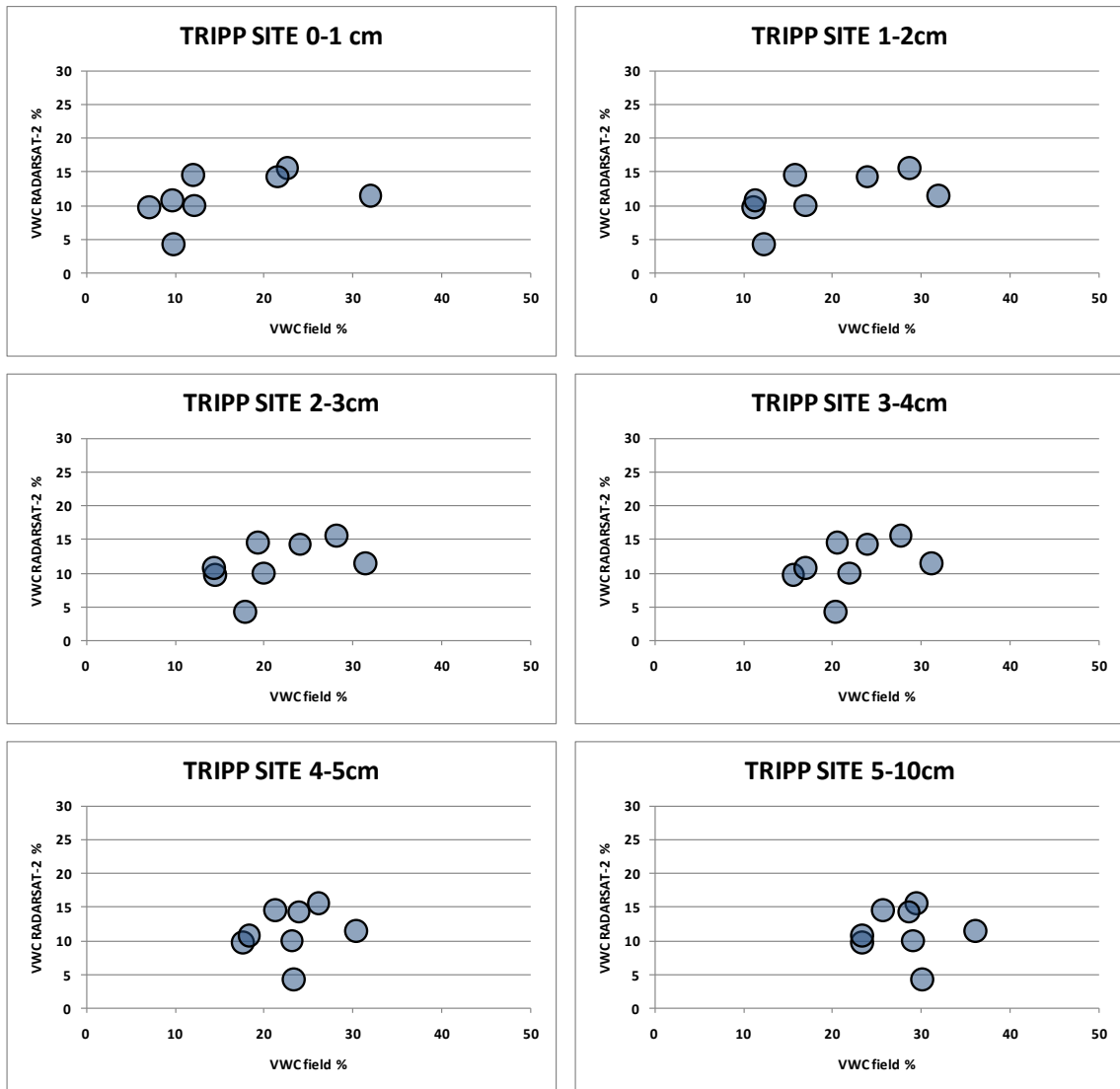


Figure 43. VWC % corrected RADARSAT-2 maps vs. VWC% field values Tripp site

5 CONCLUSIONS

Soil moisture is an important hydrological parameter incorporated into water, energy, and ecologic processes. Large spatial and temporal variability of soil moisture make ground measurements of moisture content difficult. Radar remote sensing can provide time- and cost-effective soil moisture estimates at high spatial and temporal resolution. Nevertheless, there are several factors that affect the radar signal retrieval of soil moisture, such as antecedent precipitation, vegetation coverage, surface roughness, and soil texture. RADARSAT-2 has been proposed as an efficient tool for measuring surface soil moisture under both ideal and non-ideal moisture and surface conditions (i.e. Van der Sanden, 2004). The aim of this study was to validate soil moisture maps obtained from RADARSAT-2 by comparing them with field measurements of soil moisture, to determine the correlation, accuracy and the maximum penetration depth of the radar signal.

The results show that the coverage of the area by the sensor, the correlation with field measurements and the accuracy of the RADARSAT-2 maps are strongly controlled by the moisture conditions of the site. There is also a strong influence of terrain features, such as: 1) surface roughness, 2) vegetation coverage, 3) vegetation heterogeneity, and 4) soil particle size. The results of this research indicate that the RADARSAT-2 maps have good correlation with the field measurements when the conditions of the terrain allow the application of the Oh inverse model, Oh (2004). The requirements of the model are: $0.04 < M_v < 0.28$, $\sigma_{vh}^0 < -9.6$ dB, $p < 1$, and $q < 0.11$, and $0.13 < \kappa_s < 6.98$. Temporal

variability in moisture conditions and soil texture (finer soils have higher soil moisture than coarser textured) influence the requirements needed for determining M_v (volumetric water content). Surface roughness and vegetation coverage affect the probability of reaching the conditions of the backscatter coefficient σ_{vh}^0 , co-polarized ratio p and especially the cross-polarized ratio q .

The mean of the RADARSAT-2 maps soil moisture values and ground-base VWC measurements for each site at the 10 sampling days show a high correlation for the sites where the moisture and surface conditions meet the requirements of the inversion method (Oh, 2004). The Alpha site (bare and flat surface) and the Tripp site (flat and homogeneous vegetation) show high correlation in the upper 3 cm of the soil profile. The Beta, Creosote and Nichole sites exhibit poor correlation between the sensor and the field measurements. This is because of the negative influence of the high surface roughness, heterogeneous vegetation coverage and extreme moisture conditions in the application of the Oh model.

Surface roughness, vegetation coverage and moisture conditions also influenced the accuracy of soil moisture estimation by RADARSAT-2. Under extremely dry conditions, when VWC is less than 4%, RADARSAT-2 overestimates the water content measured in the field, especially if the site is covered by vegetation, such as in the Creosote and Beta sites. Similarly, when extremely moist conditions are present in the area (the VWC is higher than 30%) and the vegetation coverage is heterogeneous, the sensor underestimates the water content compared to field measurements. The maps are

slightly more accurate when the site has moderate water content values (4-30%) and the surface is bare and/or homogeneously covered by vegetation.

Correlation between RADARSAT-2 maps and field measurements is poor between the values of the five sites at each sampling day, which can be related to the high variability in terrain conditions of the sites. Furthermore, on a smaller scale, at each sampling point, there is a generally poor correlation between the RADARSAT-2 soil moisture estimates and the field measurements. The last observations suggest that the correlation and accuracy of soil moisture maps decrease as the study scale decreases from site ($100 \times 100 \text{m}^2$) to point ($10 \times 10 \text{m}^2$) scale.

When the asymmetric volumetric correction was performed in the RADARSAT-2 maps, the correlation for the 10 sampling days remained similar to the non-corrected maps for the Alpha (high correlation, upper 3 cm) and Creosote sites (high and negative correlation, upper 3 cm). The agreement between the maps and field values decreased at the Beta and Nichole sites. However, the most critical change occurred at the Tripp site, where the correlation almost disappeared, in comparison to the high correlation of the non-corrected maps. This response may be related to the structure of the algorithm used in the asymmetric volumetric correction, which seems to deal with different geometric structures of vegetation (horizontal branches of bushes) than the ones present in the Tripp site (grasses).

Data show that the effective depth of penetration of radar signal is less than 3 cm in areas with flat and bare and/or homogeneous vegetation coverage. This result suggests that the soil moisture detected by the sensor is only representative of the upper 3 cm of

the soil profile. Care must be taken to determine whether RADARSAT-2 maps can be used in areas with different surface conditions.

Future research should consider the detailed evaluation of vegetation and roughness parameters of the study sites. This future work should improve the algorithms used in the generation of the RADARSAT-2 soil moisture maps, considering parameters such as vegetation type, soil texture and higher range in the moisture conditions ($M_v < 4\%$ and $M_v > 28\%$). This should improve the accuracy of the RADARSAT-2 soil moisture maps. The data obtained from these could be effectively used in several applications, such as hydrology and energy balance models, ecologic research, and agriculture.

6 REFERENCES

- Alkov, N. (2008). *Remote sensing of fire effects on tamarisk evapotranspiration and regeneration*. M.A. Thesis, EES department, New Mexico Institute of Mining and Technology, Socorro NM. pp, 239.
- Alvarez-Mozos, J., Verhoest, N., Larrañaga, A., Casali, J., and Gonzales-Audican, M. (2009). Influence of surface roughness spatial variability and temporal dynamics on the retrieval of soil moisture from SAR observations. *Sensors*, 9, pp. 463-489.
- Alí, Z., Barnard, I., Fox, P., Duggan, P., Gray, R., Allan, P., Brand, A., and Ste-Mari, R. (2004). Technical note. Description of RADARSAT-2 synthetic aperture radar design. *Canadian Journal of Remote Sensing*, 30 (3), pp. 246-257.
- Alí, Z., Kroupnik, G., Matharu, G., Graham, J., Barnard, I., Fox, P., and Raimondo, G. (2004). Technical note. RADARSAT-2 space segment design and its enhanced capabilities with respect to RADARSAT-1. *Canadian Journal of Remote Sensing*, 30 (3), pp. 235-245.
- Baghdadi, N., and Zribi, M. (2006). Evaluation of radar backscatter models IEM, OH and Dubois using experimental observations. *International Journal of Remote Sensing*, 27 (18), pp. 3831-3852.
- Baghdadi, N., Aubert, M., Cerdan, O., Franchisteguy, L., Viel, C., Martin, E., Zribi, M., Desprast, J.F. (2007). Operational mapping of soil moisture using Synthetic Aperture Radar: application to the Touch Basin (France). *Sensors*, 7, pp. 2458-2483.
- Baup, F., Mougin, E., de Rosnay, P., Timouk, F., and Chenérie, I. (2007). Surface soil moisture estimation over the AMMA Sahelian site in Mali using ENVISAT/ASAR data. *Remote Sensing of Environment*, 109, (4), pp. 473-481.
- Blumberg, D.G., and Freilikhher, V. (2001). Soil water-content and surface roughness retrieval using ERS-2 SAR data in the Negev Desert, Israel. *Journal of Arid Environments*, 49, (3), pp. 449-464.
- Campbell, J. (2007). *Introduction to remote sensing*. Third edition. New York: Guilford Publications, pp. 626.
- Cantón, Y., Solé-Benet, A., and Domingo, F. (2004). Temporal and spatial patterns of soil moisture in semiarid badlands of SE Spain. *Journal of Hydrology* 285, (1-4), pp. 199-214.

Cather, S., and Colpitts, R. (2005). *Preliminary geologic map of Lomas las Cañas, quadrangle, Socorro County, New Mexico*. New Mexico Bureau of Geology and Mineral Resources. Available at:
<http://geoinfo.nmt.edu/publications/maps/geologic/ofgm/details.cfm?Volume=110>.

Cody, R., and Smith, J. (1997). *Applied statistics and the SAS programming language*. Fourth edition. Prentice Hall. pp.

Dubois, P.C., vanZyl, J., and Engman, T. (1995). Corrections to "Measuring Soil Moisture with Imaging Radars". *IEEE Transactions on Geoscience and Remote Sensing*, 33, (6) pp. 1340.

Dubois, P.C., vanZyl, J., and Engman, T. (1995). Measuring soil moisture with imaging radars. *IEEE Transactions on Geoscience and Remote Sensing*, 33, (4) pp. 915-926.

D'Urso, G., and Minacapilli, M. (2006). A semi-empirical approach for surface soil water content estimation from radar data without a-priori information on surface roughness. *Journal of Hydrology*, 321, (1-4), pp. 297-310.

Engle, E. (2009). *Digital soil boundary detection using quantitative hydrologic remote sensing*. M.A. Thesis, EES department, New Mexico Institute of Mining and Technology, Socorro NM. pp. 127.

English, N.B., Weltzin, J.F., Fravolini, A., Thomas, L., and Williams, D.G. (2005). The influence of soil texture and vegetation on soil moisture under rainout shelters in a semi-desert grassland. *Journal of Arid Environments*, 63, (1), pp. 324-343.

Engman, E.T., and Chauhan, N. (1995). Status of microwave soil moisture measurements with remote sensing. *Remote Sensing of Environment*, 51, (1), pp. 189-198.

Findell, K. L., and Elfatih, A. B. E. (1997). An Analysis of the Soil Moisture-Rainfall Feedback, Based on Direct Observations from Illinois. *Water Resources Research*, 33, (4), pp. 725- 735.

Fox, P., Luscombe, A., and Thompson, A. (2004). Technical note. RADARSAT-2 SAR modes development and utilization. *Canadian Journal of Remote Sensing*, 30, (3), pp. 258-264.

Fung, A.K., Li, Z., and Chen, K.S. (1992). Backscattering from a randomly rough dielectric surface. *IEEE Transactions on Geoscience and Remote Sensing*, 30, pp. 356–369.

Gile, L.H., Hawley, J. W., Grossman, R.B. (1981). Soils and geomorphology in the basin and range area of southern New Mexico. Desert project guide book. Memory 39. New Mexico Bureau Mines and Mineral Resources (NMBMMR). Pp. 222.

Gómez-Plaza, A., Martinez, M., Albaladejo, J., Castillo, V. (2001). Factors regulating spatial distribution of soil water content in small semiarid catchments. *Journal of hydrology*, 253, pp. 211-226.

Grayson, R. B., Western, A. W., Chiew, F. H. S., and Blöschl, G. (1997). Preferred States in Spatial Soil Moisture Patterns: Local and Nonlocal Controls. *Water Resources Researched*, 33, (12), pp. 2897-2908.

Hall, F. G., Townshend, J. R., and Engman, E. T. (1995). Status of remote sensing algorithms for estimation of land surface state parameters. *Remote Sensing of Environment*, 51, (1), pp. 138-156.

Heilman, J.L, Kanemasu, E.T., Bagley, J.O., and Rasmussen, V.P. (1977). Evaluating soil moisture and yield of winter wheat in the Great Plains using Landsat data. *Remote Sensing of Environment*, 6, (4), pp. 315-326.

Huisman, J. A., Sperl, C., Bouten, W., and Verstraten, J. M. (2001). Soil water content measurements at different scales: accuracy of time domain reflectometry and ground-penetrating radar. *Journal of Hydrology*, 245, (1-4), pp. 48-58.

Kears, A. (1998). *Temporal variability of precipitation recharge in semiarid New Mexico*. M.A. Thesis, EES department, New Mexico Institute of Mining and Technology, Socorro NM. pp, 51.

Jury, W., and Horton, R. (2004). *Soil Physics*, Sixth edition, John Wiley & Sons INC. pp. 370.

Lakhankar, T., Ghedira, H., Temimi, M., Sengupta, M., Khanbilvardi, R., and Blake, R. Non-parametric methods for soil moisture retrieval from satellite remote sensing data. (2009). *Remote sensing*, 1, pp. 3-21.

Lakhankaar, T., Ghedira, H., Temimi, M., Azar, A., and Khanbilvardi, R. (2009). Effect of land cover heterogeneity on soil moisture retrieval using active microwave remote sensing data. *Remote sensing*, 1, pp. 80-91.

Li, Z., Wang, Y., Zhou, Q., Wu, J., Peng, J., and Chang, H. (2008). Spatiotemporal variability of land surface moisture based on vegetation and temperature characteristics in Northern Shaanxi Loess Plateau, China. *Journal of Arid Environments*, 72, (6), pp. 974-985.

Loew, A. (2008). Impact of surface heterogeneity on surface soil moisture retrievals from passive microwave data at the regional scale: The Upper Danube case. *Remote Sensing of Environment*, 112, (1), pp. 231-248.

Lunt, I.A., Hubbard, S.S., and Rubin, Y. (2005). Soil moisture content estimation using ground-penetrating radar reflection data. *Journal of Hydrology*, 307, (1-4), pp. 254-269.

Ma, K. M., Fu, B. J., Liu, S. L., Guan, W.B., Liu, G. H., Lü, Y. H., and Anand, M. (2004). Multiple-scale soil moisture distribution and its implications for ecosystem restoration in an arid river valley, China. *Land Degradation & Development*, 15, (1), pp. 75-85.

Mohanty, B. P., and Skaggs, T. H. Spatio-temporal evolution and time-stable characteristics of soil moisture within remote sensing footprints with varying soil, slope, and vegetation. (2001). *Advances in Water Resources*, 24, (9-10), pp. 1051-1067.

Moran, M. S., Vidal, A., Troufleau, D., Qi, J., Clarke, T. R., Pinter, P. J., Mitchell, T. A., Inoue, Y., and Neale, C. M. U. (1997). Combining multifrequency microwave and optical data for crop management. *Remote Sensing of Environment* 61, (1), pp. 96-109.

Moran, M. S., Hymer, D. C., Qi, J., and Sano, E. (2000). Soil moisture evaluation using multi-temporal synthetic aperture radar (SAR) in semiarid rangeland. *Agricultural and Forest Meteorology*, 105, (1-3), pp. 69-80.

Morena, L.C., James, K.V., and Beck, J. (2004). Technical note. An introduction to RADARSAT-2 mission. *Canadian Journal of Remote Sensing*, 30, (3), pp 221-234.

Pierdicca, N., Pulvirenti, L., and Bignami, C. (2010). Soil moisture estimation over vegetated terrains using multitemporal remote sensing data. *Remote Sensing of Environment* 114, (2), pp. 440-448.

Oh, Y., Sarabandi, K., and Ulaby, F.T. (2002). Semi-empirical model of the ensemble-averaged differential Mueller matrix for microwave backscattering from bare soil surfaces. *IEEE Transactions on Geoscience and Remote Sensing*, 40, (6), pp. 1348-1355.

Oh, Y. (2004). Quantitative retrieval of soil moisture content and surface roughness from multipolarized radar observations of bare soil surfaces. *IEEE Transactions on Geoscience and Remote Sensing*, 42, (3), pp. 596-601.

Quesney, A., Le Hégarat-Masclé, S., Taconet, O., Vidal-Madjar, D., Wigneron, J. P., Loumagne, C., and Normand, M. (2000). Estimation of Watershed Soil Moisture Index from ERS/SAR Data. *Remote Sensing of Environment*, 72, (3), pp. 290-303.

Sabins, F. (1978). Remote sensing: principles and interpretation. Library of Congress Cataloging in Publication Data, pp. 426.

Sahebi, M. R., Bonn, F., and Gwyn, Q. H. J. (2003). Estimation of the moisture content of bare soil from RADARSAT-1 SAR using simple empirical models. *International Journal of Remote Sensing* 24, (12), pp. 2575.

Sahebi, M.R., Angles, J. (2009). An inversion method based on multi-angular approaches for estimating bare soil surface parameters from RADARSAT-1. *Hydrology and Earth System Sciences Discussions*, 6, pp. 207-241.

Sanli, F.B., Kurucu, E.Y., Goksel, S.A., Hussin, Y. (2007). Comparison of soil moisture estimation from RADARSAT-1 and ASAR data using image fusion technique. *The International Archives of the Photogrammetry, Remote Sensing and Spatial Information Sciences*, 28.

Schmugge, T. (1998). Applications of passive microwave observations of surface soil moisture. *Journal of Hydrology*, 212-213, pp. 188-197.

Schmugge, T.J., Jackson, T.J., McKim, H.L. (1980). Survey of methods for soil moisture determination. *Water Resources Research*, 16, (6), pp. 961-979.

Schneider, K., Huisman, J.A., Breuer, L., Zhao, Y., and Frede, H.G. (2008). Temporal stability of soil moisture in various semi-arid steppe ecosystems and its application in remote sensing. *Journal of Hydrology*, 359, (1-2), pp. 16-29.

- Smith, K. (1998). *Methods of soil analysis*, part 1. Second edition.
- Thoma, D.P., Moran, M.S., Bryan, 109 ahman, M.M., Holifield Collins, C.D., Keefer, T.O., Noriega, R. (2008). Appropriate scale of soil moisture retrieval from high resolution radar imagery for bare and minimally vegetated soils. *Remote Sensing of Environment*, 112, (2), pp. 403-414.
- Ullaby, F., Dubuois, P., van Zyl, J. (1996). Radar mapping of surface soil moisture. *Journal of Hydrology*, 184, (1-2), pp. 57-84.
- United States Department of Agriculture USDA, Soil Conservation Service. (1988). *Soil Survey of Socorro County Area, New Mexico*. pp. 328.
- Van der Sanden, J. (2004). Anticipated applications potential of RADARSAT-2 data. *Canadian Journal of Remote Sensing*, 30, (3), pp. 369-379.
- Verhoest, N., Lievens, H., Wagner, W., Alvarez-Mozos, J., Moran, S., Mattia, F. (2008). On the soil roughness parameterization problem in soil moisture retrieval of bare surfaces from Synthetic Aperture Radar. *Sensors*, 8, (7), pp. 4213-4248.
- Walker, J., Willgoose, G., Kalma, J. (2004) In situ measurement of soil moisture: a comparison of techniques. *Journal of Hydrology*, 293, pp. 85–99.
- Wang, C., Qi, J., Moran, S., and Marsett, R. (2004). Soil moisture estimation in a semiarid rangeland using ERS-2 and TM imagery. *Remote Sensing of Environment*, 90, (2), pp. 178-189.
- Wickel, A. J., Jackson, T. J., and Wood, E. F. (2001). Multitemporal monitoring of soil moisture with RADARSAT SAR during the 1997 Southern Great Plains hydrology experiment. *International Journal of Remote Sensing*, 22, (8), pp. 1571-1583.
- Weather underground data center. Available at: <http://www.wunderground.com>.(accessed last time: November 2009)
- Western Regional Climate Center data base. Available at: <http://www.wrcc.dri.edu>. (accessed last time: September 2009).
- Yair, A. (1987). Environmental effects of loess penetration into the northern Negev Desert. *Journal of arid environment*, 13, pp 9-24.

Yamaguchi, Y., Moriyama, T., Ishido, M., and Yamada, H. (2005). Four-component scattering model for polarimetric SAR image decomposition. *IEEE Transactions on Geosciences and Remote Sensing*, 43, (8), pp. 1699-1706.

Yang, H., Shi, J., Guo, H.(2006). Temporal and spatial soil moisture change pattern detection in an agricultural area using multi-temporal Radarsat ScanSAR data. *International Journal of Remote Sensing*, 27, (10), pp. 4199-4212.

Zhang, T., Wen, J., Su, Z., van der Velde, R., Timmermans, J., Liu, R., Liu, Y, and Li, Z. (2009). Soil moisture mapping over the Chinese Loess Plateau using ENVISAT/ASAR data. *Advances in Space Research*, 43, (7), pp. 1111-1117.

Zhu, Y., and Shao, M. (2008). Variability and pattern of surface moisture on a small-scale hillslope in Liudaogou catchment on the northern Loess Plateau of China. *Geoderma*, 147, (3-4), pp. 185-191.

Zribi, M., Baghdadi, N., Holah, N., and Fafin, O. 2005. New methodology for soil surface moisture estimation and its application to ENVISAT-ASAR multi-incidence data inversion. *Remote Sensing of Environment*, 96, (3-4), pp. 485-496.

